**SCUOLA DI DOTTORATO**
**UNIVERSITÀ DEGLI STUDI *MEDITERRANEA* DI REGGIO CALABRIA**
DIPARTIMENTO DI INGEGNERIA CIVILE, DELL'ENERGIA, DELL'AMBIENTE E DEI MATERIALI (DICEAM)

DOTTORATO DI RICERCA IN
INGEGNERIA MARITTIMA, DEI MATERIALI E DELLE STRUTTURE
S.S.D. ICAR/02
XXVII CICLO

# ADVANCED ANALYSIS OF WAVE DATA FOR LONG-TERM STATISTICS AND WAVE ENERGY EXPLOITATION

PHD STUDENT:
Valentina Laface

SUPERVISOR:
Prof. Felice Arena

CO ADVISOR:
Prof. Carlos Guedes Soares

HEAD OF THE DOCTORAL SCHOOL
Prof. Felice Arena

REGGIO CALABRIA, FEBRUARY 2015

VALENTINA LAFACE

THIS PAGE INTENTIONALLY LEFT BLANK

# ADVANCED ANALYSIS OF WAVE DATA FOR LONG-TERM STATISTICS AND WAVE ENERGY EXPLOITATION

*To my parents that have always believed in my ability, that did not allow me to leave when I did not believe enough, and especially for having teaching me that everything is possible in my life**é** BUT I HAVE TO BE THE FIRST TO BELIEVE**é** ..*

*To my brother and his future wife, because I feel that they are with me now and they will be with me in the future, each time I will need their help and support**é** .*

*To anyone has lived through this experience with me**é** . Making it **ñ**our PhD**ò**...*

*To all people of my family and all my friends because what I have become is the results of the growth among them**é** .*

Il Collegio dei docenti del Dottorato di Ricerca in
*Ingegneria Marittima, dei Materiali e delle Strutture*
è composto da:

Felice Arena (coordinatore)
Giuseppe Barbaro
Guido Benassai
Paolo Boccotti
Vittoria Bonazinga
Michele Buonsanti
Salvatore Caddemi
Enzo D'Amore
Giuseppe Failla
Vincenzo Fiamma
Pasquale Filianoti
Enrico Foti
Paolo Fuschi
Sofia Giuffrè
Carlos Guedes Soares
Giovanni Leonardi
Antonina Pirrotta
Aurora Angela Pisano
Alessandra Romolo
Adolfo Santini
Francesco Scopelliti
Pol D. Spanos
Alba Sofi

UNIONE EUROPEA
Fondo Sociale Europeo


REPUBBLICA
ITALIANA

REGIONE
CALABRIA
Assessorato Cultura,
Istruzione e Ricerca
Dipartimento 11


“**La presente tesi è cofinanziata con il sostegno della Commissione Europea, Fondo Sociale Europeo e della Regione Calabria. Lôautore è il solo responsabile di questa tesi e la Commissione Europea e la Regione Calabria declinano ogni responsabilità sullôuso che potrà essere fatto delle informazioni in essa contenute**”.

“**This thesis is co-funded with support of the European Commission, the European Social Fund and the Regione Calabria. The author is solely responsible for this thesis and the European Commission and the Regione Calabria responsible for any use that may be made of the information contained therein**”.

## Table of Contents

# Introduction

*The thesis deals with wave data analysis for the long-term statistics of sea storms and wave energy resources estimation. The correct evaluation of extreme values of significant wave height is one of the most important areas of scientific interest in maritime engineering because of its relevant contribution to the design stage of maritime structures and wave energy devices. The thesis gives an overview of the various methodologies employed in extreme values analysis of wave height focusing on the ñEquivalent Storm Modelsò. Belonging to this category are the Equivalent Triangular Storm (ETS) and Equivalent Power Storm (EPS) models. They enable us to analyze storms by representing them through a simpler geometric shape associating to each actual storm a statistically equivalent one, defined by means of two parameters: the first representative of storm intensity and assumed equal to the maximum significant wave height in the actual storm, the latter representative of storm duration, determined assuming that the maximum expected wave heights in the actual and equivalent storms are the same. They provide a solution for the return period $R(H_s>h)$ of a storm whose maximum significant wave height is greater than a fixed threshold h, and for the mean persistence $D_m(h)$ above h. In the case of ETS model the solution of both $R(H_s>h)$ and $D_m(h)$ are achieved in a closed form, while the solutions for EPS model have to be solved numerically. The EPS model gives a more realistic representation of storms affording more conservative predictions. In the thesis a new model called Equivalent Exponential Storm Model is developed in order to combine all together the advantages of the previous ones. Several interesting results are obtained applying the new model. Furthermore the thesis presents various original analyses performed applying the three ñEquivalent Storms Modelsò and processing different kinds of wave data. The variability of parameters of intensity and duration of equivalent storms with the assumption of different time interval between two consecutive records is investigated and its influence on long-term predictions is evaluated. A sensitivity analysis of return values to storm threshold is performed applying both the EES and Peak Over Threshold methods. Furthermore, considering the importance of wave direction when an angle dependent structure or device has to be designed, the thesis addresses the problem of directional analysis, providing a criterion to classify storms as ñdirectional stormsò with wave direction pertaining to a given directional sector. The introduced methodology concerns also the identification of the appropriate center and width of the sector. Another analysis performed in the present work deals about the long term statistics of ocean storms starting from time series of partitioned sea states, considering separated wind and swell seas. The ETS model is applied for long term predictions to time series of significant*

*wave height calculated considering both contributions, and the wind sea only, in order to evaluate variability of return values due to having neglected swell contribution. Concerning the estimation of wave energy resource, in the thesis a simplified formula for the calculation of average wave power in deep water is applied for wave energy mapping of Mediterranean Sea in parallel to extreme values mapping, showing how the conjunction of these two information is fundamental at the design stage of wave energy device.*

*The thesis is made up by eight chapters. Each of them contains results that have been already published by the author and are proposed here in a more detailed version.*

# Chapter 1 ï Introduction to extreme values analysis of storm waves

*This chapter gives an overview on the methodologies for extreme values analysis of wave data. A classification of the various methods is provided. First the classical approaches are discussed, and then the short and the long-term statistics are introduced for extreme analysis and predictions of sea storm via the Equivalent Storm Models. Finally several kinds of wave data used for extreme wave analysis are discussed.*

## 1.1. Overview and classification of methods for extreme values analysis of wave data

Extreme values analysis of waves plays a significant role at the design stage of marine structures and wave energy converters. The use of an appropriate methodology in estimation of extreme wave condition is then a key point. A lack in the selection of the design wave involves an overdesigned structure, if the design wave is overestimated, making the investment unattractive from the economical point of view. Vice versa, an underestimated design wave may imply the failure of the structure. Extreme wave heights, also referred as *m-year* return values, are wave height that will occur in average once in a period of *m* years. In the selection of an extreme wave height, when designing for survivability, 100-yr return values are often used because of the low probability of occurrence associated with them. Wave energy converters are usually designed for a service life of 20-30 years, but return values of longer periods (50-100 yrs.) have to be considered in the evaluation of extreme conditions. Depending on the methodology employed in the selection of data sample from a given time series, may be distinguished two different approaches for extreme values analysis:

- Total Sample Method;
- Peak Value Method.

The former, called also Initial Distribution method or Cumulative Distribution function method, utilizes the whole available data of wave heights observed visually or instrumentally during a

number of years. It was proposed by *Draper (1966)* when wave observation projects were at their initial stage and wave data availability in terms of time of observation was limited. It is applicable even when time series are few years long. The latter consists in dividing time series in storms/time windows of a given duration and to pick up the largest wave height per each window. If the block has duration of one year and only the maximum wave height per each block is taken into account in the analysis, the method is called Annual Maxima. Instead, it if only storm peaks greater than a given threshold are considered it is called Peak Over Threshold (POT) *(Coles, 2001; Goda et al. 1994; Goda, 2000; Ferreira and Guedes Soares, 1998)*. An alternative approach that may be considered belonging to the category of Peak Values Method is based on the Equivalent Storm Models *(Boccotti 1986, 2000; Arena and Pavone, 2006, 2009; Fedele and Arena 2010)*. These models utilize the geometric representation of storms replacing actual storm with a statistically equivalent one characterized by a simpler geometric shape. Starting from a given time series storms are identified by means of a sea storm definition *(Boccotti 1986, 2000)* and each of them is replaced with the equivalent one. The equivalent storm is determined by means of two parameters: the first representative of storm intensity and equalled to the maximum significant wave height in the actual storm, the latter representative of storm duration, calculated by imposing the equality between the maximum expected wave heights of actual and equivalent storms. The sequence of actual storms is the actual sea, while the sequence of equivalent storms represents the "Equivalent Sea". The actual and equivalent seas are characterized by same number of storms, each of them with the same maximum $H_s$. As a consequence the return period of a storm whose maximum $H_s$ is greater than a fixed threshold $h$ is the same in the actual sea and in the equivalent sea. This approach has been introduced by *Boccotti (1986, 2000)* with the Equivalent Triangular Storm (ETS) model and then developed in a more general form by *Fedele and Arena (2010)* via the Equivalent Power Storm (EPS) model. In the case of ETS a triangular shape is considered, while with EPS storm history is given by a power law with $\lambda$ exponent ($\lambda$=1 gives linear law of $H_s(t)$ and triangular shape). For these models a solution for the calculation of the return period $R(H_s>h)$ of a storm whose maximum significant wave height is greater than a fixed threshold $h$, has been developed basing on the concept of "Equivalent Sea".

One important aspect in preparing a statistical sample is to satisfy the requisites of stochastic independence and homogeneity. Stochastic independence means that individual data has to be statistically independent of each other (correlation coefficient of successive data close to zero). Concerning homogeneity, it requires that individual data in a sample have a common parent

distribution, all belonging to a single group of data, which is called population. The choice of methodology must be done taking into account the above conditions. Total Sample method is very easy to be used, but violates the stochastic independence between individual data. In fact, regularly recorded wave data are mutually correlated with a correlation coefficient remaining over 0.3 – 0.5 for a time lag of 24 hours *(Goda, 1979)*. The Peak Value Method category satisfies the condition of stochastic independence. The Annual Maxima to be applied requires the availability of time series of several decades long to have enough points for curve fitting. In fact, a small size of the sample involves a large confidence interval and low reliability in a statistical sense. For these reasons the recommended approaches are Peak Over Threshold and Equivalent Storm Models, which are the ones used herein. It is worth mentioning that POT and equivalent storm models have some analogies in sample selection, but are quite different approaches. Applying POT data are analysed in a form of cumulative distribution to be fitted by several distribution functions. Once the function that gives the best fit of the data is selected, return values are determined by extrapolating the distribution function at the level of probability corresponding to the given period of years, considered in the design process. In the case of equivalent storm models, return values are calculated by means of the return period $R(H_s>h)$. It is based on the concept of Equivalent Sea and depends upon two functions: significant wave height distribution and a base-height regression $\bar{b}(a)$ which gives the relationship between parameters of intensity $a$ and duration $b$ of equivalent storms. In this way return values are not determined directly from data fitting and because of that are more accurate, especially if return period of 50-100 yrs. are considered. In following sections POT, ETS and EPS models will be treated.

## 1.2 Peak Over Threshold method

The Peak Over Threshold method is a statistical approach utilized for extreme wave analysis that uses only the maxima of wave height in time series data. The sample of the maxima is selected by dividing time series into storms of given duration $\Delta t$ and by taking into account only the storm maxima above a fixed threshold $h_{crit}$. The choice of the duration $\Delta t$ and of the threshold $h_{crit}$ plays a significant role on the predicted wave height *(Coles 2001)*. In order to perform a correct analysis individual data point need to be statistically independent of each other and because of that $\Delta t$ it needs to be adequately large (in general a $\Delta t$ from two to four days should be appropriate) *(Mathiesen et al 1994, Coles 2001)*. Furthermore the POT is threshold dependent and then $h_{crit}$ needs to be chosen carefully because the assumption of different $h_{crit}$ may produce significant differences on the predicted wave heights *(Neelamani*

*2009)*. Once the sample has been selected two parameters are important for the analysis: the average number of event/year *l* and the total number *N* of events involved in the analysis. Then by arranging data in a descending order the probability of exceedance *P*(*m*) of the *mth* order may be calculated by means of one of the plotting position formulas given in literature *(Goda 2000)*. The best known position formula is the Weibull formula:

$$P(m) = \frac{m}{N+1} \tag{1.1}$$

where *m* is the order number. Then the theoretical distribution of best fit has to be identified. The candidate functions often employed are *(Goda, 2000)*:

1) Gumbel distribution

$$F(h) = 1 - \exp\left[-\exp\left(-\frac{h-B}{A}\right)\right] \qquad -\infty < h < \infty \tag{1.2}$$

2) Frechèt distribution

$$F(h) = 1 - \exp\left[-\left(1+\frac{h-B}{kA}\right)^{-k}\right] \qquad B - kA \le h < \infty \tag{1.3}$$

3) Weibull distribution

$$F(h) = 1 - \exp\left[-\left(\frac{h-B}{A}\right)^{k}\right] \qquad B \le h < \infty \tag{1.4}$$

4) Lognormal distribution

$$f(h) = \frac{1}{\sqrt{2\pi}Ah} - \exp\left[-\frac{(\ln h - B)^2}{2A^2}\right] \qquad 0 < h < \infty \tag{1.5}$$

Where *F*(*h*) and *f*(*h*) denote the cumulative distribution and probability density function respectively.

These functions have two or three parameters. Parameter *A* is called the scale parameter because it governs the linear scale of *h*, *B* is the location parameter because it fixes the location of the axis of *h* and *k* is the shape parameter because it determines the functional shape of distribution. The parameter k is dimensionless, while *A* and *B* have the same dimension of *h* except for lognormal distribution. There are several methods of fitting a theoretical distribution function to a sample of extreme data and estimating the parameters values. The most common are:

1) graphical fitting method;
2) least square method;
3) method of moments;
4) maximum likelihood method.

Both the graphical fitting method and the least square method require the representation of data in the probabilistic paper of the considered distribution in the way that the distribution may be represented by a straight line. In the first case the line is drawn by visual judgment, while the least square method enables an objective comparison of the goodness of fit. With the method of moments parameters are determined by calculating mean and standard deviation of the sample and equating them to the characteristics of the distributions which are tabled. The maximum likelihood method is another approach to estimate parameters distribution. It is applied by means of likelihood function. The searched parameters are those that maximize the mentioned function *(See Goda 2000)*.

The relationship between probability of exceedance *P* and the return period *R* is given by:

$$P = \frac{1}{lR} \tag{1.6}$$

Follows that and considering the Weibull distribution the return values of wave height $h(R)$ for a given return period *R* may be calculated as:

$$h(R) = B + A\left[\ln(lR)\right]^{1/k} \tag{1.7}$$

It is worth noting that the same procedure followed to apply POT may be used in the case of Annual Maxima, simply by considering the time interval $\Delta t$ of one year and the threshold $h_{crit}$ equal to zero.

## 1.3 Sea waves at different time scale: short and long term statistics

The sea surface elevation is a non-stationary stochastic process which is studied as a series of stationary Gaussian processes describing the sea-state in short periods. During each of these short periods, the sea surface elevation process is completely characterized by a spectral function and is summarized by spectral parameters such as the significant wave height, $H_s$, the common indicator of sea-state severity, the peak period $T_p$, and the dominant wave direction. In this context, a sea state is a sequence of a few hundred of waves. The number of waves has to be sufficiently large to well represent statistical properties of sea condition and enough small to have quasi-stationary conditions (usually 100-300 waves). A sea storm is defined as a sequence of sea states during which the significant wave height $H_s$ is above a certain threshold $h_{crit}$ and does not fall below it for a certain time interval *(Boccotti 1986, 2000)*. Commonly, the time interval is assumed 12 hours, while the threshold $h_{crit}$ is related to the average significant wave height $\overline{H}_s$ at the given location. Thus, it depends on the characteristics of the recorded sea states at the considered site. Boccotti proposed a value of the threshold $h_{crit}$ equal to $1.5\,\overline{H}_s$.

### *1.3.1 Statistical properties of waves in a sea state: probability distribution of crest-to-trough wave height*

The statistical distribution of crest-trough wave height has been determined by considering that the free surface to a first order in a Stokes expansion is a random Gaussian process of time. *Longuet-Higgins (1952)* obtained that the crest-to-trough heights have a Rayleigh distribution, for an infinitely narrow spectrum; therefore the probability that a wave has crest-to-trough height greater than $H$, in a sea state with significant wave height $H_s = h$ (being $H_s \equiv 4\sigma$, where $\sigma$ is the standard deviation of the surface displacement) is:

$$P(H; H_s = h) = \exp\left[-2\left(\frac{H}{h}\right)^2\right] \tag{1.8}$$

Later, both field data and numerical simulation *(Earle, 1975; Haring et al., 1976; Forristall, 1978; Boccotti, 1989; Arena, 1999; Prevosto et al. 2000)* showed that Rayleigh distribution

overestimates the wave height. This overestimation is a consequence of the finite spectral bandwidth *(Longuet-Higgins, 1980; Boccotti, 1982; Forristall, 1984)*. The general form of the probability of exceedance for finite bandwidth was obtained analytically by *Boccotti (1981, 1989, 1997, 2000)* as a corollary of the quasi-determinism theory. It is given by:

$$P(H;H_s=h)=\exp\left[-\frac{4}{1+\psi^*}\left(\frac{H}{h}\right)^2\right] \tag{1.9}$$

where $\gamma^*$ is a narrow bandedness parameter of the spectrum, defined as the absolute value of the quotient between the absolute minimum $\gamma(T^*)$ and the absolute maximum $\gamma(0)$ of the autocovariance of the surface displacements. The parameter is equal to 1 for an infinitely narrow spectrum [in this condition, Equation (1.9) gives the Rayleigh distribution (1.8)] and tends to 0 as the bandwidth grows. Some characteristic values are $\gamma^*$ = 0.73 for a mean JONSWAP spectrum *(Hasselmann et al., 1973)* and $\gamma^*$ = 0.65 for a Pierson-Moskowitz spectrum *(Pierson and Moskowitz, 1964)*. Equation (1.9) was derived analytically in the limit as $H / h \to \infty$. Field data showed that it well fits the height data for $H / h > 0.8 \div 1$ *(Boccotti, 1989, 2000)*.

### *1.3.2 Long term variability of $H_s$: significant wave height distribution*

The long term variability of the significant wave height describes the wave climate at a given site. Several models have been proposed to represent this variability, especially for the estimation of extreme values. The most used distributions have been the Log-normal *(Jaspers, 1956)* and the Weibull *(Battjes, 1971; Guedes Soares and Henriques, 1996, Boccotti 1986, 2000)*. A part from these other models have been considered, such as a mixture of Log-normal and Weibull distributions *(Haver, 1985)*, the Generalized Gamma distribution *(Ochi, 1992)*, or the Beta distributions *(Ferreira and Guedes Soares, 1999)*. Here in the three-parameters Weibull distribution is considered:

$$P(H_s>h)=\exp\left[-\left(\frac{h-h_l}{w}\right)^u\right] \qquad \text{defined for } H_s>h_l \tag{1.10}$$

The parameters of the distribution (1.10) are estimated by applying an iterative procedure *(see Goda, 1999)*: for fixed values of the shape parameter, the values of $h_l$ and $w$ are evaluated by applying the least square method. We choose the value of $u$ and consequently the values of $h_l$

and $w$ which maximizes the correlation coefficient between the sample data and the estimate distribution (the closer the correlation coefficient is to 1 the better the fitting). If the parameter $h_l$ is equal to zero the two parameter Weibull distribution is considered which is achieved from Equation (1.10) with $h_l$=0.

For the directional long term distribution of $H_s$, *Boccotti (2000)* proposed an asymptotic law to fit the directional extreme significant wave heights. Specifically, he proposed to describe such a probability as a difference between two Weibull distributions. That is,

$$P(H_s > h;\Delta\vartheta) = \exp\left[-\left(\frac{h-h_l}{w_\alpha}\right)^u\right] - \exp\left[-\left(\frac{h-h_l}{w_\beta}\right)^u\right] \tag{1.11}$$

In Equation (1.11) $u$ is the shape parameter pertaining to Equation (1.10) and the parameters $w_\alpha$ and $w_\beta$ depend on the sector $\Delta\vartheta$. Parameters $w_\alpha$ and $w_\beta$, are positive with $w_\beta < w_\alpha \leq w$, where $w$ is the scale parameter pertaining to Equation (1.10).

### *1.3.3 Statistical properties of waves in a sea storm*

Statistical properties of waves during storms were investigated by *Borgman (1970, 1973)*, who obtained the probability of exceedance of the maximum wave height during a sea storm $P(H_{\max} > H)$. By representing a sea storm as a sequence of $N_s$ sea states, we have

$$P(H_{\max} > H) = 1 - \prod_{i=1}^{N_s} \left[1 - P(H; H_s = h_i)\right]^{D_t / \overline{T}(h_i)} \tag{1.12}$$

where the $i^{\text{th}}$ sea state has the significant wave height $H_s = h_i$, the mean zero up-crossing wave period $\overline{T}(h_i)$, and the duration $D_t$. Following Borgman, Equation. (1.12) may be rewritten in the integral form as

$$P(H_{\max} > H) = 1 - \exp\left\{\int_0^D \frac{\ln\left[1 - P\left(H; H_s = h(t)\right)\right]}{\overline{T}[h(t)]} \mathrm{d}t\right\} \tag{1.13}$$

where $D$ is the storm duration. Finally, the maximum expected wave height $\overline{H_{\max}}$ during the sea storm is obtained as the integral over $(0,\infty)$ of the probability of exceedance $P(H_{\max} > H)$ given by Equation (1.13):

$$\overline{H}_{\max} = \int_0^{\infty} 1 - \exp\left\{ \int_0^D \frac{\ln\left[1 - P\left(H; H_s = h(t)\right)\right]}{\overline{T}[h(t)]} \mathrm{d}t \right\} dH \tag{1.14}$$

## 1.4 Equivalent Storm Models

The equivalent storm models utilize the approach to extrapolate sea storms from time series of significant wave height and to associate to each actual storm a statistically equivalent one via the equivalent storm models, the knowledge of the storms sequence together with the probability distribution of significant wave height at a given location enables to calculate return periods of storms with given characteristics.

### *1.4.1 Equivalent Triangular Storm (ETS) model*

The ETS model allows associating to each actual storm an equivalent triangular one by means of two parameters: the triangle height *a*, representing the storm intensity and the triangle base *b*, representative of the storm duration. The triangle height *a* is equal to the maximum significant wave height of the real storm (Figure 1.1), while the triangle base *b* is determined by following an iterative procedure imposing the equality between the maximum expected wave heights of the ETS *(Boccotti 1986, 2000)* and of the real storm (Equation 1.14). The sequence of ETSs obtained replacing each real storm with the related ETS is called "equivalent triangular sea". By relying on the concept of equivalent triangular sea, *Boccotti (1986, 2000)* developed an analytical solution for the return period $R(H_s>h)$ of a storm whose maximum significant wave height is greater than a fixed threshold $h$, and for the mean persistence $D_m(h)$ above $h$. The solution for $R(H_s>h)$ is given by the following equation:

$$R(H_s > h) = \frac{\bar{b}(h)}{hp(H_s = h) + P(H_s > h)} \tag{1.15}$$

where $\bar{b}(h)$ is the base-height regression for ETSs, $P(H_s>h)$ is the probability of exceedance of $H_s$ and $p(H_s=h)$ is the probability density function of the $H_s$ ($=-dP(H_s>h)/dh$).

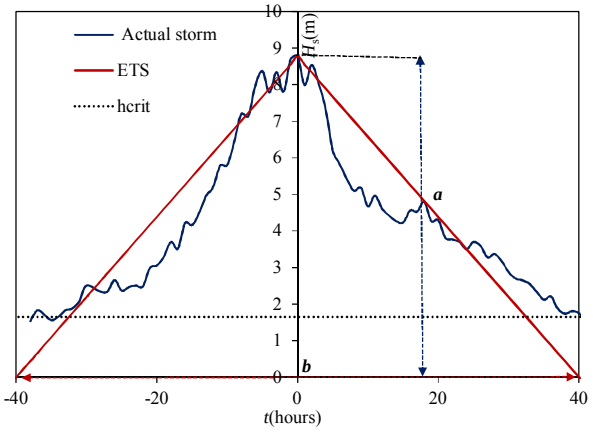


**Figure. 1.1 ï** Example of actual storm and associated ETS.

The function $\bar{b}(h)$ for Mediterranean Sea has the form of a linear regression as the following:

$$\bar{b}(h) = b_{10}(k_1 \frac{h}{a_{10}} + k_2) \tag{1.16}$$

where $a_{10}$ and $b_{10}$ are the average values of bases and heights respectively, of the $N=10n_{yrs}$ strongest storms ($n_{yrs}$ is the number of years of observation). Parameters $k_1$, $k_2$ are characteristics parameters of the location and are determined by representing all the couples $(a,b)$ in a Cartesian plot normalized respect to $a_{10}$ and $b_{10}$ and fitting the data by a linear law. In Oceans an exponential law *(see Boccotti, 2000; Arena and Barbaro, 1999)* as the following is considered:

$$\bar{b}(h) = b_{10}k_1 \exp\left(k_2 \frac{h}{a_{10}}\right) \tag{1.17}$$

The mean persistence $D_m(h)$ is the average time interval during which $H_s$ is above $h$ in the storms exceeding the threshold $h$. It may be calculated as the ratio between the total time interval in which $H_s>h$, during an appropriately large time interval $\tau$ and the number of storm during $\tau$ with maximum significant wave height greater than $h$:

$$D_m(h) = \frac{\tau P(H_s > h)}{\tau / R(H_s > h)} \tag{1.18}$$

Considering the three-parameter Weibull distribution (1.10), Equations (1.15) and (1.18) may be rewritten as:

$$R(H_s > h) = \frac{\bar{b}(h)}{1 + u\frac{h}{w^u}\left(\frac{h - h_l}{w}\right)^{u-1}} \exp\left[\left(\frac{h - h_l}{w}\right)^u\right] \tag{1.19}$$

$$D_m(h) = \frac{\bar{b}(h)}{1 + u\frac{h}{w^u}\left(\frac{h - h_l}{w}\right)^{u-1}} \tag{1.20}$$

Along the same line of Boccotti (2000), *Arena, et al. (2013)* derived the "directional" return period $R(H_s>h;\Delta\boldsymbol{\theta})$. That is, the return period of a sea storm in which the maximum significant wave height exceeds a fixed threshold, $h$, and the dominant wave direction belongs to a given sector $\Delta\boldsymbol{\theta}$. Specifically, they showed that, in this context, Equation (1.15) holds if $p(H_s=h)$ and $P(H_s>h)$ are replaced by, respectively, $p(H_s=h;\Delta\boldsymbol{\theta})$ and $P(H_s>h;\Delta\boldsymbol{\theta})$. Thus, by adopting the directional probability distribution given by Equation (1.11), the following equation is derived:

$$R(H_s > h;\Delta\theta) = \frac{\bar{b}(h)}{\exp\left[-\left(\frac{h - h_l}{w_\alpha}\right)^u\right]\left[1 + u\frac{h}{w_\alpha^u}\left(\frac{h - h_l}{w_\alpha}\right)^{u-1}\right] - \exp\left[-\left(\frac{h - h_l}{w_\beta}\right)^u\right]\left[1 + u\frac{h}{w_\beta^u}\left(\frac{h - h_l}{w_\beta}\right)^{u-1}\right]} \tag{1.21}$$

This solution is based on the assumption that the dominant wave direction of a sea storm, at the apex phase of its development, is constant and that the base-height regression $\bar{b}(h)$ is not dependent on the dominant direction.

### *1.4.2 Equivalent Power Storm (EPS) model*

The Equivalent Power Storm model by *Fedele and Arena (2010)* generalized the concept of triangular storm: the significant wave height in time domain, during a storm, is represented with a $\lambda$ power law ($\lambda$>0), as:

$$H_s(t) = a\left[1 - (2|t|/b_\lambda)^\lambda\right] \tag{1.22}$$

where the peak of the storm (equal to $a$) occurs at $t$=0 (see Figure 1.2). Note that $H_s(t)$ in Equation (1.22) is defined for $-b/2 \le t \le b/2$. For a given value of $\boldsymbol{\theta}$, the EPS is defined by

means of the height $a$ and the base $b_\lambda$ which are achieved as for the ETS. The maximum expected wave height in a power storm with height $a$ and base $b_\lambda$, is:

$$\overline{H_{\max}}(a,b_\lambda)=\int_0^\infty 1-\exp\left\{\frac{b}{\lambda a}\int_0^a \frac{\ln\{1-P(H\mid H_s=h)\}}{\bar{T}(h)}\left(1-\frac{h}{a}\right)^{1/\lambda-1}dh\right\}\mathrm{d}H. \tag{1.23}$$

The EPS model was introduced to give a better representation of the storms, and for the extreme values of wave heights (Fedele and Arena, 2010). They showed that the EPS model has a good stability for λ>0.7. Furthermore, the value of λ characterizes the storm: we have a parabolic storm for λ=2, a cubic storm for λ=3, a cusp-storm for λ=0.5 and so on (Figure 1.2). For λ=1 we have triangular storms. The authors showed that the optimal value λ, for the modelling of extreme sea storms, is 0.75; finally they determined $R(H_s>h)$ by considering the EPS model.

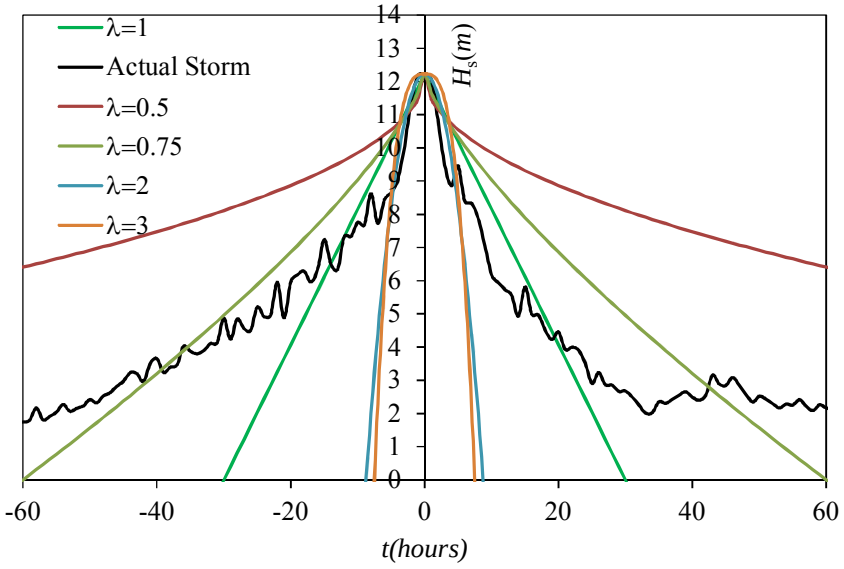


**Figure. 1.2 ï** Example of actual storm and associated EPSs ($\lambda$=0.5, 0.75, 1, 2, 3).

It is given by the equation

$$R(H_s>h)=\frac{1}{\int_h^\infty \frac{a}{\bar{b}(a)}G(\lambda,a)da} \tag{1.24}$$

where $\bar{b}(a)$ is the mean base-height regression, which relates the mean value of duration $b$ to the intensity $a$ of the EPSs and $G(\lambda,a)$ is a function related to the probability density function of

the EPS intensities. The expression of $\bar{b}(a)$ is derived from strictly empirical arguments, as it is highly dependent on the location under examination. Analysis of several data has shown that the mean base-height regression formula in the form of an exponential law (see previous section) provides a good estimation of $R(H_s>h)$. The function $G(\lambda,a)$ is defined as:

$$G(\lambda,a)=\begin{cases}\dfrac{\sin(\pi/\lambda)}{\pi/\lambda}\displaystyle\int_1^{\infty}\left.\frac{d^2P(H_s>z)}{dz^2}\right|_{a,x}(x-a)^{-1/\lambda}dx \\ if \quad \lambda>1; \\ \dfrac{d^2P(H_s>a)}{da^2} \qquad\qquad if \quad \lambda=1; \\ \dfrac{(-1)^n a^n}{n!}\dfrac{\sin(\pi\mu)}{\pi\mu}\displaystyle\int_1^{\infty}\left.\frac{d^{n+2}P(H_s>z)}{dz^{n+2}}\right|_{a,x}(x-1)^{-\mu}dx \\ if \quad \lambda=(n+\mu)^{-1}<1.\end{cases} \tag{1.25}$$

## 1.5. Wave data sources

Several data sources are used as input for extreme wave analysis. They may be classified in:

- instrumentally measured data;
- visually observed data;
- hindcasted data;
- forecasted data.

Instrumentally measured data are the best source, provided that they cover a sufficiently long time span and the downtime is kept minimum. Hindcasted data of storm waves are the second best source, provided that the wave hindcasting method has been well calibrated with several storm wave records in the area of interest. Wave forecasting has been carried out in recent years by meteorological agencies of many countries. The data bank accumulated trough this work has proved to provide a good source of extreme wave data in the near future. However, the accuracy of wave height information would be inferior to instrumental records and hindcasted wave data, because wave forecasting is made on uncertain weather condition forecasted in advance. There are two types of visually observed data: one is the observation made at a fixed station at regular interval, the other is a compilation of ship report data, which

are presented in a form of joint distribution of wave heights and periods. Visual observation data should be used as the last recourse, because the accuracy of individual data is low. In the analyses proposed in the thesis only two of the above typologies are used: buoys data from both NOAA-NDBC (National Oceanic and Atmospheric Administration's – National Data Buoy Center, USA) and Italian buoys network (RON – Rete Ondametrica Nazionale - managed by ISPRA), and hindcasted data from HIPOCAS project *(Guedes Soares et al., 2002; Pilar et al., 2008)*, from HOMERE database *(Boudiere et al., 2013)*, and from wave simulation in Mediterranean Sea (ENEA). The NOAA manages the NDBC, which consists of many buoys moored along the US coasts, both in the Pacific Ocean and in the Atlantic Ocean. Some buoys were moored in the late 1970s, so that more than 35 years of data are available. The historical wave data give hourly significant wave height, peak and mean period. Only few buoys are directional. The Italian buoys network (RON) started measurements in 1989, with 8 directional buoys located off the coasts of Italy. Currently, the network consists of 15 buoys, moored in deep water. RON buoys give up to two records per hour; for each record, the data of significant wave height, peak and mean period and dominant direction are given. The HIPOCAS project (Hindcast of Dynamic processes of the Ocean and Coastal Areas of Europe) provided a simulation of 44-years (1958-2001) wind, waves, sea level data and current climatology. The hindcast wave model used in HIPOCAS is the third generation wave model WAM cycle 4 modified for two-way nesting by *Gòmez* and *Carretero (1997)*, which gives the following output parameters: significant wave height $H_s$, wave direction, mean period $T_m$, peak period $T_p$ with a time step of three hours. HOMERE is a sea-states hindcast database, based on WAVEWATCH III model (version 4.09) on a unstructured grid covering the English Channel and Bay of Biscay (NGUG) over 1994-2012 period (19 years). The data set includes 37 global parameters and the frequency spectra on a very high resolution grid (~110 000 points) as well as directional spectra on a high resolution grid (4096 points), with a one hour time step. Wave simulations in Mediterranean Sea have been performed using a parallel version of WAM wave model Cycle 4.5.3 *(Günther and Behrens, 2011)*. WAM is a third generation spectral wave model, largely used in wave forecasting systems, that solves the spectral energy balance equation without any a priori assumption on the spectral shape. The model domain used covers the entire Mediterranean Sea from 5.50°W to 36.126°E of longitude and has been discretized with a regular grid in spherical coordinates at the uniform resolution of 1/16° in each direction. The resulting grid cell has a size of about 5-7 Km. Model bathymetry has been derived from the General Bathymetric Chart of the Oceans (GEBCO) 30 arc-second gridded data set (GEBCO) by averaging the depths of data points falling in each computational cell. The directional wave

energy spectrum has been discretized using 36 directional bins and 32 frequencies starting from 0.06 Hz and increasing with relative size increment of 0.1 to a final frequency of 1.15. The climatology has been produced for the period 2001-2010 using as surface forcing for the model six-hourly wind analysis fields produced operatively by ECMWF at ¼° spatial resolution. The main wave parameters, including significant wave height ($H_s$), wave direction ($\boldsymbol{d}_m$) and mean period ($T_m$) have been estimated every 3 hours for all points in the domain.

THIS PAGE INTENTIONALLY LEFT BLANK

# Chapter 2 ï A new approach for long-term statistics of ocean waves: the Equivalent Exponential Storm (EES) model

*The idea to represent the time history of an ocean storm with a triangular shape was introduced by Boccotti (2000) in the equivalent triangular storm model.*

*The generalization to a general power law (equivalent power storm model) was achieved by Fedele and Arena (2010), and their work concluded that a storm should be represented with a power law with an exponent equal to 0.75.*

*Both models have been applied to derive, with an analytical approach, several solutions for the return period of severe storms (Boccotti, 2000; Arena and Pavone, 2006, 2009; Fedele and Arena, 2010).*

*In this chapter, a new equivalent exponential storm model is introduced to modeling sea storms with an exponential law to determine the long-term statistics of ocean waves. The expression of the return period of a sea storm in which the maximum significant wave height exceeds a given threshold is achieved in a closed form. Then, it is shown that the duration of the equivalent exponential storms well represents the duration of actual storms. Finally, comparisons with the previous models are given.*

## 2.1. Introduction

Stochastic modeling of significant wave height time series has allowed for the development of statistical methods that can predict extreme waves (*Krogstad*, 1985; *Boccotti*, 2000; *Prevosto et al.*, 2000). The various steps involved in the procedure to predict extreme wave heights such as data collection (time series of significant wave heights over many years), selection of the adequate distribution, and selection of the wave height corresponding to a given return period have been reviewed by *Isaacson and Mackenzie* (1981). Reviews of several such methods may also be found in *Goda* (1999). *Guedes Soares* (1989) proposed a method to combine information coming from different predictions in a single design value. If individual crest-to-trough wave heights or crest heights are modeled, one needs to combine the wave statistics

during the sea state (i.e., short-term statistics - *Rice*, 1944; *Boccotti*, 2000; *Forristall*, 2000; *Fedele and Arena*, 2005) with the distribution of significant wave heights at a given location (long-term statistics). In this context, a storm is a non-stationary process defined as a sequence of sea states with a significant wave height greater than a fixed threshold. Each of them is considered as a homogeneous and stationary process that is fully defined by knowledge of the directional spectrum of the sea surface and the associated moments. Starting from a significant wave height time series, *Boccotti* (1986, 2000) introduced the concept of the equivalent triangular sea, which involves substituting the sequence of actual storms extrapolated from the given time series with a sequence of equivalent storms having a triangular shape; this is called the equivalent triangular storm (ETS). The ETS associated with a given storm is defined by two parameters: one gives the storm intensity and the other the storm duration. Once the actual storm time history is known, the intensity parameter can be equated to the maximum significant wave height in the actual storm and the duration can be achieved by an iterative procedure through imposing equality between the maximum expected wave height of the actual storm (*Borgman* 1970, 1973) and the equivalent storm (*Boccotti*, 2000). On the basis of the notion of the equivalent triangular sea, *Boccotti* (2000) developed a procedure to determine an analytical solution for the return period $R(H_s > h)$ of a sea storm in which the maximum significant wave height is greater than the fixed threshold *h*, and further for the return period $R(H)$ of a sea storm in which the maximum individual wave height exceeds the fixed threshold *H* (*Boccotti* 1986, 2000; *Arena and Pavone*, 2006). *Arena and Pavone* (2009) determined the analytical solution of the return periods $R_N$ and $R_{\geq N}$ of a sea storm in which *N* or at least *N* waves higher than a fixed threshold occur. Recently, *Fedele and Arena* (2010) (see also *Arena et al.*, 2014) proposed the equivalent power storm (EPS), a generalization of Boccotti's ETS model that includes different shapes for equivalent storms characterized by a more realistic description of the significant wave heights in the temporal history; specifically, a generic storm is described by a power law with $\lambda$ exponent (if $\lambda = 1$, we have the ETS model). The EPS model was exploited to choose the best value of $\lambda$ (which is also a shape parameter) that best fits the maximum wave height distribution of the actual storm. The searched value proved to be equal to 0.75, and the predictions were slightly more conservative than those of the ETS model. Note that the EPS model does not use a closed form solution for $R(H_s > h)$. The equivalent exponential storm model presented here aims to introduce a model that is based on the same principles of the previous ones, but which is able to combine together the benefits of both the two previous

models, i.e., predictions close to the those obtained by the EPS model with $\lambda = 0.75$ and a closed form solution for $R(H_s > h)$.

## 2.2. Equivalent Exponential Storm (EES) model

A sea storm is a non-stationary process where the significant wave height varies randomly in the time domain. Here, the equivalent exponential storm (EES) model is introduced, which represents the storm history of any actual storm as an EES whose significant wave height *h* varies in time *t* according to an exponential law, as follows:

$$h(t) = a\exp(-\alpha|t|) \tag{2.1}$$

where $\alpha$ is a shape parameter. We impose that

$$\begin{cases} h(t=0) = a \\ \\ h(t = \pm b_E / 2) = h_{crit} \end{cases} \tag{2.2}$$

where *a* represents the storm intensity and is equal to the maximum significant wave height during the actual storm and $b_E$ is the time interval in which *h* is above the storm threshold $h_{crit}$.

From Equation (2.2) it follows that

$$h_{crit} = a\exp(-\alpha\, b_E / 2)\,, \tag{2.3}$$

and then it is possible to express the shape parameter $\alpha$ as a function of $h_{crit}$ and $b_E$:

$$\alpha = -\frac{2}{b_E}\ln(h_{crit} / a)\,. \tag{2.4}$$

By means of the above expression, Equation (2.1) may be rewritten as

$$h(t) = a\exp\left[\frac{2}{b_E}\ln(h_{crit} / a)|t|\right]. \tag{2.5}$$

We may conclude that an EES is defined by means of two parameters:

- the storm intensity *a*, which is equal to the maximum significant wave height during the actual storm;
- the storm duration $b_E$, which is such that the maximum expected wave height is the same in the EES and in the actual storm.

Parameter *a* is achieved directly from the storm history, while parameter $b_E$ is determined by following an iterative procedure.

Let us consider an EES with intensity *a* and duration $b_E^{'}$. The maximum expected wave height will be given by

$$\overline{H_{\max}}(a,b_E^{'}) = \int_0^{\infty} 1 - \exp\left\{ -\frac{b_E^{'}}{\ln(h_{crit}/a))} \int_{h_{crit}}^{a} \frac{\ln\left[1 - P(H;H_s = h)\right]}{\overline{T}(h)} \frac{1}{h} \mathrm{d}h \right\} \mathrm{d}H \,. \qquad (2.6)$$

Where $P(H;H_s = h)$ is the crest to trough wave height distribution (1.9). To determine the EES duration $b_E$, first the maximum expected wave height in the actual storm $\overline{H_{\max}}$ has to be calculated by means of Borgman Equation (1.14). Then starting from the obtained value of $\overline{H_{\max}}$, we fix the tentative value $b_E^{'}$. Next, if $\overline{H_{\max}}$ of the actual storm is greater than $\overline{H_{\max}}(a,b_E^{'})$, we have to fix a larger value for *b* (because $b_E > b_E^{'}$) and vice versa. We iterate in this way until the equality $\overline{H_{\max}} = \overline{H_{\max}}(a,b_E)$ will be satisfied.

Note that the base $b_E$ of the EES is slightly different with respect to the base definition given by *Boccotti* (2000) for the ETS and by *Fedele and Arena* (2010) for the EPS. This is because in previous definitions the storm base is referred to $H_s = 0$. For the EESs, because $H_s$ goes asymptotically to zero for increasing values of *t*, the base $b_E$ is determined for $H_s = h_{crit}$. In other words, $b_E$ represents the time in which $H_s$ is above $h_{crit}$ in the EES.

### 2.2.1. Distribution of storm peaks $p_A(a)$

The distribution of storm peaks $p_A(a)$ is determined by following the logic introduced by *Boccotti* (1986, 2000) for the ETS, that is by imposing the condition that the average time during which $H_s$ is above *h* is the same both in the actual sea and in the equivalent storm

sequence. Here, the sequence of EESs is considered, which is achieved by replacing each actual storm with an EES using the procedure described in the previous section. Let us consider a large time span $\tau$ ; the time in which $H_s > h$ during $\tau$ is

$$\tau P(H_s > h) \tag{2.7}$$

where $P(H_s > h)$ represents the probability of exceedance of the significant wave height at the given location. This time may be also given by

$$T_{EES}(h) = \int_{a=h}^{\infty} \int_{b_E=0}^{\infty} t_s(h, h_{crit}, a, b_E)\, \mathrm{d}N(a, b_E) \tag{2.8}$$

where $\mathrm{d}N(a, b_E)$ is the number of exponential equivalent storms with peak amplitude $A$ in $(a, a+\mathrm{d}a)$ and duration $B$ in $(b_E, b_E+\mathrm{d}b_E)$ during $\tau$ . More explicitly,

$$\mathrm{d}N(a, b_E) = N(\tau)\, p_A(a)\, p_{B|A}(b_E \mid a)\mathrm{d}b_E \mathrm{d}a \tag{2.9}$$

where $N(\tau)$ is the number of storms during $\tau$.

The time $t_s$ in which the significant wave height is above $h$ in the EES is given by

$$t_s(h, h_{crit}, a, b_E) = b_E \frac{\ln(h/a)}{\ln(h_{crit}/a)}. \tag{2.10}$$

It follows that

$$T_{EES}(h) = \int_{a=h}^{\infty} \int_{b_E=0}^{\infty} b_E \frac{\ln(h/a)}{\ln(h_{crit}/a)} N(\tau)\, p_A(a)\, p_{B|A}(b_E \mid a)\mathrm{d}b_E \mathrm{d}a\,, \tag{2.11}$$

and by considering Equation (2.7), we obtain

$$\tau\, P(H_s > h) = \int_{a=h}^{\infty} \overline{b_E}(a)\, N(\tau) \frac{1}{\ln(h_{crit}/a)}\, p_A(a) \ln(h/a) \mathrm{d}a \tag{2.12}$$

where

$$\overline{b_E}(a) = \int_{b_E=0}^{\infty} b_E \, p_{B|A}(b_E \mid a) \mathrm{d}b_E \, . \tag{2.13}$$

From Equation (2.12), by defining

$$G(a) = \overline{b_E}(a) \frac{N(\tau)}{\tau} \frac{p_A(a)}{\ln(h_{crit}/a)} \tag{2.14}$$

an integral Volterra equation of the first kind for $G$ is obtained as

$$P(H_s > h) = \int_{a=h}^{\infty} G(a) \ln(h/a) \mathrm{d}a \, . \tag{2.15}$$

The solution for $G$ proceeds by differentiating both members of Equation (2.15) twice with respect to $h$ and setting $h = a$:

$$G(a) = -\frac{dP(H_s > a)}{da} - a \frac{\mathrm{d}^2 P(H_s > a)}{\mathrm{d}a^2}, \tag{2.16}$$

and finally from Equation (2.14):

$$p_A(a) = -\frac{1}{\overline{b_E}(a)} \frac{\tau}{N(\tau)} \left( \frac{dP(H_s > a)}{da} + a \frac{\mathrm{d}^2 P(H_s > a)}{\mathrm{d}a^2} \right) \ln\left( \frac{h_{crit}}{a} \right). \tag{2.17}$$

Note that the probability density function $p_A(a)$ is achieved in a closed form as a function of the probability of exceedance of significant wave heights at the examined location. The logic followed is this section is similar to the original logic by *Boccotti* (1986, 2000), who obtained the $p_A(a)$ in a closed form, and to the logic of *Fedele and Arena* (2010), who derived it for the EPS without solving the integral in Equation (2.15), which requires a numerical calculation.

### 2.2.2. Return period $R(H_s>h)$ of a storm in which the maximum significant wave height exceeds the threshold $h$

The return period $R(H_s > h)$ of a sea storm where the maximum significant wave height exceeds $h$ is equal to the return period of an EES whose peak $A$ exceeds $h$. Thus,

$$R(H_s > h) = \frac{\tau}{N(\tau; A > h)} \tag{2.18}$$

where $\tau$ is a large time interval and

$$N(\tau; A > h) = \int_{a=h}^{\infty} \int_{b_E=0}^{\infty} \mathrm{d}N(a, b_E) = N(\tau) \int_{h}^{\infty} p_A(a)\mathrm{d}a \tag{2.19}$$

is the average number of EESs whose peak $A$ exceeds $h$ during $\tau$. It follows that

$$R(H_s > h) = \frac{1}{\int_{h}^{\infty} \frac{1}{\overline{b_E}(a)} \ln\left(\frac{h_{crit}}{a}\right) G(a)\mathrm{d}a} \tag{2.20}$$

where $G(a)$ is defined by Equation (2.16).

Because the convergence of the integral in Equation (2.20) is very quick and the function $\overline{b_E}(a)$ varies gradually, we may assume $\overline{b_E}(a)$ is constant in the integration domain and consider $\overline{b_E}(a) = \overline{b_E}(h)$. Then, by substituting expression (2.16) of $G(a)$ in Equation (2.20) follows that:

$$R(H_s > h) = \frac{\overline{b_E}(h)}{I_1 + I_2} \tag{2.21}$$

where

$$I_1 = -\int_{a=h}^{\infty} \ln\left(\frac{h_{crit}}{a}\right) \frac{dP(H_s > a)}{da} da \tag{2.22}$$

$$I_2 = -\int_{a=h}^{\infty} a \ln\left(\frac{h_{crit}}{a}\right) \frac{d^2P(H_s > a)}{da^2} da \tag{2.23}$$

Finally, by integrating per parts $I_2$ and taking into account that:

$$\lim_{a \to \infty} P(H_s > a) = 0 \tag{2.24}$$

$$\lim_{a\to\infty} ap(H_s = a) = 0 \tag{2.25}$$

it follows that

$$I_1 + I_2 = -h\ln\left(\frac{h_{crit}}{h}\right)p(H_s = h) + P(H_s > h) \tag{2.26}$$

Then, the $R(H_s > h)$ is obtained in a closed form:

$$R(H_s > h) = \frac{\overline{b_E}(h)}{-h\ln\left(\frac{h_{crit}}{h}\right)p(H_s = h) + P(H_s > h)} \tag{2.27}$$

where $p(H_s = h) = -\frac{dP(H_s > h)}{dh}$ is the probability density function of the significant wave height $H_s$. Assuming that the significant wave height is distributed as a lower-bounded three parameter Weibull distribution (1.10), the following expression is obtained:

$$R(H_s > h) = \frac{\overline{b_E}(h)}{-hu\frac{(h-h_l)^{u-1}}{w^u}\ln\left(\frac{h_{crit}}{h}\right)+1}\exp\left[\left(\frac{h-h_l}{w}\right)^u\right] \tag{2.28}$$

where the parameters $(h_l, u, w)$ characterize the significant wave height distribution at the examined location.

### 2.2.3. Base-heights regression for EESs

In the previous sections, it has been shown that each EES is represented by two parameters: the height *a* and the base *b*. Furthermore, it has been shown that, starting from the equivalent sea, which is achieved by substituting an EES for each actual storm, the expression of the return period $R(H_s > h)$ is given by Equation (2.28). Its expression depends upon function $\overline{b_E}(h)$, which represents the average base of the EESs with height *h*. To determine this function, a set of *N* storms in the given location must be analyzed by determining *N* values of ( $a_i, b_{E_i}$ ) with *i* = 1,..*N* for the corresponding EES. Then, function $\overline{b_E}(h)$ is achieved by considering a well

defined law to describe the regression of the ( $a_i, b_{E_i}$ ) dataset. In this paper (see Applications), a linear regression will be considered for the EESs, which is given by

$$\overline{b_E}(a) = k_1 a + k_2 \tag{2.29}$$

where ( $k_1, k_2$ ) are characteristic parameters of the location.

## 2.3. Data analysis

Data of three buoys from the National Oceanic and Atmospheric Administration's National Data Buoys Center (NOAA-NDBC), which were obtained off the U.S. coast, have been processed (Figure 2.1). The buoys used include buoy 42001 in the Gulf of Mexico, buoy 46042 in North Pacific Ocean, and buoy 46001 in the Gulf of Alaska. The analysis was carried out with the significant wave height time series.

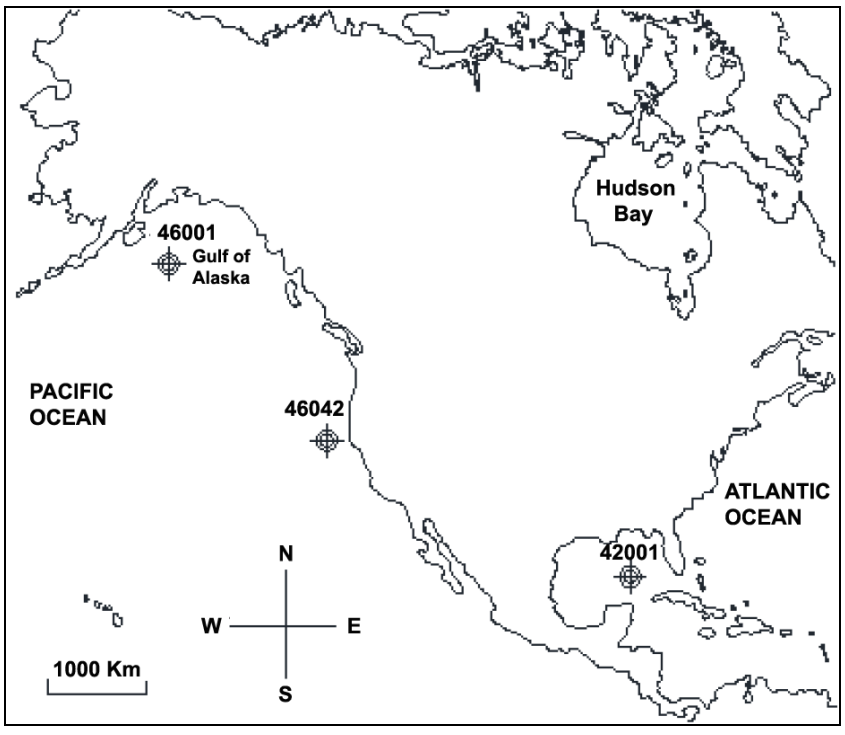


**Figure. 2.1 ï** Locations of the analyzed buoys from the National Oceanic and Atmospheric Administration's National Data Buoys Center (NOAA-NDBC) (USA).

First, the average value of significant wave height $\overline{H_s}$ was calculated (Table 2.1) and the storm threshold $h_{crit}$ was fixed equal to 1.5 times the $\overline{H_s}$. Then, all storms in the dataset were identified and analyzed by means of the ETS, EPS (with λ = 0.75), and EES models. Figure 2.2 shows the strongest storm recorded at buoy 46042.

| Buoy | Available data | $H_{s\max}$ [m] | $\overline{H_s}$ [m] | $h_{crit}$ [m] |
|---|---|---|---|---|
| 42001 | 08-13-1975/12-31-2012 | 11.20 | 1.1 | 1.7 |
| 46042 | 06-17-1987/12-31-2012 | 9.92 | 2.2 | 3.3 |
| 46001 | 10-01-1972/12-31-2012 | 14.8 | 2.7 | 4.1 |

**Table. 2.1 ï** Maximum and average significant wave heights and storm thresholds $h_{crit}$.

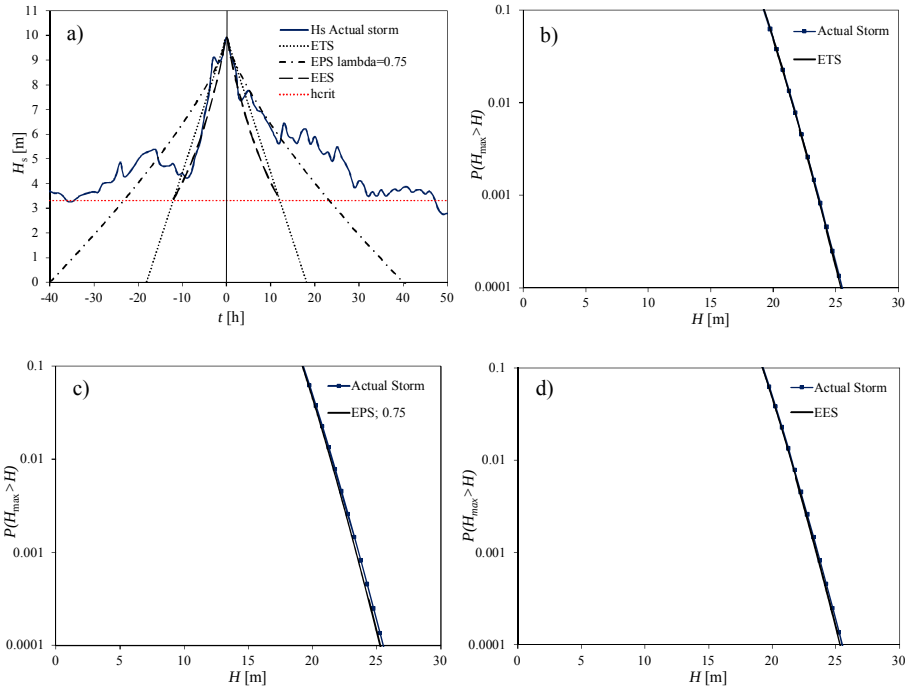


**Figure. 2.2**– (a) Strongest actual storm at the 46042 buoy and associated equivalent triangular storm (ETS), equivalent power storm (EPS) ($\lambda = 0.75$), and equivalent exponential storm (EES). Comparisons of the probability of exceedances for the maximum wave height calculated for the actual storm and for (b) ETS, (c) EPS with $\lambda = 0.75$, and (c) EES.

### 2.3.1. Correlation between intensity and duration of actual and equivalent seas (ETS, EPS, EES) and the base-height regression $b_E(a)$

In this section, the correlations between the intensities and durations of both actual storms and equivalent storms (ETSs, EPSs, EESs) are investigated. The results show that for the ETSs and EPSs the correlation coefficients between storm parameters *a* and *b* are small and negative (in agreement with the results of *Arena and Pavone*, 2006, for the ETSs): these values ranged between -0.281 and -0.154 for the ETSs and between -0.286 and -0.160 for the EPSs (see Table 2.2).

For the EESs, the correlations coefficients between $a$ and $b_E$ were positive and larger (in terms of the absolute value), and the values ranged between 0.432 and 0.551.

In addition, the correlation coefficients between the duration $D$ of actual storms and the intensity of storms $a$ were investigated, where the duration $D$ is defined as the time in which the significant wave height stays above the storm threshold $h_{crit}$: the values ranged between 0.604 and 0.673 (see Table 2.2). Note that only storms with durations $D \geq 12$ hours were considered in the analysis.

| | ETS | | EPS | | EES | | Actual storms |
|---|---|---|---|---|---|---|---|
| Buoy | $\rho_{a,b}$ | $\rho_{b,D}$ | $\rho_{a,b}$ | $\rho_{b,D}$ | $\rho_{a,b_E}$ | $\rho_{b_E,D}$ | $\rho_{a,D}$ |
| 42001 | -0.154 | 0.216 | -0.160 | 0.210 | 0.551 | 0.652 | 0.604 |
| 46042 | -0.281 | 0.114 | -0.286 | 0.108 | 0.495 | 0.640 | 0.673 |
| 46001 | -0.263 | 0.095 | -0.267 | 0.090 | 0.432 | 0.549 | 0.661 |

**Table. 2.2** – Correlation coefficients between parameters *a* and *b* and between *b* and duration *D* for actual storms and ETSs, EPSs ($\lambda = 0.75$), and EESs; the coefficients of correlation between *a* and duration *D* for actual storms (storms with duration $D \geq 12$ hours have been considered).

The result is that while for the ETS and for the EPS we could assume bases $b$ independent from storm intensity $a$ (*Arena and Pavone*, 2006), for the EESs we should consider function $\overline{b_E}(a)$. Figure 2.3 shows the plots $(a, b_E)$ for each storm and the resulting linear regression $\overline{b_E}(a)$ given by Equation (2.29) whose parameters are summarized in Table 2.3.

| Buoy | $k_1$ [hm$^{-1}$] | $k_2$ [hours] |
|---|---|---|
| 42001 | 6.080 | 29.480 |
| 46042 | 5.010 | 2.600 |
| 46001 | 1.380 | 21.720 |

**Table. 2.3 ï** Coefficients $k_1, k_2$ of the linear base-height regressions for EESs.

It is noteworthy that the base-height regression $\bar{b}(a)$ for ETS and EPS is usually a monotonically slightly decreasing function (*Boccotti*, 2000; *Arena and Pavone*, 2006, 2009; *Fedele and Arena*, 2010; *Arena et. al.*, 2014). For the EESs, the average values of bases $b_E$ increase with storm intensity $a$ (see Figure 2.3). This trend of the EES is in agreement with the results given for actual storms, i.e., from $a$ and $D$. Finally, the coefficients of correlation between the duration $D$ of actual storms and the bases of ETS, EPS, and EES are investigated. For the ETSs and EPSs, the $\rho_{b,D}$ ranges were (0.095–0.216) and (0.090–0.210), respectively. For the EESs, the $\rho_{b_E,D}$ was higher, and it ranged between 0.549 and 0.652. In conclusion, we may consider the parameter $b_E$ of the EESs as more representative of the storm duration with respect to parameter $b$ of the ETSs and EPSs.

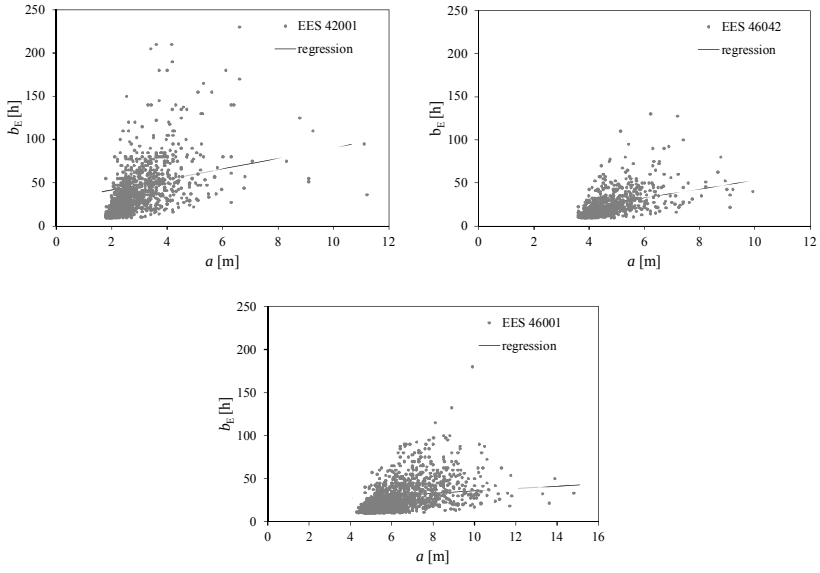


**Figure. 2.3 ï** Parameters $b_E$ versus parameters $a$ and the linear base-height regression $\bar{b}(a)$ of EESs.

### 2.3.2. Comparison of the long-term statistics for the actual sea and equivalent sea as represented by the ETS, EPS ($\lambda$=0.75), and EES models

A basic assumption of Boccotti's ETS model, as well as of the EPS and the new EES models, is that the actual sea is substituted by an equivalent sea. In this section, comparisons are made among the probabilities of exceedance of significant wave height for the actual sea and the ETS, EPS (with $\lambda = 0.75$), and EES. This comparison is necessary to verify the differences among the actual sea and equivalent seas.

Data are presented in Figures 2.4–2.6 as Weibull plots. Then, the distribution is fitted with a three parameters according to the Weibull law (1.10), and the parameters are reported in Tables 2.4 and 2.5. The results show good agreement between the $P(H_s > h)$ for the actual sea and the equivalent seas. Furthermore, the EES well represented the significant wave height distribution.

| Buoy | $u$ | $w$ [m] | $h_l$ [m] |
|---|---|---|---|
| 42001 | 0.671 | 0.262 | 1.10 |
| 46042 | 1.176 | 1.042 | 1.30 |
| 46001 | 1.209 | 1.591 | 1.50 |

**Table. 2.4** – Parameters $u$, $w$, and $h_l$ of the significant wave height distribution $P(H_s > h)$ for the actual sea.

| Buoy | $u$ | $w$ [m] | $h_l$ [m] |
|---|---|---|---|
| 42001 | 0.651 | 0.232 | 1.10 |
| 46042 | 1.242 | 1.103 | 1.30 |
| 46001 | 1.343 | 2.094 | 0.40 |

**Table. 2.5** – Parameters $u$, $w$, $h_l$ of the significant wave height distribution $P(H_s > h)$ for EESs.

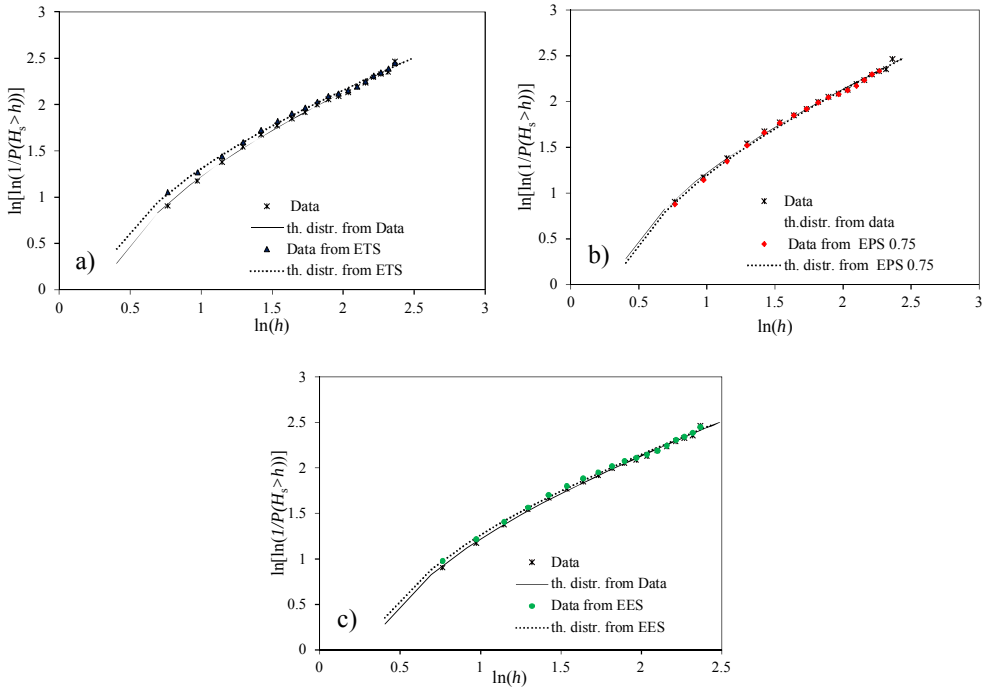


**Figure. 2.4 ï** Comparison between the significant wave height distribution $P(H_s>h)$ of the actual sea and of the equivalent sea at 42001 for (a) ETS, (b) EPS ($\lambda = 0.75$), and (c) EES.

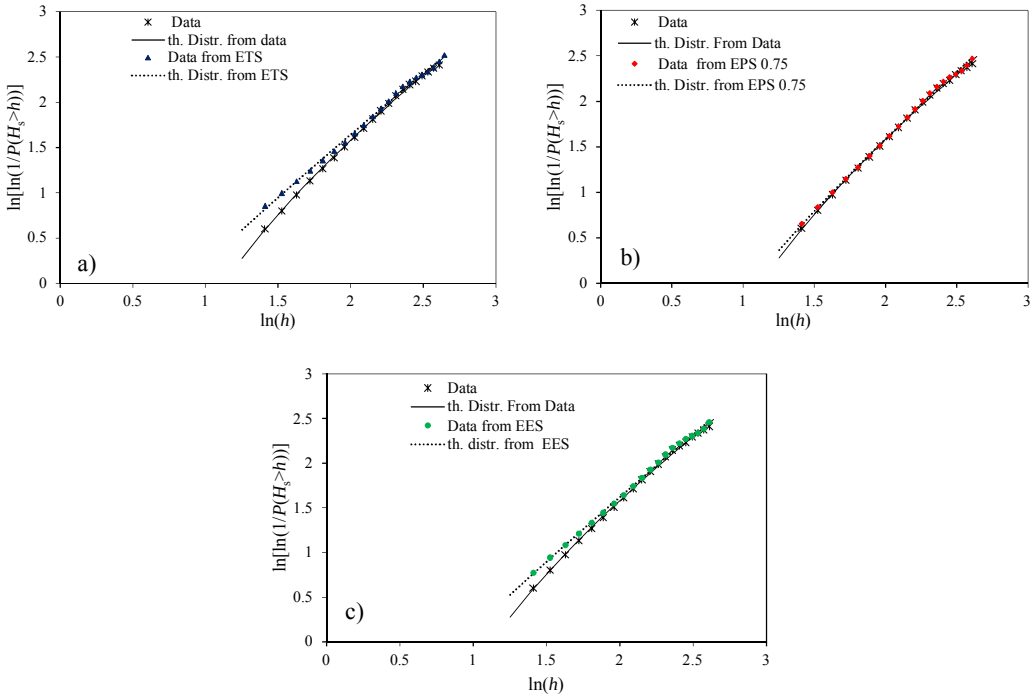


**Figure. 2.5 ï** Comparison between the significant wave height distribution $P(H_s>h)$ of the actual sea and of the equivalent sea at 46042 for (a) ETS, (b) EPS ($\lambda = 0.75$), and (c) EES.

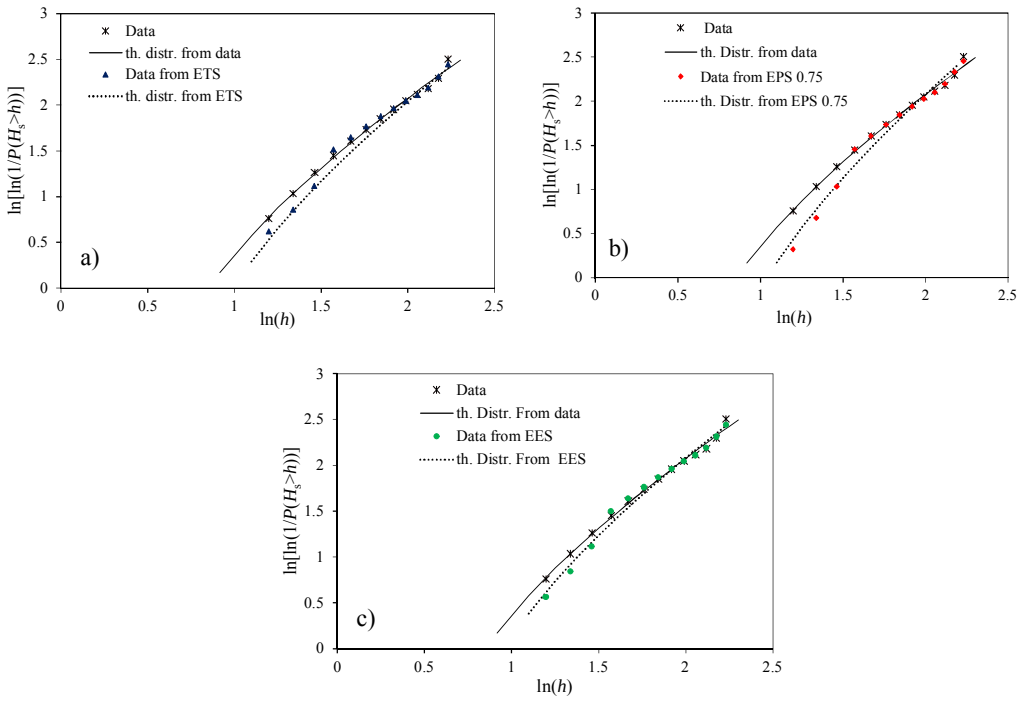


**Figure. 2.6** – Comparison between the significant wave height distribution $P(H_s > h)$ of the actual sea and of the equivalent sea at 46001 for (a) ETS, (b) EPS ($\lambda = 0.75$), and (c) EES.

Finally, comparisons were made between the return periods $R(H_s>h)$ calculated with the parameters of the $P(H_s>h)$ distribution for the actual sea and the EES (see Tables 2.4 and 2.5); the data is shown in Figure 2.7. As we can see, the differences are negligible for return values calculated for $R$ = 100 years, i.e., the differences are smaller than 4%. Hence, we can conclude that the EES model well represents the actual sea for calculations of the return period for extreme storms.

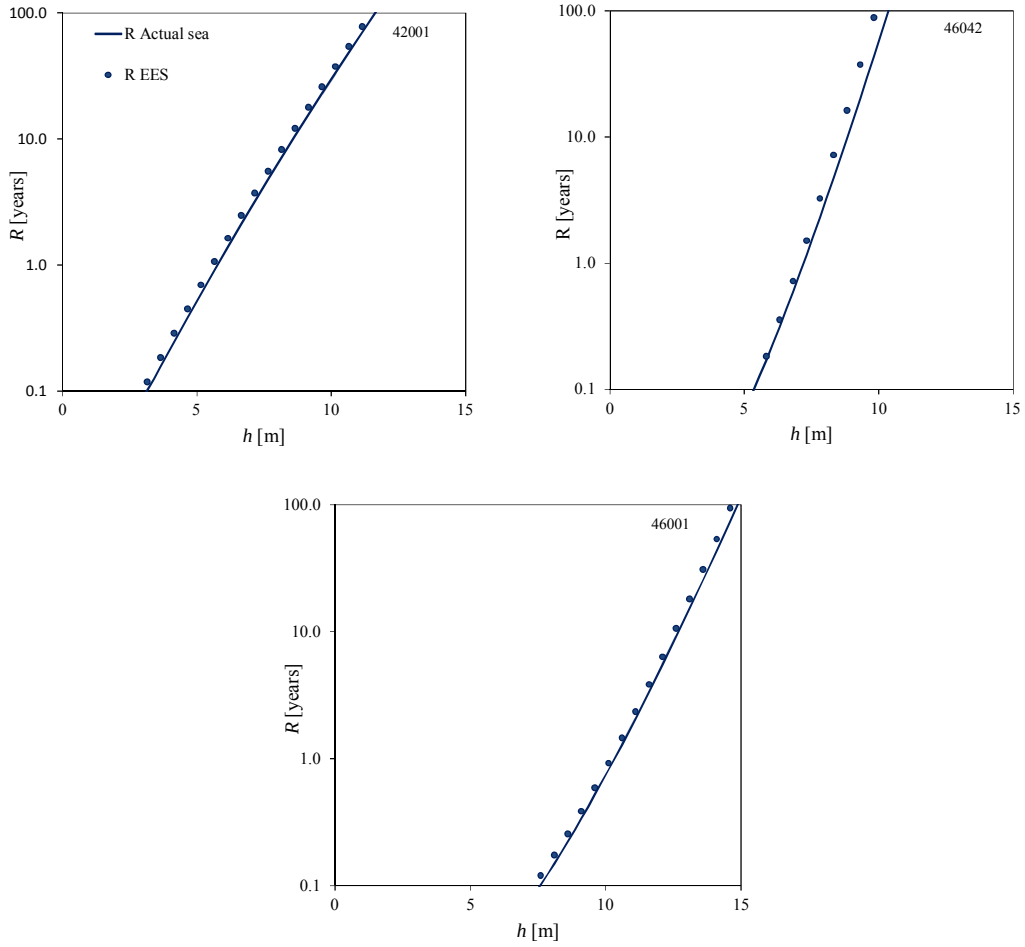


**Figure. 2.7** – Return periods $R(H_s > h)$ of the actual sea and of the equivalent exponential sea at buoys: (a) 42001; (b) 46042; (c) 46001.

## 2.4. Conclusions

A new model called the equivalent exponential storm model has been introduced to represent sea storms. Following the previous works of *Boccotti (2000), Arena and Pavone (2006, 2009)*, and *Fedele and Arena (2010)* regarding the representation of a storm with a triangular law or with a more general power law (so as to have parabolic storms, cusp storms, and so on), the new model represents a storm history with an exponential law with two parameters. One parameter represents the storm intensity and the other the storm duration.

*Fedele and Arena* (2010), by applying their EPS model, concluded that a power law with an exponent $\lambda$ smaller than 1 (equal to 0.75; it is 1 for triangular storms) well represents ocean

storms. The EES model is less than linear, like the one proposed in their paper for $\lambda = 0.75$. In addition, with respect to the EPS, the new model has some advantages. The solution for the return period in which the significant wave height exceeds a given threshold has been derived in a closed form, and therefore it may be calculated easily. The bases of the EESs represent the storm duration better than those of the previous models (ETS and EPS). Additionally, it was found that the storm duration increases with the storm intensity.

THIS PAGE INTENTIONALLY LEFT BLANK

# Chapter 3 ï On sampling between data of significant wave height for long term statistics with equivalent storm models

*In this chapter a sensitivity analysis of equivalent storm models to the time interval $\Delta t$ between successive data is performed. A different sampling $\Delta t$ between successive data may produce differences in the recorded sea state and in the storms history. In this chapter the Equivalent Triangular Storm (ETS) and the Equivalent Exponential Storm (EES) models are applied for the analysis in order to evaluate the variability of parameters of intensity and duration of equivalent storms calculated starting from time series with different sampling $\Delta t$ between successive data. Finally the effect of the variability of parameters of equivalent storms on the long-term statistics is investigated by means of the return period $R(H_s>h)$.*

## 3.1. Data analysis

The analysis is performed starting from significant wave height time series given by four buoys of NOAA-NDBC (National Oceanic and Atmospheric Administration's – National Data Buoy Center) network (USA) moored in Pacific Ocean: the 46035, 46028, 46006 and the 44005 (Figures 3.1a and 3.1b). The analysis is carried out by applying both the ETS and the EES models, assuming for the data acquisition different time intervals $\Delta t$ (1, 3, 6 hours) between two consecutive records.

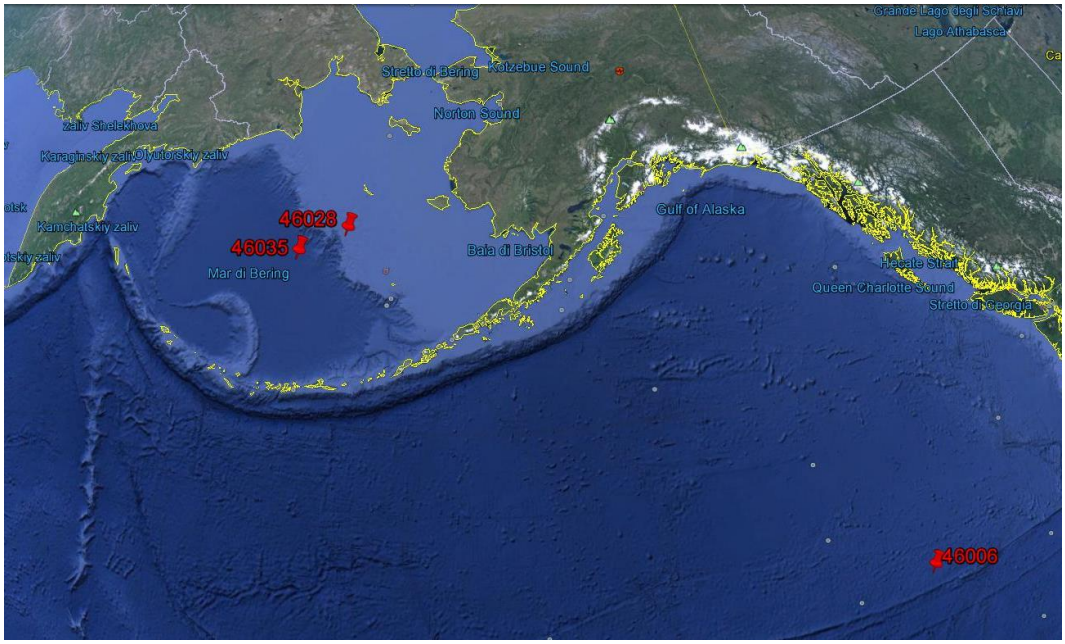


**Figure. 3.1a ï** Locations of NOAA-NDBC 46035, 46028, 46006 buoys.

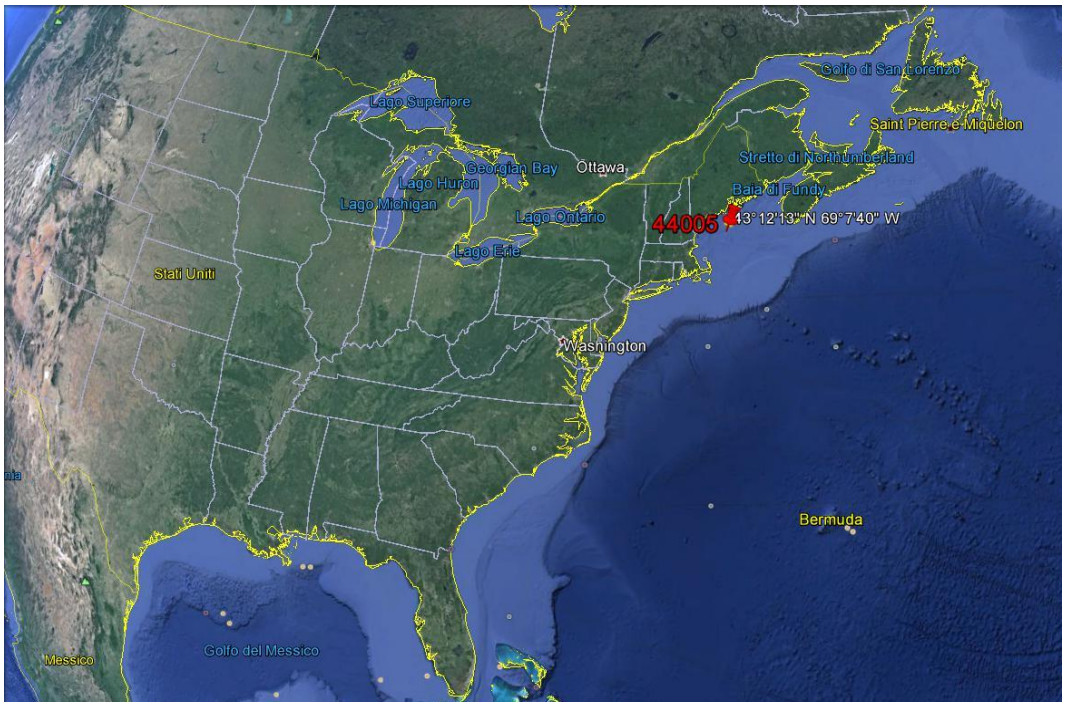


**Figure. 3.1b ï** Location of NOAA-NDBC 44005 buoy.

The analysis consists of the following stages:

- Calculation of parameters of the distribution of significant wave height (1.10);
- extrapolation of actual storm sequences from time series of significant wave height with time interval between successive data $\Delta t$ equal to 1, 3, 6 hours by means of the definition (1.3);
- calculation of parameters of both ETSs and EESs starting from each of the above actual storm sequences;
- calculation of the related base-height regressions for both ETSs and EESs;
- calculation of return period $R(H_s>h)$ for both ETSs and EESs by means of Equations (1.19) and (2.28) respectively;
- calculation of return values of significant wave heights $h(R)$ for fixed return periods $R$ (10, 20, 50, 100 years) by means of Equations (1.19) and (2.28) respectively;
- evaluation of the variability of $h(R)$ due to the assumption of different $\Delta t$.

## 3.2. Significant wave height distribution $P(H_s>h)$ at the examined locations

For this application the lower bounded three-parameters Weibull distribution (1.10) is considered to fit data of the significant wave height at the examined locations. The parameters of the distributions (Table 3.1 and Figure 3.2) are calculated by following the procedure presented in (1.3.2).

| Buoy | u | w[m] | $h_l$[m] |
|---|---|---|---|
| **46035** | 1,269 | 2,064 | 0,7 |
| **46028** | 1,226 | 1,117 | 1,3 |
| **46006** | 1,145 | 1,268 | 1,4 |
| **44005** | 1,233 | 1,434 | 0,0 |

**Table. 3.1 ï** Parameters u, w, $h_l$, of significant wave height distribution $P(H_s>h)$.

Results show that at 46035, 46028 and 46006 the three-parameter Weibull distribution well fits the data, while at 44005 a two parameters one may be considered.

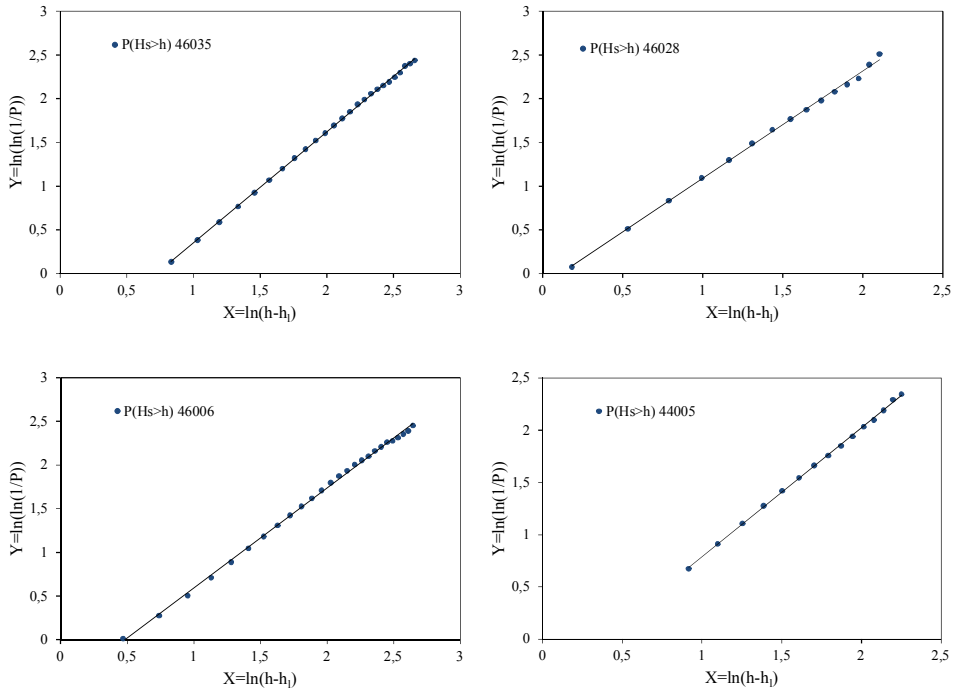


**Figure. 3.2 ï** Significant wave height distribution $P(Hs>h)$ at the considered locations.

## 3.3. Extrapolation of actual storm sequences, calculation of ETSs and EESs, determination of the base-height regression functions

As explained previously for the analysis proposed in this chapter time series with different time interval $\Delta t$ (1, 3, 6 hours) between successive data are used as input. Data of NOAA-NDBC are recorded every one hour so first the original time series are considered (case $\Delta t$=1hour). Then from the original time series only data with $\Delta t=3$ hours are considered, and finally only data with $\Delta t=6$ hours. In this way three time series of significant wave height are analysed at each considered location. From each of them the actual storm sequence is extrapolated and for each actual storm the related ETS and EES are calculated. Once the ETSs and EESs sequences are known the linear base-height regression functions may be calculated by representing the couple $(a,b)$ of ETSs and EESs in a Cartesian diagram and by determining the least square line. Figures 3.3-3.6, show linear base-height regression functions for ETSs (top) and EESs (bottom) for each the different $\Delta t$ (1, 3, 6 hours) considered (from left to right), for 46035, 46028, 46006 and 44005 buoys, respectively. Parameters $k_1$, $k_2$ of the above functions are summarized in Tables 3.2-3.4.

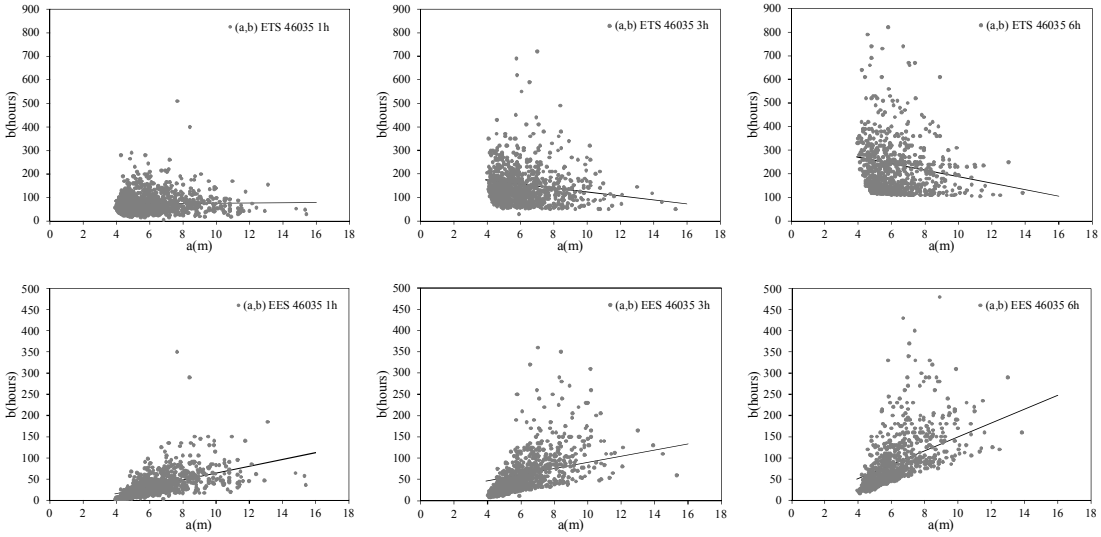


**Figure. 3.3ï** Linear base-height regression function for ETSs (Top) and for EESs (bottom) calculated starting from time series with time interval $\Delta t$ between successive data of 1, 3, 6 hours, for 46035 buoy.

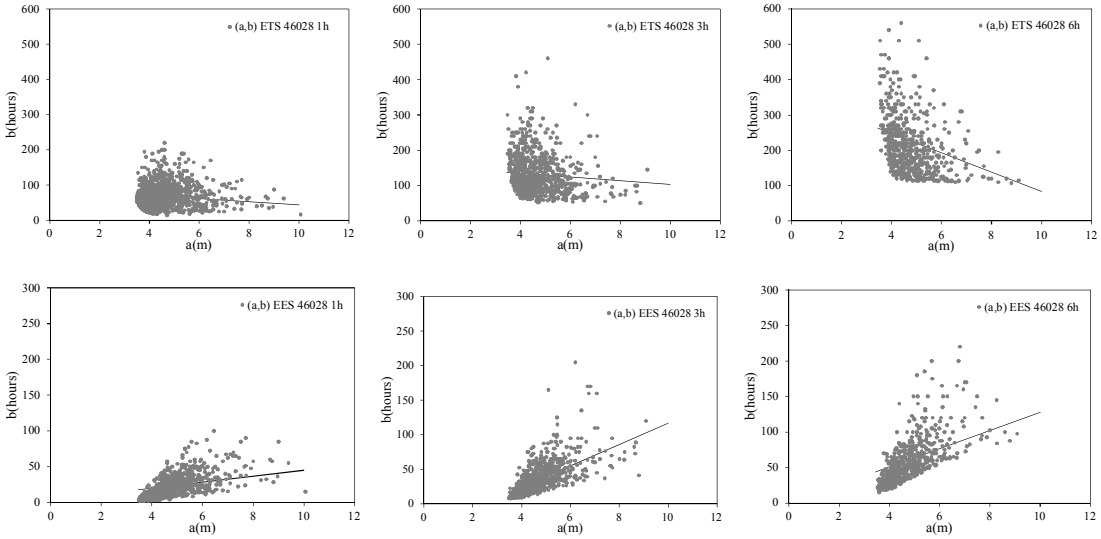


**Figure. 3.4 ï** Linear base-height regression function for ETSs (Top) and for EESs (bottom) calculated starting from time series with time interval $\Delta t$ between successive data of 1, 3, 6 hours, for 46028 buoy.

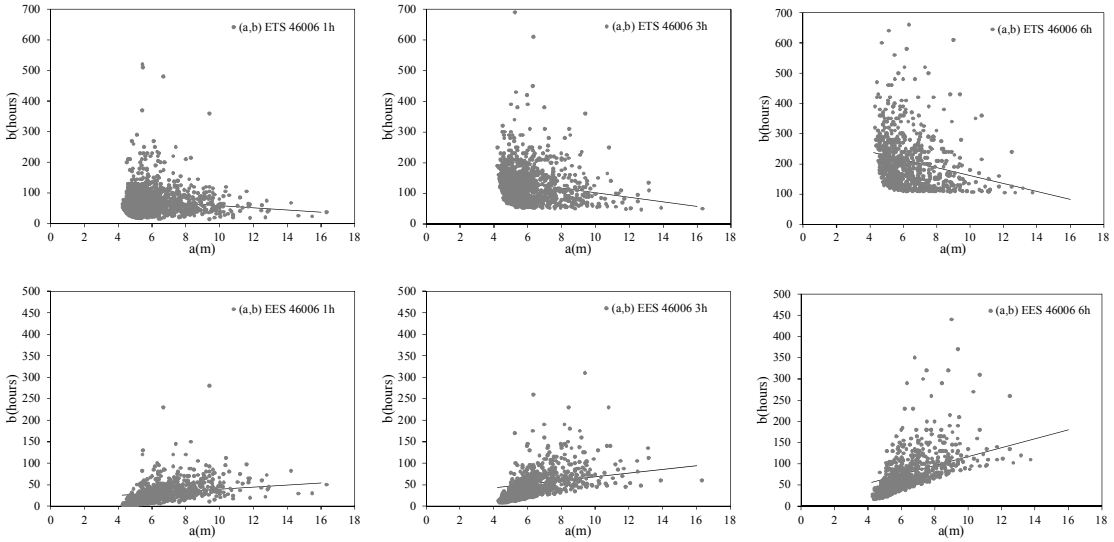


**Figure. 3.5 ï** Linear base-height regression function for ETSs (Top) and for EESs (bottom) calculated starting from time series with time interval $\Delta t$ between successive data of 1, 3, 6 hours, for 46006 buoy.

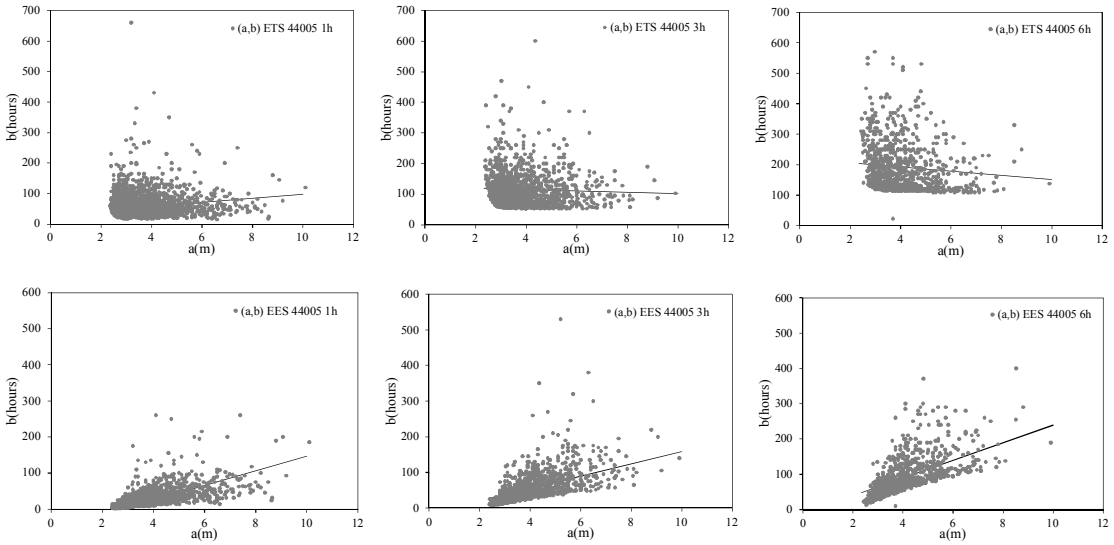


**Figure. 3.6 ï** Linear base-height regression function for ETSs (Top) and for EESs (bottom) calculated starting from time series with time interval $\Delta t$ between successive data of 1, 3, 6 hours, for 44005 buoy.

| Δt=1h | ETS | | EES | |
|---|---|---|---|---|
| **Buoy** | **$K_1$[h/m]** | **$K_2$[hours]** | **$K_1$[h/m]** | **$K_2$[hours]** |
| **46035** | 0,432 | 72,256 | 8,041 | -16,125 |
| **46028** | -4,448 | 88,870 | 4,196 | 3,098 |
| **46006** | -3,533 | 93,912 | 2,495 | 14,790 |
| **44005** | 6,627 | 32,563 | 20,175 | -55,317 |

**Table. 3.2 ï** Parameters $k_1$, $k_2$, of linear base-height regression of ETSs and EESs calculated from time series with time interval $\Delta t$ = 1 hour.

| Δt=3h | ETS | | EES | |
|---|---|---|---|---|
| **Buoy** | **$K_1$[h/m]** | **$K_2$[hours]** | **$K_1$[h/m]** | **$K_2$[hours]** |
| **46035** | -8,455 | 207,870 | 7,281 | 17,248 |
| **46028** | -5,127 | 155,030 | 15,503 | -37,952 |
| **46006** | -7,381 | 175,830 | 4,257 | 26,274 |
| **44005** | -2,288 | 124,550 | 17,180 | -13,669 |

**Table. 3.3 ï** Parameters $k_1$, $k_2$, of linear base-height regression of ETSs and EESs calculated from time series with time interval $\Delta t$ = 3 hours.

| Δt=6h | ETS | | EES | |
|---|---|---|---|---|
| **Buoy** | **$K_1$[h/m]** | **$K_2$[hours]** | **$K_1$[h/m]** | **$K_2$[hours]** |
| **46035** | -13,814 | 326,770 | 16,471 | -15,359 |
| **46028** | -27,340 | 356,960 | 12,830 | -0,648 |
| **46006** | -13,199 | 294,060 | 10,564 | 11,784 |
| **44005** | -6,874 | 220,140 | 24,991 | -10,482 |

**Table. 3.4 ï** Parameters $k_1$, $k_2$, of linear base-height regression of ETSs and EESs calculated from time series with time interval $\Delta t$ =6 hours.

Looking at the base-height regression functions it is possible to see that considering increasing time interval $\Delta t$ the duration $b$ of both ETSs and EESs grow. To understand this phenomenon it is needed to look at the modifications of the single storm. Considering increasing $\Delta t$ the significant wave height corresponding to the storm peak may be not intercepted and the maximum significant wave height $H_{s\,max}$ of the actual storm may be smaller (see Figure 3.7). In this way the structure of the actual storm in correspondence of the storm peak is modified becoming flatter and causing an increase of the duration $b$. In fact the duration $b$ depends upon the sea states near the storm peak and tend to increase as flatter is the structure of the actual storm. If this effect is verified in a big number of storms it produces an increase of the bases.

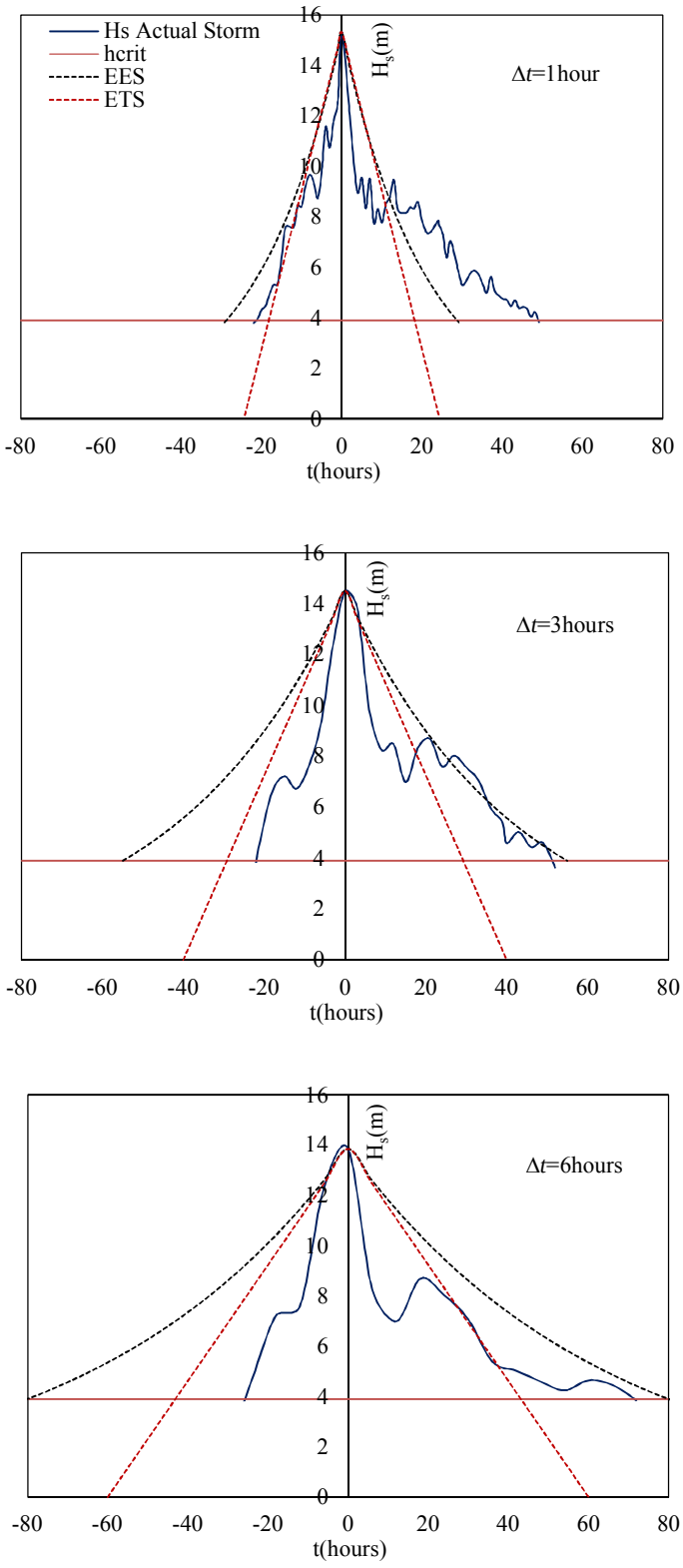


**Figure. 3.7 ï** Actual storm and associated EESs and ETSs for Δ*t*= 1, 3, 6 hours at 46035 buoy.

## 3.4. Calculation of return period $R(H_s>h)$ and of return values of significant wave heights $h(R)$

The return period $R(H_s>h)$ depend upon two functions: the probability distribution of the significant wave height $P(H_s>h)$ and the base-height regression function $b(a)$. In this section the effects due to the variation of the base-height regression functions on the calculation of return period of ETSs and EESs are evaluated. Return period $R(H_s>h)$ is calculated for both ETSs and EESs by considering the three different base-height regression function ($\Delta t$=1, 3, 6 hours) determined in previous section. Results are shown in Figures 3.8 and 3.9. Results show that in the greatest part of the cases for fixed return period $R$ the return values of significant wave height $h(R)$ tend to decrease if the base-height regression function corresponding to increasing $\Delta t$ are considered (see Tables 3.5-3.7). Tables 3.8, 3.9 show the variation $\Delta h$ of $h(R)$ in percentage passing from $\Delta t$=1 hour to $\Delta t$=3 hours and passing from $\Delta t$=3 hour to $\Delta t$=6 hours, respectively.

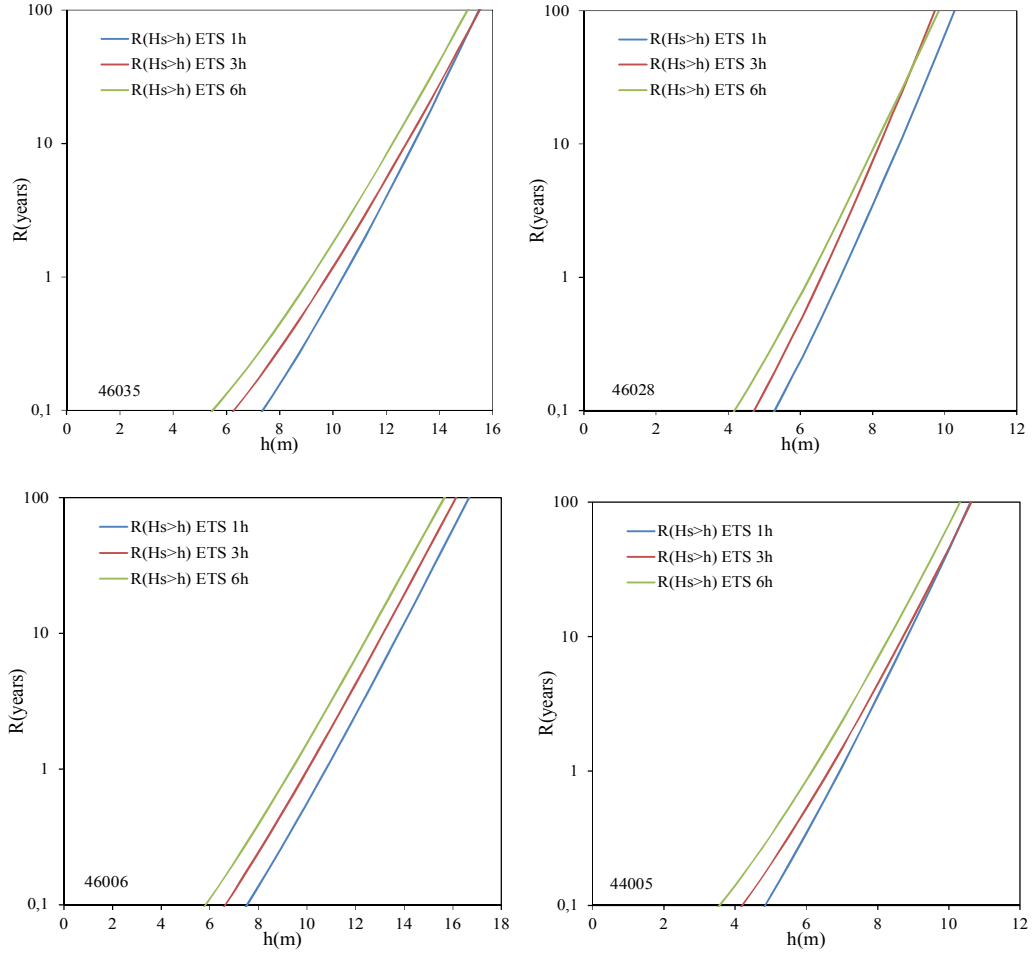


**Figure. 3.8 ï** Return period $R(Hs>h)$ for ETSs at the considered locations.

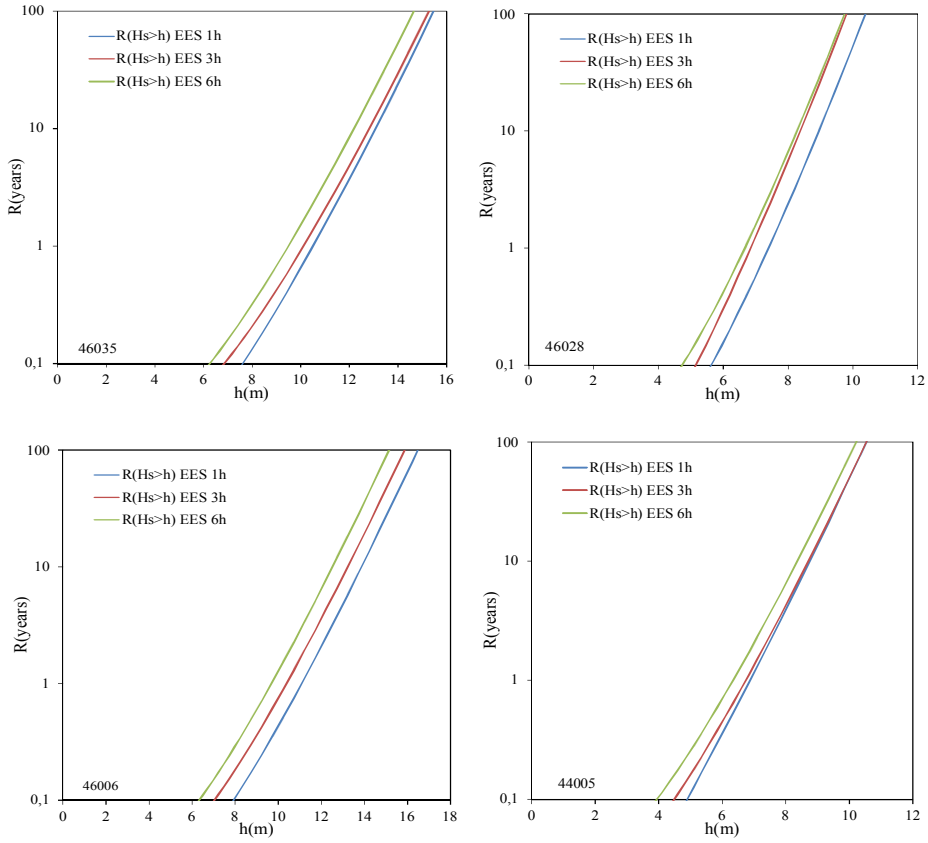


**Figure. 3.9 ï** Return period *R*(*Hs*>*h*) for EESs at the considered locations.

| Δt=1h | ETS | | | | EES | | | |
|---|---|---|---|---|---|---|---|---|
| **Buoy** | **h(R=10yrs) [m]** | **h(R=20yrs) [m]** | **h(R=50yrs) [m]** | **h(R=100yrs) [m]** | **h(R=10yrs) [m]** | **h(R=20yrs) [m]** | **h(R=50yrs) [m]** | **h(R=100yrs) [m]** |
| **46035** | 13,00 | 13,80 | 14,80 | 15,50 | 13,10 | 13,80 | 14,80 | 15,50 |
| **46028** | 8,74 | 9,21 | 9,82 | 10,27 | 8,95 | 9,39 | 9,96 | 10,38 |
| **46006** | 13,78 | 14,66 | 15,80 | 16,66 | 13,87 | 14,66 | 15,7 | 16,47 |
| **44005** | 8,83 | 9,38 | 10,09 | 10,61 | 8,8 | 9,35 | 10,06 | 10,58 |

**Table. 3.5 ï** Return Values *h*(*R*) for Δ*t*=1hour.

| Δt=3h | ETS | | | | EES | | | |
|---|---|---|---|---|---|---|---|---|
| **Buoy** | **h(R=10yrs) [m]** | **h(R=20yrs) [m]** | **h(R=50yrs) [m]** | **h(R=100yrs) [m]** | **h(R=10yrs) [m]** | **h(R=20yrs) [m]** | **h(R=50yrs) [m]** | **h(R=100yrs) [m]** |
| **46035** | 12,80 | 13,60 | 14,70 | 15,50 | 12,80 | 13,60 | 14,60 | 15,30 |
| **46028** | 8,20 | 8,67 | 9,28 | 9,72 | 8,37 | 8,81 | 9,38 | 9,80 |
| **46006** | 13,13 | 14,04 | 15,23 | 16,13 | 13,22 | 14,04 | 15,09 | 15,87 |
| **44005** | 8,72 | 9,31 | 10,07 | 10,63 | 8,71 | 9,27 | 10,00 | 10,54 |

**Table. 3.6 ï** Return Values *h*(*R*) for Δ*t*=3hours.

| Δt=6h | ETS | | | | EES | | | |
|---|---|---|---|---|---|---|---|---|
| **Buoy** | **h(R=10yrs) [m]** | **h(R=20yrs) [m]** | **h(R=50yrs) [m]** | **h(R=100yrs) [m]** | **h(R=10yrs) [m]** | **h(R=20yrs) [m]** | **h(R=50yrs) [m]** | **h(R=100yrs) [m]** |
| **46035** | 12,20 | 13,10 | 14,20 | 15,1 | 12,20 | 13,00 | 13,90 | 14,70 |
| **46028** | 8,08 | 8,61 | 9,30 | 9,83 | 8,28 | 8,73 | 9,31 | 9,75 |
| **46006** | 12,56 | 13,49 | 14,72 | 15,64 | 12,52 | 13,32 | 14,37 | 15,15 |
| **44005** | 8,34 | 8,95 | 9,74 | 10,32 | 8,36 | 8,93 | 9,67 | 10,21 |

**Table. 3.7 ï** Return Values $h(R)$ for $\Delta t$=6hours.

| 1h-3h | ETS | | | | EES | | | |
|---|---|---|---|---|---|---|---|---|
| **Buoy** | **Δh(10yrs) [%]** | **Δh(20yrs) [%]** | **Δh(50yrs) [%]** | **Δh(100yrs) [%]** | **Δh(10yrs) [%]** | **Δh(20yrs) [%]** | **Δh(50yrs) [%]** | **Δh(100yrs) [%]** |
| **46035** | 2,1 | 1,3 | 0,4 | -0,1 | 2,1 | 1,7 | 1,4 | 1,2 |
| **46028** | 6,2 | 5,9 | 5,5 | 5,4 | 6,5 | 6,2 | 5,8 | 5,6 |
| **46006** | 4,7 | 4,2 | 0,6 | 1,1 | 4,7 | 4,2 | 3,9 | 3,6 |
| **44005** | 1,2 | 0,7 | 0,2 | -0,2 | 1,0 | 0,9 | 0,6 | 0,4 |

**Table. 3.8 ï** Variation in percentage between return values calculated with $\Delta t$=1hour and $\Delta t$=3hours.

| 3h-6h | ETS | | | | EES | | | |
|---|---|---|---|---|---|---|---|---|
| **Buoy** | **Δh(10yrs) [%]** | **Δh(20yrs) [%]** | **Δh(50yrs) [%]** | **Δh(100yrs) [%]** | **Δh(10yrs) [%]** | **Δh(20yrs) [%]** | **Δh(50yrs) [%]** | **Δh(100yrs) [%]** |
| **46035** | 4,0 | 3,7 | 3,3 | 3,0 | 4,8 | 4,6 | 4,3 | 4,1 |
| **46028** | 1,5 | 0,7 | -0,2 | -1,1 | 1,1 | 0,9 | 0,7 | 0,5 |
| **46006** | 4,3 | 3,9 | 3,3 | 3,0 | 5,3 | 5,1 | 4,8 | 4,5 |
| **44005** | 4,4 | 3,9 | 3,3 | 2,9 | 4,0 | 3,7 | 3,3 | 3,1 |

**Table. 3.9 ï** Variation in percentage between return values calculated with $\Delta t$=3hours and $\Delta t$=6hours.

Results show that $\Delta h$ decreases with increasing values of $R$ both for ETSs and EESs, but for ETSs the reduction of $\Delta h$ is greater than EESs.

## 3.5. Conclusions

The analysis proposed in this chapter has shown how the structure of the storms changes with different values of the time span $\Delta t$ between two consecutive records. The variability of the intensity and duration of the storms, represented with both the ETS and EES models, has been investigated, for increasing value of time $\Delta t$ between two consecutive records in the range (1, 6 hours). Value of 6 hours is widely used for analysis of significant wave heights from

meteorological models (for example, the WAM-ECMWF). The result is that for increasing values of $\Delta t$ the storm duration is increased significantly, and the storm intensity may be smaller. This error produces changes in the base-height regression functions and may be important for long-term analysis based on the ETS and EES models. In fact return values of significant wave height $h(R)$ calculated via the ETS or EES models decrease increasing $\Delta t$ and because of that return values $h(R)$ calculated starting from time series with sampling $\Delta t$ between data of 1 hour are more conservative than those calculated with greater time sampling $\Delta t$ (3-6 hours) .

# Chapter 4 ï Sensitivity analysis of return values to storm threshold for Peak Over Threshold and Equivalent Exponential Storm models

*This chapter proposes a comparison between two statistical approaches used for long-term predictions of extreme significant wave heights: the Equivalent Exponential Storm (EES) model and the Peak Over Threshold (POT) method. One important aspect when a statistical analysis is done is the choice of the sample in order to have individual data statistically independent of each other. For this purpose the mentioned methodologies identify storms from time series. In the case of the EES model, storms are identified by means of a storm definition linked to a threshold $h_{crit}$ of significant wave height. For what concerns the POT method, storms are extrapolated from time series of significant wave height by dividing time history in storms of a given duration $\Delta t$ and by taking into account only storms with maximum significant wave height greater than a fixed threshold $h_{crit}$. As the methods are defined they are both threshold dependent. In the paper the variability of return values of significant wave height due to the assumption of different thresholds is investigated both for EES model and POT method. In addition a further analysis is carried out for POT method by assuming different storm durations $\Delta t$. Results confirm that both methodologies are affected by a certain sensibility to the threshold, which is limited in the case of EES model.*

## 4.1. Introduction

The extreme wave analysis aims to estimate return values of wave height that will occur once in a long time period of, say, 50 or 100 years. These values are essential for the correct evaluation of safety and design condition of marine structures. A lack in the estimation of the design wave may imply either an unsafe structure (if return values are underestimated) or an over-designed and uneconomical structure (if return values are overestimated). This kind of analysis requires a series of observed or hindcasted data adequately large (a decade or more). The fundamental purpose of long-term statistics is to determine the relationship between large

wave heights and their occurrence probability and to calculate their return period. There is no theoretical foundation for the choice of the extreme events distribution and the most commonly used approach is to test several distributions and to select the one that provides the best fit. There are several works on extreme values prediction of wind and waves. The first who has developed a statistical method for extreme values prediction of natural random events is *Gumbel (1958)*. Several statistical methods that may be applied to carry out extreme values analysis are discussed in *Mathiesen et al. (1994), Goda (1992, 1993, 2000)*. A review of the various steps involved in the procedure applied for prediction of extreme wave height, such as data collection, selection of the adequate distribution, the selection of the wave height corresponding to a given return period, may be found in *Isaacson and Mackenzie (1981)*. One of the most commonly method applied for extreme wave analysis is the Peak Over Thresholds (POT) in which only wave data above a fixed threshold are taken into account. Information about POT may be found in Goda (2000), Coles (2001) and in *Ferreira and Guedes Soares (1998)*. An alternative approach is the Equivalent Triangular Storm (ETS) model proposed by *Boccotti (1986, 2000)* to predict return period of extreme wave events starting from a given sequence of storms in time. Approaches inspired by ETS model are the Equivalent Power storm (EPS) model of *Fedele and Arena (2010)* and the Equivalent Exponential Storm (EES) model by *Arena and Laface (2015)*. In this chapter data from buoys of NOOA-NDBC are processed to predict return values of significant wave height $h(R)$ corresponding to return periods $R$ of 10, 20, 50, 100 years, by applying both POT and EES approaches. Sensitivity analyses are carried out with respect to variability of threshold $h_{crit}$ value both for POT and EES and with respect to the variability of the storm duration $\Delta t$ for POT, in order to evaluate the robustness of the methodologies.

## 4.2. Data analysis

In this section a brief explanation of the various steps involved in the analysis done with EES model and POT method is presented and results are given and compared. The analysis has been carried out by considering data given from two buoys of NOAA-NDBC (National Data Buoy Center): the 46035 and the 46006 (Figure 4.1.). For both buoys more than 25 years of data are available. The EES and POT approaches have been applied to calculate return values of significant wave height $h(R)$ corresponding to different return periods $R$ (10, 20, 50, 100 years), by varying the threshold $h_{crit}$ from 1.5 times the average significant wave height $\overline{H}_s$ to $4\,\overline{H}_s$ with a step of $0.25\,\overline{H}_s$ (see Table 4.1).

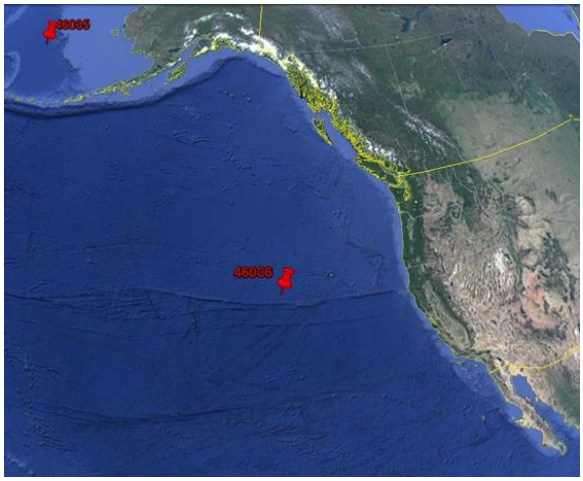


**Figure. 4.1 ï** Locations of the analysed buoys.

| $h_{crit}$ | 46035 $h_{crit}$(m) | 46006 $h_{crit}$(m) |
|---|---|---|
| $\overline{H_s}$ | 2.6 | 2.8 |
| $1.5\overline{H_s}$ | 3.9 | 4.2 |
| $1.75\overline{H_s}$ | 4.6 | 4.9 |
| $2\overline{H_s}$ | 5.2 | 5.6 |
| $2.25\overline{H_s}$ | 5.9 | 6.3 |
| $2.5\overline{H_s}$ | 6.5 | 7.0 |
| $2.75\overline{H_s}$ | 7.2 | 7.7 |
| $3\overline{H_s}$ | 7.8 | 8.4 |
| $3.25\overline{H_s}$ | 8.5 | 9.1 |
| $3.5\overline{H_s}$ | 9.1 | 9.8 |
| $3.75\overline{H_s}$ | 9.8 | 10.5 |
| $4\overline{H_s}$ | 10.4 | 11.2 |

**Table. 4.1 ï** Average significant wave height $\overline{H_s}$ and value of each threshold $h_{crit}$ (from $1.5\overline{H_s}$ to $4\overline{H_s}$) considered for the analysis at the given locations.

### 4.2.1 Analysis with Peak Over Threshold (POT) method

As explained in the previous section, the calculation of return values of significant wave height $h(R)$ for different return periods $R$ by applying POT is done by considering different threshold $h_{crit}$ (from $1.5\overline{H_s}$ to $4\overline{H_s}$) and different storm duration $\Delta t$ (24, 48, 72, 96 hours). The first step is the selection of the data sample starting from time series. The fact to consider 11 thresholds $h_{crit}$ and 4 values of storm duration $\Delta t$ involves that 44 data sample are analyzed at each considered location. Each sample is achieved from time series by extrapolating storms

with the fixed duration $\Delta t$ and by taking into account only the storm maxima above the considered threshold $h_{crit}$. Once the samples are selected each of them is analyzed by means of the same procedure which consists in the following steps:

- arranging data in a descending order;
- calculation of the probability of exceedance be means of the plotting position formulas (1.1);
- testing different distribution to identify the one that gives the best fit of the data;
- calculation of the parameters of the selected distribution;
- calculation of return values $h(R)$ corresponding to R=10, 20, 50, 100 years .

At both considered location the Weibull distribution (1.4) is selected and return values $h(R)$ are calculated by means of Equation (1.7). Tables 4.2-4.9 show $h(R)$ for fixed $\Delta t$ and different $h_{crit}$. For fixed $\Delta t$ the variability of return values $h(R)$ due to the assumption of different thresholds $h_{crit}$ is investigated. Tables 4.10 and 4.11 show for fixed $\Delta t$ and $R$, the maximum difference in percentage between the maximum and the minimum $h(R)$ calculated by varying the thresholds $h_{crit}$. Results show that for a given storm duration $\Delta t$ the maximum variation $\Delta h_{max}$ of return values increases for increasing values of return periods $R$ reaching values greater than 15% and 12% at 46035 and 46006, respectively, for $R$=100 years.

| $h_{crit}$ (m) | 10 years h(m) | 20 years h(m) | 50 years h(m) | 100years h(m) |
|---|---|---|---|---|
| 3.9 | 13.73 | 14.60 | 14.90 | 15.61 |
| 4.6 | 13.88 | 14.80 | 14.89 | 15.60 |
| 5.2 | 13.84 | 14.77 | 14.93 | 15.64 |
| 5.9 | 13.86 | 14.81 | 14.93 | 15.64 |
| 6.5 | 13.91 | 14.88 | 14.98 | 15.69 |
| 7.2 | 13.85 | 14.80 | 15.00 | 15.70 |
| 7.8 | 13.88 | 14.86 | 15.04 | 15.75 |
| 8.5 | 13.92 | 14.94 | 15.03 | 15.74 |
| 9.1 | 13.96 | 15.12 | 15.11 | 15.82 |
| 9.8 | 13.95 | 15.19 | 15.16 | 15.88 |
| 10.4 | 13.92 | 15.26 | 15.29 | 16.00 |

**Table. 4.2 ï** Return values of significant wave height $h(R)$ for different return periods $R$, calculated by applying the POT method assuming different thresholds $h_{crit}$ and a storm duration $\Delta t$ of 24 hours, for 46035 buoy.

| $h_{crit}$ (m) | 10 years h(m) | 20 years h(m) | 50 years h(m) | 100years h(m) |
|---|---|---|---|---|
| 3.9 | 13.67 | 14.55 | 15.68 | 16.52 |
| 4.6 | 13.87 | 14.81 | 16.04 | 16.96 |
| 5.2 | 13.89 | 14.86 | 16.12 | 17.07 |
| 5.9 | 13.97 | 14.97 | 16.29 | 17.28 |
| 6.5 | 13.91 | 14.90 | 16.20 | 17.18 |
| 7.2 | 13.91 | 14.90 | 16.19 | 17.16 |
| 7.8 | 13.87 | 14.84 | 16.12 | 17.08 |
| 8.5 | 13.92 | 14.94 | 16.28 | 17.29 |
| 9.1 | 13.96 | 15.12 | 16.70 | 17.94 |
| 9.8 | 13.96 | 15.18 | 16.89 | 18.24 |
| 10.4 | 13.92 | 15.25 | 17.15 | 18.68 |

**Table. 4.3 ï** Return values of significant wave height $h(R)$ for different return periods $R$, calculated by applying the POT method assuming different thresholds $h_{crit}$ and a storm duration $\Delta t$ of 48 hours, for 46035 buoy.

| $h_{crit}$ (m) | 10 years h(m) | 20 years h(m) | 50 years h(m) | 100years h(m) |
|---|---|---|---|---|
| 3.9 | 13.65 | 14.49 | 15.56 | 16.34 |
| 4.6 | 13.74 | 14.62 | 15.74 | 16.56 |
| 5.2 | 13.80 | 14.71 | 15.88 | 16.75 |
| 5.9 | 13.92 | 14.90 | 16.16 | 17.10 |
| 6.5 | 13.93 | 14.92 | 16.22 | 17.19 |
| 7.2 | 13.87 | 14.84 | 16.10 | 17.05 |
| 7.8 | 13.90 | 14.90 | 16.22 | 17.21 |
| 8.5 | 13.92 | 14.96 | 16.33 | 17.37 |
| 9.1 | 13.97 | 15.16 | 16.78 | 18.05 |
| 9.8 | 13.97 | 15.23 | 17.00 | 18.40 |
| 10.4 | 13.92 | 15.28 | 17.24 | 18.83 |

**Table. 4.4 ï** Return values of significant wave height $h(R)$ for different return periods $R$, calculated by applying the POT method assuming different thresholds $h_{crit}$ and a storm duration $\Delta t$ of 72 hours, for 46035 buoy.

| $h_{crit}$ (m) | 10 years h(m) | 20 years h(m) | 50 years h(m) | 100years h(m) |
|---|---|---|---|---|
| 3.9 | 13.64 | 14.47 | 15.53 | 16.30 |
| 4.6 | 13.72 | 14.60 | 15.71 | 16.52 |
| 5.2 | 13.89 | 14.84 | 16.06 | 16.95 |
| 5.9 | 13.87 | 14.82 | 16.06 | 16.97 |
| 6.5 | 13.89 | 14.86 | 16.13 | 17.06 |
| 7.2 | 13.94 | 14.94 | 16.25 | 17.22 |
| 7.8 | 13.96 | 14.99 | 16.34 | 17.35 |
| 8.5 | 13.96 | 15.02 | 16.42 | 17.48 |
| 9.1 | 13.95 | 15.08 | 16.61 | 17.80 |
| 9.8 | 13.97 | 15.24 | 17.01 | 18.42 |
| 10.4 | 13.93 | 15.22 | 17.03 | 18.47 |

**Table. 4.5 ï** Return values of significant wave height $h(R)$ for different return periods $R$, calculated by applying the POT method assuming different thresholds $h_{crit}$ and a storm duration $\Delta t$ of 96 hours, for 46035 buoy.

| $h_{crit}$ (m) | 10 years h(m) | 20 years h(m) | 50 years h(m) | 100years h(m) |
|---|---|---|---|---|
| 4.2 | 13.64 | 14.56 | 15.75 | 16.64 |
| 4.9 | 13.66 | 14.60 | 15.83 | 16.74 |
| 5.6 | 13.71 | 14.68 | 15.94 | 16.89 |
| 6.3 | 13.77 | 14.77 | 16.08 | 17.07 |
| 7.0 | 13.78 | 14.81 | 16.18 | 17.21 |
| 7.7 | 13.93 | 15.08 | 16.63 | 17.82 |
| 8.4 | 14.02 | 15.33 | 17.14 | 18.57 |
| 9.1 | 13.88 | 15.01 | 16.52 | 17.67 |
| 9.8 | 14.01 | 15.30 | 17.06 | 18.42 |
| 10.5 | 13.95 | 15.32 | 17.22 | 18.71 |
| 11.2 | 13.93 | 15.28 | 17.13 | 18.57 |

**Table. 4.6 ï** Return values of significant wave height $h(R)$ for different return periods $R$, calculated by applying the POT method assuming different thresholds $h_{crit}$ and a storm duration $\Delta t$ of 24 hours, for 46006 buoy.

| $h_{crit}$ (m) | 10 years h(m) | 20 years h(m) | 50 years h(m) | 100years h(m) |
|---|---|---|---|---|
| 4.2 | 13.74 | 14.69 | 15.92 | 16.83 |
| 4.9 | 13.73 | 14.70 | 15.95 | 16.87 |
| 5.6 | 13.76 | 14.75 | 16.03 | 16.98 |
| 6.3 | 13.79 | 14.80 | 16.11 | 17.09 |
| 7.0 | 13.91 | 15.00 | 16.45 | 17.54 |
| 7.7 | 13.94 | 15.09 | 16.61 | 17.77 |
| 8.4 | 14.03 | 15.31 | 17.07 | 18.43 |
| 9.1 | 14.03 | 15.34 | 17.15 | 18.56 |
| 9.8 | 14.04 | 15.36 | 17.14 | 18.53 |
| 10.5 | 14.02 | 15.31 | 17.03 | 18.35 |
| 11.2 | 13.95 | 15.28 | 17.11 | 18.53 |

**Table. 4.7 ï** Return values of significant wave height $h(R)$ for different return periods $R$, calculated by applying the POT method assuming different thresholds $h_{crit}$ and a storm duration $\Delta t$ of 48 hours, for 46006 buoy.

| $h_{crit}$ (m) | 10 years h(m) | 20 years h(m) | 50 years h(m) | 100years h(m) |
|---|---|---|---|---|
| 4.2 | 13.76 | 14.73 | 15.96 | 16.86 |
| 4.9 | 13.84 | 14.85 | 16.15 | 17.12 |
| 5.6 | 13.84 | 14.87 | 16.20 | 17.19 |
| 6.3 | 13.87 | 14.92 | 16.28 | 17.30 |
| 7.0 | 13.97 | 15.10 | 16.60 | 17.73 |
| 7.7 | 13.98 | 15.15 | 16.72 | 17.91 |
| 8.4 | 13.89 | 15.00 | 16.46 | 17.57 |
| 9.1 | 14.05 | 15.39 | 17.23 | 18.67 |
| 9.8 | 14.05 | 15.33 | 17.04 | 18.35 |
| 10.5 | 14.02 | 15.31 | 17.03 | 18.35 |
| 11.2 | 13.93 | 15.24 | 16.97 | 18.28 |

**Table. 4.8 ï** Return values of significant wave height $h(R)$ for different return periods $R$, calculated by applying the POT method assuming different thresholds $h_{crit}$ and a storm duration $\Delta t$ of 72 hours, for 46006 buoy.

| $h_{crit}$ (m) | 10 years h(m) | 20 years h(m) | 50 years h(m) | 100years h(m) |
|---|---|---|---|---|
| 4.2 | 13.69 | 14.62 | 15.79 | 16.65 |
| 4.9 | 13.74 | 14.70 | 15.93 | 16.84 |
| 5.6 | 13.81 | 14.83 | 16.13 | 17.09 |
| 6.3 | 13.89 | 14.96 | 16.35 | 17.40 |
| 7.0 | 13.96 | 15.10 | 16.62 | 17.77 |
| 7.7 | 13.98 | 15.17 | 16.77 | 17.98 |
| 8.4 | 14.07 | 15.41 | 17.25 | 18.68 |
| 9.1 | 14.06 | 15.43 | 17.31 | 18.78 |
| 9.8 | 14.05 | 15.34 | 17.07 | 18.40 |
| 10.5 | 14.02 | 15.32 | 17.07 | 18.41 |
| 11.2 | 14.00 | 15.29 | 17.06 | 18.39 |

**Table. 4.9 ï** Return values of significant wave height $h(R)$ for different return periods $R$, calculated by applying the POT method assuming different thresholds $h_{crit}$ and a storm duration $\Delta t$ of 96 hours, for 46006 buoy.

| *R(years)* | 24 hours $\Delta h_{max}$(%) | 48 hours $\Delta h_{max}$(%) | 72 hours $\Delta h_{max}$(%) | 96 hours $\Delta h_{max}$(%) |
|---|---|---|---|---|
| 10 | 2.18 | 1.66 | 2.35 | 2.45 |
| 20 | 4.81 | 4.48 | 5.47 | 5.29 |
| 50 | 9.34 | 9.30 | 10.83 | 9.64 |
| 100 | 13.08 | 13.29 | 15.25 | 13.33 |

**Table. 4.10 ï** Maximum variation $\Delta h_{max}$ of return values $h(R)$ due to the assumption of different threshold $h_{crit}$, for EES model for each storm duration $\Delta t$ and each return period $R$, for 46035 buoy.

| *R(years)* | 24 hours $\Delta h_{max}$(%) | 48 hours $\Delta h_{max}$(%) | 72 hours $\Delta h_{max}$(%) | 96 hours $\Delta h_{max}$(%) |
|---|---|---|---|---|
| 10 | 2.80 | 2.26 | 2.07 | 2.77 |
| 20 | 5.28 | 4.52 | 4.51 | 5.77 |
| 50 | 9.27 | 7.70 | 7.99 | 9.60 |
| 100 | 12.42 | 10.24 | 10.72 | 12.77 |

**Table. 4.11 ï** Maximum variation $\Delta h_{max}$ of return values $h(R)$ due to the assumption of different threshold $h_{crit}$, for EES model for each storm duration $\Delta t$ and each return period $R$, for 46006 buoy.

Considering the return value $h(R)$ corresponding to a given threshold $h_{crit}$ and to a fixed return period $R$, for each of the considered storm duration $\Delta t$ (24, 48, 72, 96 hours) return values variability due to the assumption of different storm duration $\Delta t$ is investigated. The maximum variation in percentage between the maximum and the minimum return values is calculated and results are given in Tables 4.12 and 4.13. Results indicate that the variability of return values $h(R)$ due to the assumption of different storm duration $\Delta t$ is lower than that due to the thresholds

$h_{crit}$, being limited to the 3% and 7%, at 46035 and 46006 buoys respectively, for return period of 100 years. It decreases if for fixed $h_{crit}$ lower values of return period $R$ are considered.

| $h_{crit}$ (m) | 10 years $\Delta h_{max}$(%) | 20 years $\Delta h_{max}$(%) | 50 years $\Delta h_{max}$(%) | 100years $\Delta h_{max}$(%) |
|---|---|---|---|---|
| 3.9 | 0.70 | 0.89 | 1.19 | 1.44 |
| 4.6 | 1.10 | 1.45 | 2.10 | 2.63 |
| 5.2 | 0.69 | 1.01 | 1.50 | 1.89 |
| 5.9 | 0.75 | 1.09 | 1.57 | 1.94 |
| 6.5 | 0.30 | 0.41 | 0.58 | 0.72 |
| 7.2 | 0.65 | 0.95 | 1.28 | 1.50 |
| 7.8 | 0.61 | 0.97 | 1.37 | 1.63 |
| 8.5 | 0.32 | 0.56 | 0.87 | 1.08 |
| 9.1 | 0.18 | 0.51 | 1.02 | 1.42 |
| 9.8 | 0.13 | 0.39 | 0.74 | 0.98 |
| 10.4 | 0.06 | 0.44 | 1.24 | 1.91 |

**Table. 4.12 ï** Maximum variation $\Delta h_{max}$ of $h(R)$ for fixed $h_{crit}$ due to the assumption of different $\Delta t$ (from 24 hours to 96 hours), for 46035 buoy.

| $h_{crit}$ (m) | 10 years $\Delta h_{max}$(%) | 20 years $\Delta h_{max}$(%) | 50 years $\Delta h_{max}$(%) | 100years $\Delta h_{max}$(%) |
|---|---|---|---|---|
| 4.2 | 0.95 | 1.15 | 1.29 | 1.33 |
| 4.9 | 1.31 | 1.68 | 2.04 | 2.24 |
| 5.6 | 0.95 | 1.28 | 1.59 | 1.76 |
| 6.3 | 0.87 | 1.29 | 1.68 | 1.90 |
| 7.0 | 1.34 | 1.97 | 2.76 | 3.28 |
| 7.7 | 0.37 | 0.62 | 0.94 | 1.18 |
| 8.4 | 1.28 | 2.74 | 4.76 | 6.29 |
| 9.1 | 1.23 | 2.76 | 4.78 | 6.28 |
| 9.8 | 0.30 | 0.36 | 0.61 | 0.96 |
| 10.5 | 0.49 | 0.12 | 1.10 | 1.97 |
| 11.2 | 0.16 | 0.24 | 0.93 | 1.60 |

**Table. 4.13 ï** Maximum variation $\Delta h_{max}$ of $h(R)$ for fixed $h_{crit}$ due to the assumption of different $\Delta t$ (from 24 hours to 96 hours), for 46006 buoy.

### 4.2.2 Analysis with Equivalent Exponential Storm (EES) model

The calculation of return values of significant wave height $h(R)$ for given return periods $R$ by applying the EES model is performed by means of the following steps:

- fix a storm threshold $h_{crit}$ of significant wave height;
- identification of actual storm from time series of significant wave height by means of definition given in section (1.3);
- calculation of parameters $a$ and $b_E$ of EES associated to each actual storm;
- determination of base-height regression $\overline{b_E}(h)$ function for EESs;

- determination of the parameters $u$, $w$, $h_l$ of the distribution (1.10) of significant wave height;
- fixed $R$, solving iteratively Equation (2.28).

This procedure is repeated for $R$=10, 20, 50, 100 years and for each threshold $h_{crit}$ given in Table 4.1. The obtained return values of significant wave height are summarized in Tables 4.14 and 4.15. For each return period $R$ the difference in percentage between the maximum and the minimum return values $h(R)$ are calculated (Table 4.16). Results confirm a certain sensibility of the model to the threshold $h_{crit}$, but it is worth noting that it is quite limited and the maximum variation $\Delta h_{max}$ of return values $h(R)$ with the storm threshold $h_{crit}$ is less than 3% at each considered location.

| $h_{crit}$ (m) | 10 years h(m) | 20 years h(m) | 50 years h(m) | 100years h(m) |
|---|---|---|---|---|
| 3.9 | 13.20 | 13.94 | 14.90 | 15.61 |
| 4.6 | 13.20 | 13.93 | 14.89 | 15.60 |
| 5.2 | 13.23 | 13.98 | 14.93 | 15.64 |
| 5.9 | 13.23 | 13.98 | 14.93 | 15.64 |
| 6.5 | 13.28 | 14.02 | 14.98 | 15.69 |
| 7.2 | 13.30 | 14.04 | 15.00 | 15.70 |
| 7.8 | 13.32 | 14.07 | 15.04 | 15.75 |
| 8.5 | 13.34 | 14.08 | 15.03 | 15.74 |
| 9.1 | 13.42 | 14.16 | 15.11 | 15.82 |
| 9.8 | 13.40 | 14.18 | 15.16 | 15.88 |
| 10.4 | 13.50 | 14.29 | 15.29 | 16.00 |

**Table. 4.14 ï** Return values of significant wave height $h(R)$ for different return periods $R$, calculated applying the EES model for different thresholds $h_{crit}$, for 46035 buoy.

| $h_{crit}$ (m) | 10 years h(m) | 20 years h(m) | 50 years h(m) | 100years h(m) |
|---|---|---|---|---|
| 4.2 | 13.87 | 14.68 | 15.72 | 16.50 |
| 4.9 | 13.95 | 14.76 | 15.80 | 16.58 |
| 5.6 | 13.95 | 14.75 | 15.80 | 16.57 |
| 6.3 | 14.00 | 14.81 | 15.86 | 16.64 |
| 7.0 | 14.03 | 14.83 | 15.87 | 16.64 |
| 7.7 | 14.09 | 14.90 | 15.95 | 16.73 |
| 8.4 | 14.13 | 14.98 | 16.08 | 16.88 |
| 9.1 | 14.21 | 15.00 | 16.03 | 16.79 |
| 9.8 | 14.27 | 15.06 | 16.08 | 15.84 |
| 10.5 | 14.24 | 15.03 | 16.04 | 16.80 |
| 11.2 | 14.28 | 15.10 | 16.15 | 16.92 |

**Table. 4.15 ï** Return values of significant wave height $h(R)$ for different return periods $R$, calculated applying the EES model for different thresholds $h_{crit}$, for 46006 buoy.

| *Buoy* | 10 years $\Delta h_{max}(\%)$ | 20 years $\Delta h_{max}(\%)$ | 50 years $\Delta h_{max}(\%)$ | 100years $\Delta h_{max}(\%)$ |
|---|---|---|---|---|
| 46035 | 2.27 | 2.58 | 2.69 | 2.56 |
| 46006 | 2.96 | 2.86 | 2.74 | 2.55 |

**Table. 4.16 ï** Maximum variation $\Delta h_{max}$ of return values $h(R)$ due to the assumption of different threshold $h_{crit}$, for EES model for each return period $R$.

## 4.3. Conclusions

In this chapter a comparative extreme values analysis has been proposed by applying the EES and POT models. In particular a sensitivity analysis of the models to the threshold value has been carried out. Furthermore for the case of POT a further analysis is proposed to evaluate return values variability with different storm duration $\Delta t$ (24, 48, 72, 96 hours). Concerning the return values variability due to the storm threshold $h_{crit}$ the analysis has been performed by considering 11 threshold values from 1.5 times the average significant wave height $\overline{H}_s$ to 4 $\overline{H}_s$, with a step of 0.5 $\overline{H}_s$. The results have showed that for EES the difference between the maximum and the minimum wave heights predicted assuming different thresholds is less than 2.7% at 46035 and 3.2% at 46006. For POT this variation is about 15,25% at 46035 and 12.77% at 46006. For what concerns the amplitude of time interval $\Delta t$, the variation on the predicted wave height is less than 3% at 46035 and less than 7% at 46006. From a comparison of the results given by the two models it is clear that in both cases a certain sensibility to the thresholds is observed, which is limited in the case of EES and is quite important in the case of POT. Furthermore for POT method the sensibility to the threshold is combined with the sensibility to the storm duration and because of that this method is in general less efficient than the EES one.

# Chapter 5 ï Directional analysis of sea storms

*The chapter deals with the directional analysis of sea storms in the Atlantic and Pacific Oceans and in the Mediterranean Sea. The main focus of the study presented here is the investigation of variability of wave directions during sea storms. The analysis is carried out starting from significant wave height and wave direction time series. At the first stage storms are selected from time series without any condition on wave direction. Subsequently the directional analysis of each identified storm is performed by considering the wave direction associated with each sea state during the storm. A methodology to classify the selected storms as* ***ñ****directional storms****ò*** *pertaining to a certain directional sector is proposed. Finally a technique to determine the main directions of occurrence of the strongest sea storms and the appropriate width of directional sectors centred on these directions is suggested. Results are useful for different kind of applications such as directional long-term predictions for the design process of angle-dependent structures or for wave energy converter devices.*

## 5.1. Introduction

It is important, for engineering applications, to consider directionality during storms to develop criteria for the prediction of extremes values that take into account the wave direction, and enable to determine the long-term statistics for any directional sector. This approach may be very useful in determining the directional extreme values offshore, which will be propagated in coastal areas to calculate the design wave for any maritime structure. Recently *Jonathan and Evans (2007)* developed an approach to establish appropriate directional criteria and an associated omnidirectional criterion. *Jonathan et al. (2008)* showed that a directional extreme model is generally better than a model which ignores directionality and omnidirectional criteria derived from a directional model are more accurate and should be preferred. Many models such as Peak Over Thresholds divide a single storm in sub-sets associated to different directional sectors, but could be more appropriate to develop criteria that enable to associate each storm to a given directional sector. The main objective of the analysis presented here is to introduce the

concept of directional storm that could be the base for a physically based model for directional long-term analysis. The variability of direction during storm history (which is defined as the significant wave height in time domain during the evolution of the storm) is investigated. Then a criterion to classify storms as "directional storms" pertaining to a certain sector is proposed. Furthermore a methodology for the determination of the centre and the width of the directional sector is given. This kind of analysis are useful for several kind of application such us directional long-term predictions, design process of angle-dependent devices *(Arena et al. 2014)*, but also to check the correct operation of buoys if data of different kind are compared.

## 5.2. Directional sea storms

To define a sea storm as a "directional storm" pertaining to a certain sector $(\vartheta_i \pm \Delta\vartheta)$ the variability of wave direction during the storm has to be investigated. The analysis proposed in this chapter (see section 5.4) shows that during the storms a certain variability of wave direction is observed: it is quite relevant in storm queues (lower sea states) and tend to reduces itself near storm peak (stronger sea states). Directional sea storms may be defined as a sequence of sea states in which the significant wave height exceeds a given threshold $h_{crit}$ and the wave direction is within a given sector $(\vartheta_i \pm \Delta\vartheta)$. Because of the strong variability of wave direction in storm queues to introduce a directional criterion should be appropriate to refer to the wave direction of the sea state above a fixed threshold $h$'.

Let us determine the sea storms from the whole time series of significant wave height (whichever the wave direction is). From the whole set of sea storms, we may define:

(i) a sea storm as a " directional storm" with wave direction within the sector $(\vartheta_i \pm \Delta\vartheta)$, if the wave direction at the maximum significant wave height $H_{s\max}$ falls in $(\vartheta_i \pm \Delta\vartheta)$;

(ii) a sea storm as a " directional storm" with wave direction within the sector $(\vartheta_i \pm \Delta\vartheta)$, if the average wave direction $\overline{\vartheta}(t)$ calculated for the sea states with $H_s > h'$ falls in $(\vartheta_i \pm \Delta\vartheta)$.

Note that in (ii), if $h' = h_{crit}$ the whole storms are considered. Furthermore definition (ii) is related to the wave direction trend above a fixed threshold of significant wave height. In the

paper it is applied for threshold $h' \geq 0.5 H_{s\max}$. Figures 5.2 and 5.3, show some examples of sea storms with wave direction during the sea states which characterize the storms.

Concerning to the sector $(\vartheta_i \pm \Delta\vartheta)$ it is defined starting from the direction $\vartheta_i$ and the width $\Delta\vartheta$. It is worth noting that it has no meaning to refer to directional sector of minor relevance from which a few number of (less intense) storms occur, when a directional analysis is done. For this reason the sectors to which is appropriate to focalize are those centered on the main or secondary (if any) directions from which the strongest storms occur. Thus to classify directional storms first the main and secondary directions have to be identified and then the most appropriate $\Delta\vartheta$ has to be determined. Increasing $\Delta\vartheta$ it will result an increasing number of storms belonging to any considered sector.

## 5.3. Statistical properties of waves in a directional sea storm

The statistical properties of waves during storms were investigated by *Borgman (1970, 1973)*, who obtained the cumulative distribution function $P(H_{\max} < H)$ of the extreme individual wave height in a sea storm. This probability is obtained starting from the crest-to-trough wave height cumulative distribution in a sea state.

To generalize the Borgman's results to a directional storm associated to a direction $\vartheta_i \pm \Delta\vartheta$, by assuming the stochastic independence of wave heights, we have

$$P(H_{\max} < H; \vartheta_i \pm \Delta\vartheta) = \prod_{i=1}^{N_s} \left[ P(H; H_s = h_i, \vartheta_i \pm \Delta\vartheta) \right]^{D_t / \overline{T}(h_i)} \tag{5.1}$$

where $D_t$ is the sea state duration, $\overline{T}$ the mean period *(Rice, 1958)* and $N_s$ is the number of sea states during the storms.

The probability that a wave has height smaller than $H$ in a sea state with significant wave height $H_s$ equal to $h$ is related to the wave direction sector $\vartheta_i \pm \Delta\vartheta$ by means of:

$$P(H; H_s = h, \vartheta_i \pm \Delta\vartheta) = \begin{cases} = 1 - \exp\left[ -\dfrac{4}{1+\psi^*} \left( \dfrac{H}{h} \right)^2 \right] & \text{if } \vartheta_i - \Delta\vartheta < \vartheta_d \leq \vartheta_i + \Delta\vartheta \\ = 1 \quad \text{otherwise} \end{cases} \tag{5.2}$$

where $\vartheta_d$ is the dominant wave direction of the sea state and $\psi^*$ is the narrow bandedness parameter of the spectrum and it is equal to the ratio, in absolute value, between the absolute minimum and the absolute maximum of the covariance function of the sea state. It is equal to 1 for an infinitely narrow spectrum [note that in this condition, Equation (5.2) gives the Rayleigh distribution, to 0.73 for a mean JONSWAP spectrum (*Hasselmann et al.*, 1973) and to 0.65 for a *Pierson-Moskowitz* (1964) spectrum. Then, the cumulative distribution function $P(H_{\max} < H; \vartheta_i \pm \Delta\vartheta)$, following the Borgman's logic, is written in an integral form as

$$P(H_{\max} < H; \vartheta_i \pm \Delta\vartheta) = \exp\left\{\int_0^D \frac{\ln\left[1 - P\left(H; H_s = h(t), \vartheta_i \pm \Delta\vartheta\right)\right]}{\overline{T}[h(t)]} \mathrm{d}t\right\} \tag{5.3}$$

where $D$ is the storm duration. Finally, the maximum expected wave height $\overline{H_{\max}}$ during the sea storm is obtained as the integral over $(0, \infty)$ of the probability of exceedance $1 - P(H_{\max} < H; \vartheta_i \pm \Delta\vartheta)$.

## 5.4. Data analysis

This chapter deals with the directional analysis of sea storms carried out by processing wave data coming from different sources: data given by directional buoys of RON and NOAA networks, and by HIPOCAS project (see section 1.5). Six locations in Atlantic Ocean from HIPOCAS (Figure 5.1a), one in central Mediterranean Sea (Figure 5.1a) from RON network and one in US coast in Pacific Ocean (Figure 5.1b) from NOAA-NDBC are considered. The analysis is performed by processing significant wave height and wave direction time series. At the first stage sea storms are extrapolated from significant wave height time series by means of the definition given in section (1.3) which doesn't take into account the wave direction, but it is only related to the average significant wave height at the considered site (see Table 5.1). Then the directional analysis is done by considering the sequence of sea states during each sea storm with the sequence of the related wave directions (see Figures 5.2 and 5.3). First only the wave direction associated to the peak of the storm $H_{s\,\max}$ is regarded. Figures 5.4 and 5.5 (left) show the wave direction at the sea state with the maximum significant wave height (storm peak) $H_{s\max}$ versus $H_{s\max}$ (each point represents a storm). From the figures it is clear that at each considered site it is possible to identify one or more main directions from which the strongest storms occur.


**Figure. 5.1 ï** a) Locations of the analysed points from HIPOCAS and of Mazara del Vallo buoy from RON network; b) Location of 46042 buoy from NOAA-NDBC.

| Location | $\overline{H_s}$(m) | $h_{crit}$(m) | N°storm($H_{smax}$>2$h_{crit}$) |
|---|---|---|---|
| HIPOCAS(1) | 2,4 | 3,6 | 137 |
| HIPOCAS(2) | 2,79 | 4,19 | 115 |
| HIPOCAS(3) | 2,272 | 4,08 | 163 |
| HIPOCAS(4) | 3,31 | 4,96 | 215 |
| HIPOCAS(5) | 3,55 | 5,32 | 269 |
| HIPOCAS(6) | 3,51 | 5,27 | 227 |
| MAZARA(RON) | 0,97 | 1,45 | 232 |
| 46042- NDBC | 2,21 | 3,31 | 34 |

**Table. 5.1 ï** Average significant wave height $\overline{H}_s$, critical threshold $h_{crit}$ and number of storms with maximum significant wave height $H_{s\max} \geq 2h_{crit}$.

For example, one at HIPOCAS (1) ($\vartheta_1 = 300°$), two at RON ($\vartheta_1 = 280°$, $\vartheta_2 = 140°$), three at HIPOCAS (6) ($\vartheta_1 = 80°$, $\vartheta_2 = 190°$, $\vartheta_3 = 360°$) and three at NOAA 46042 ($\vartheta_1 = 320°$, $\vartheta_2 = 160°$, $\vartheta_3 = 10°$), (see Tables 5.2 and 5.3). Subsequently the average wave direction during the whole storm is calculated starting from wave direction of all sea states (Figures 5.4 and 5.5 right). Then a comparison between the average direction and the direction at storm peak is shown in Figure 5.6: these two directions are very close to each other for most of the storms, but in some cases a difference is observed. Then, a deeper analysis is proposed by considering the strongest storms ($H_{smax} \geq 2h_{crit}$), by calculating the standard deviation of wave direction and by considering its average values for classes of maximum significant wave height $H_{smax}$. The same calculation is done for the whole storm history first and then by considering only sea sates above a fixed threshold $h^{\hat{o}}$ (from $0{,}5H_{smax}$ to $0{,}8H_{s\,max}$) of significant wave height. Figure 5.7 shows the average value of the standard deviation of direction versus the average maximum significant wave height $\overline{H}_{s\max}$ for storms with $H_{smax}$ in given classes of $H_s$. The results show that during the storms a certain variability of wave direction it is observed: it is quite relevant if the whole storm history is considered and tends to reduce itself if only sea states above a fixed threshold $h^{\hat{o}}$ of significant wave height are taken into account. In particular the standard deviation of wave direction decreases for increasing thresholds $h^{\hat{o}}$. It is due to the strong variability of wave direction in storm queues (less intense sea states). Starting from the above results the definitions 5.2(i) and 5.2(ii) of directional storm are introduced and applied to classify the identified storms (without any condition of wave direction) as directional storms pertaining

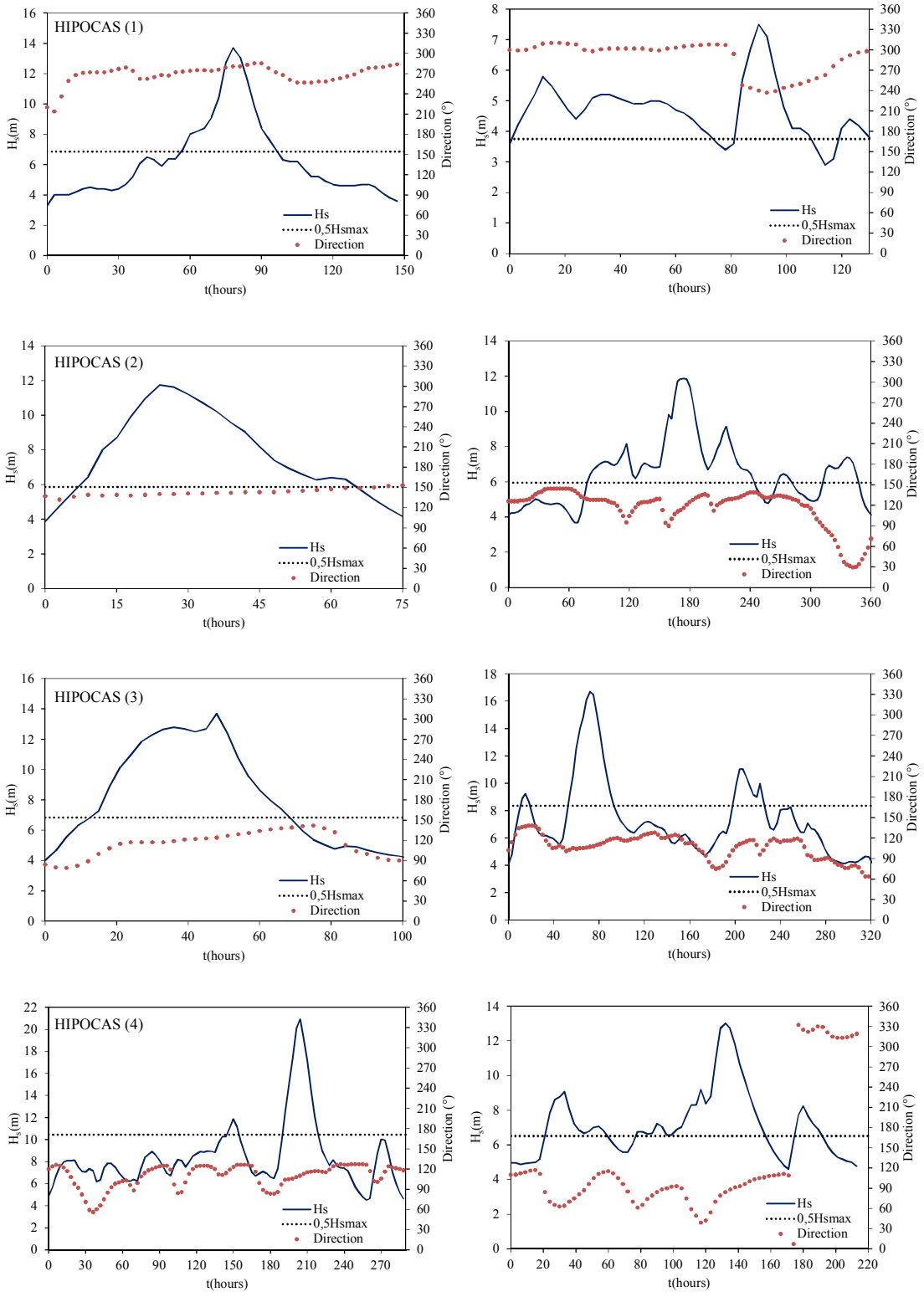


**Figure. 5.2** – Some storms histories: significant wave height $H_s$ and related wave direction during the storms with quite regular (left) and irregular (right) trends of wave direction.

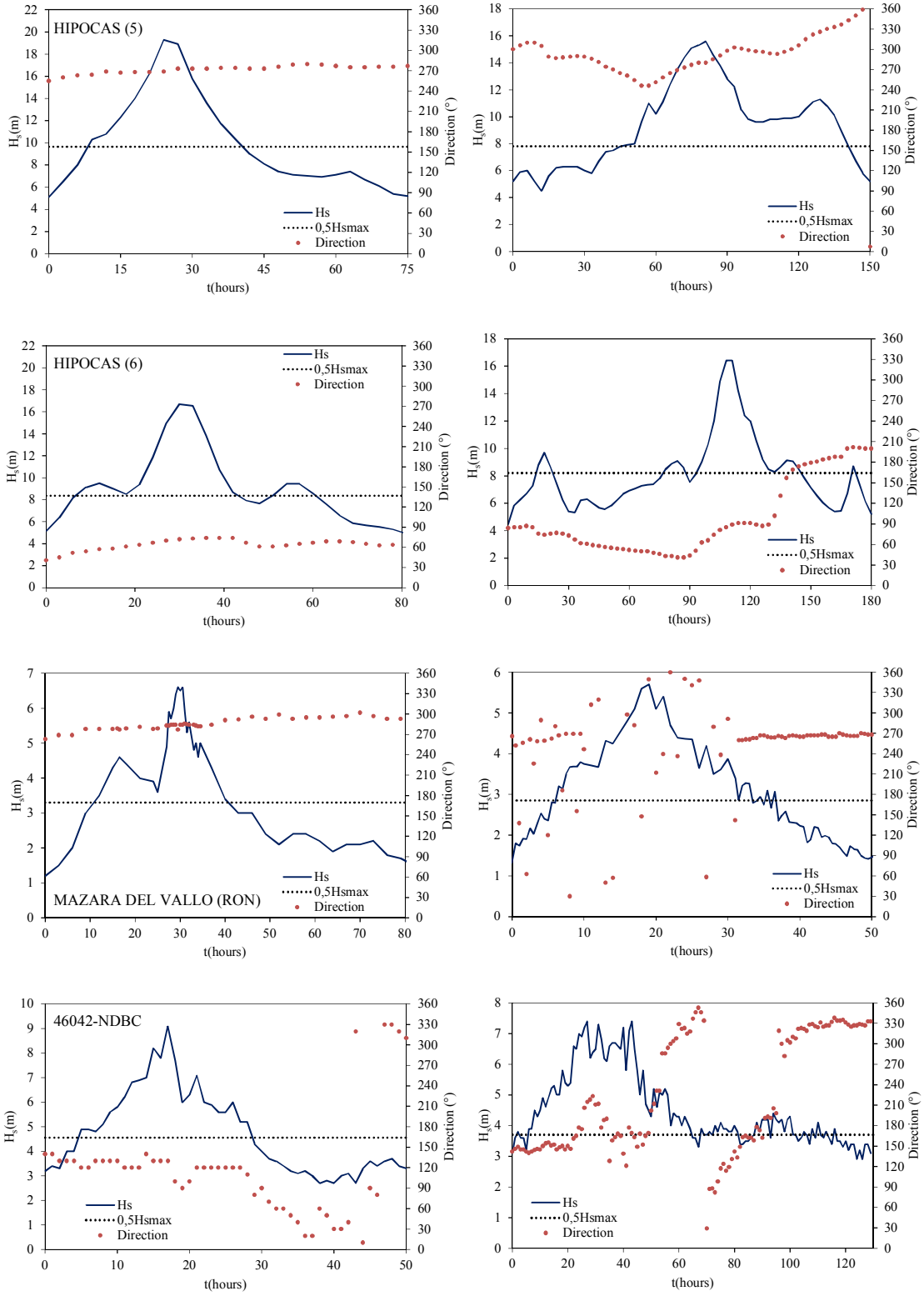


**Figure. 5.3 ï** Some storms histories: significant wave height $H_s$ and related wave direction during the storms with quite regular (left) and irregular (right) trends of wave direction.

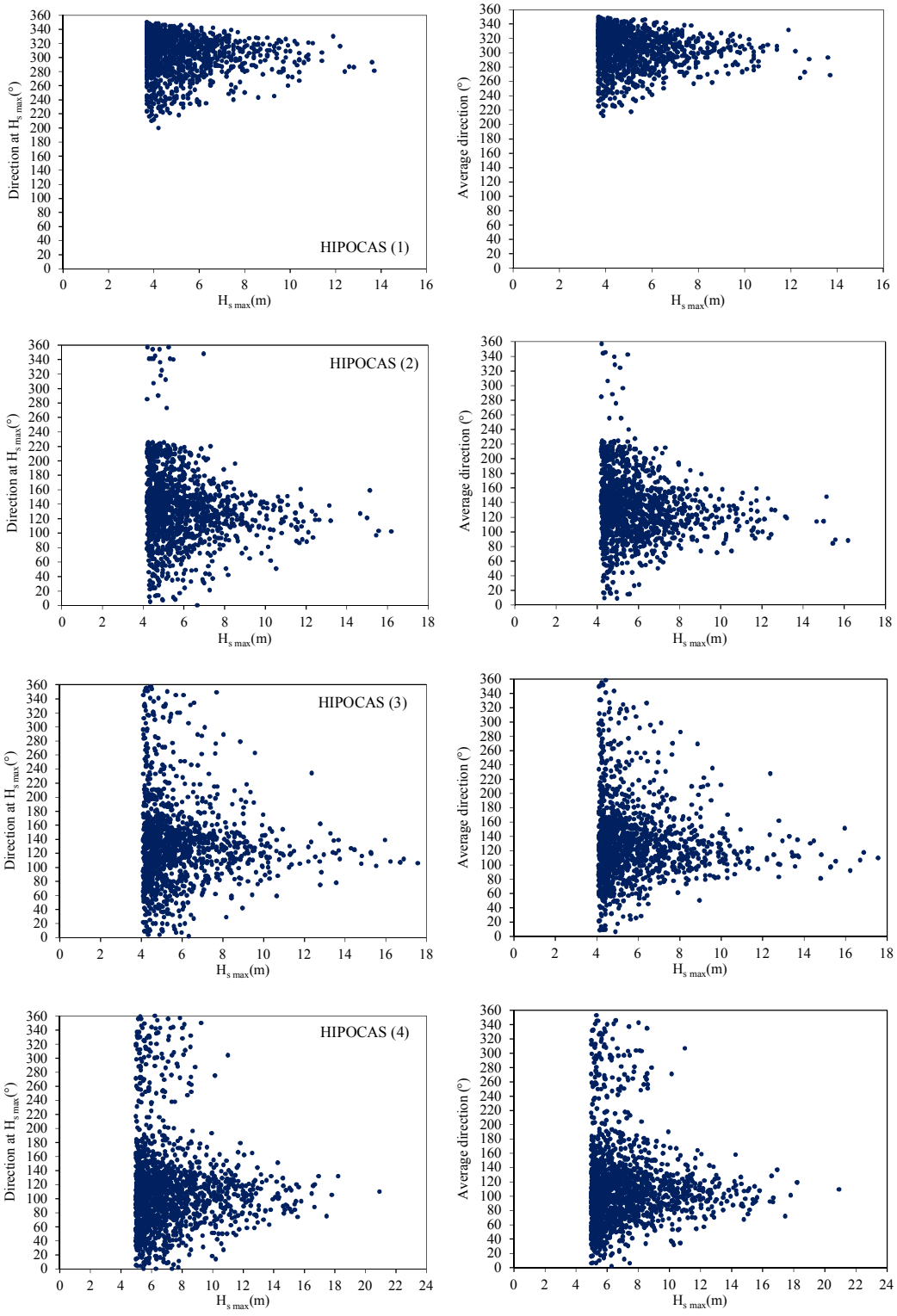


**Figure. 5.4 ï** Wave direction at maximum significant wave height $H_{s\,max}$ versus $H_{s\,max}$ (left), average wave direction during the storm versus $H_{s\,max}$ (right).

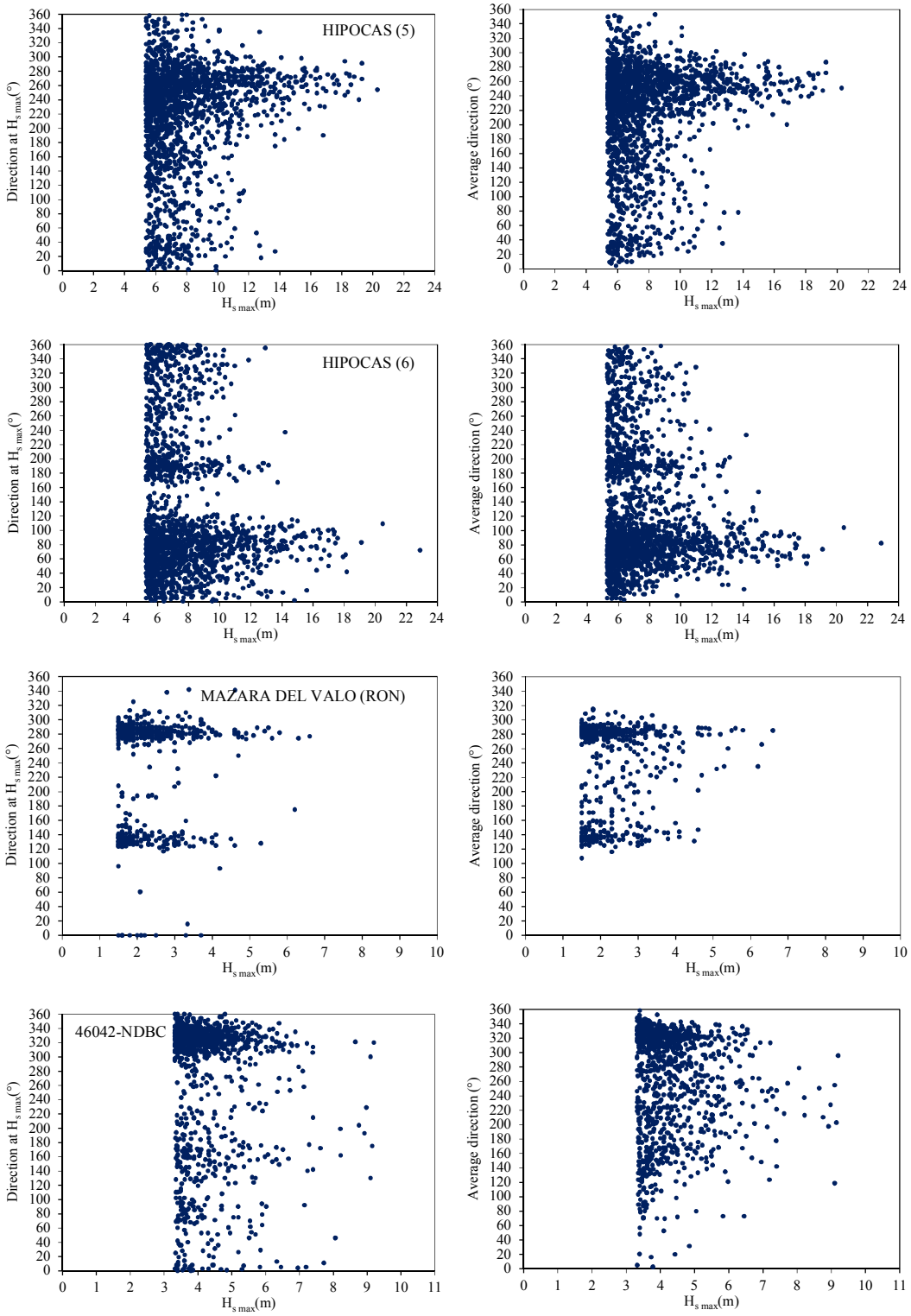


**Figure. 5.5 ï** Wave direction at maximum significant wave height $H_{s\,max}$ versus $H_{s\,max}$ (left), average wave direction during the storm versus $H_{s\,max}$ (right).

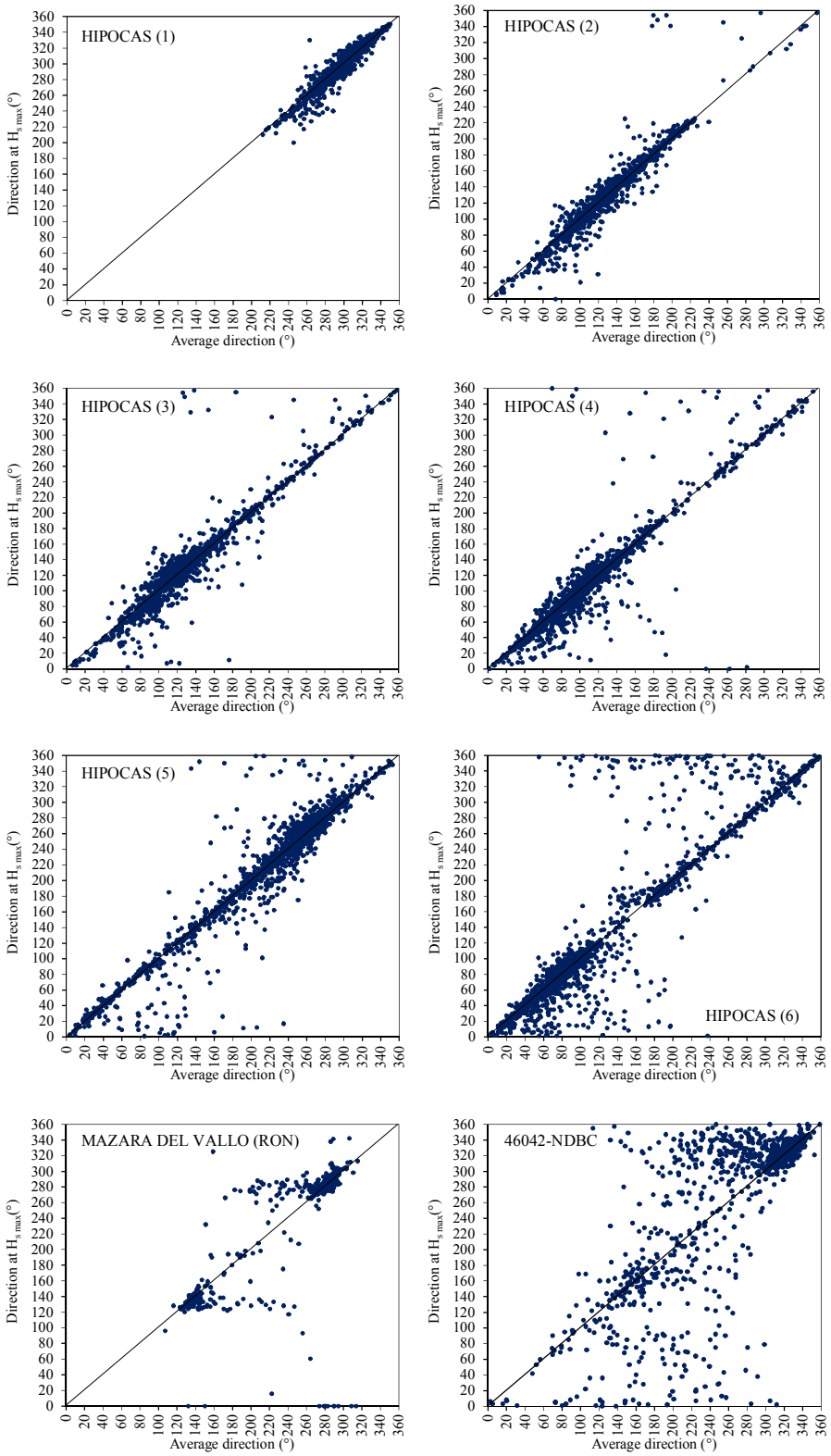


**Figure. 5.6 ï** Wave direction at maximum significant wave height $H_{s\,max}$ versus average wave direction during the storm.

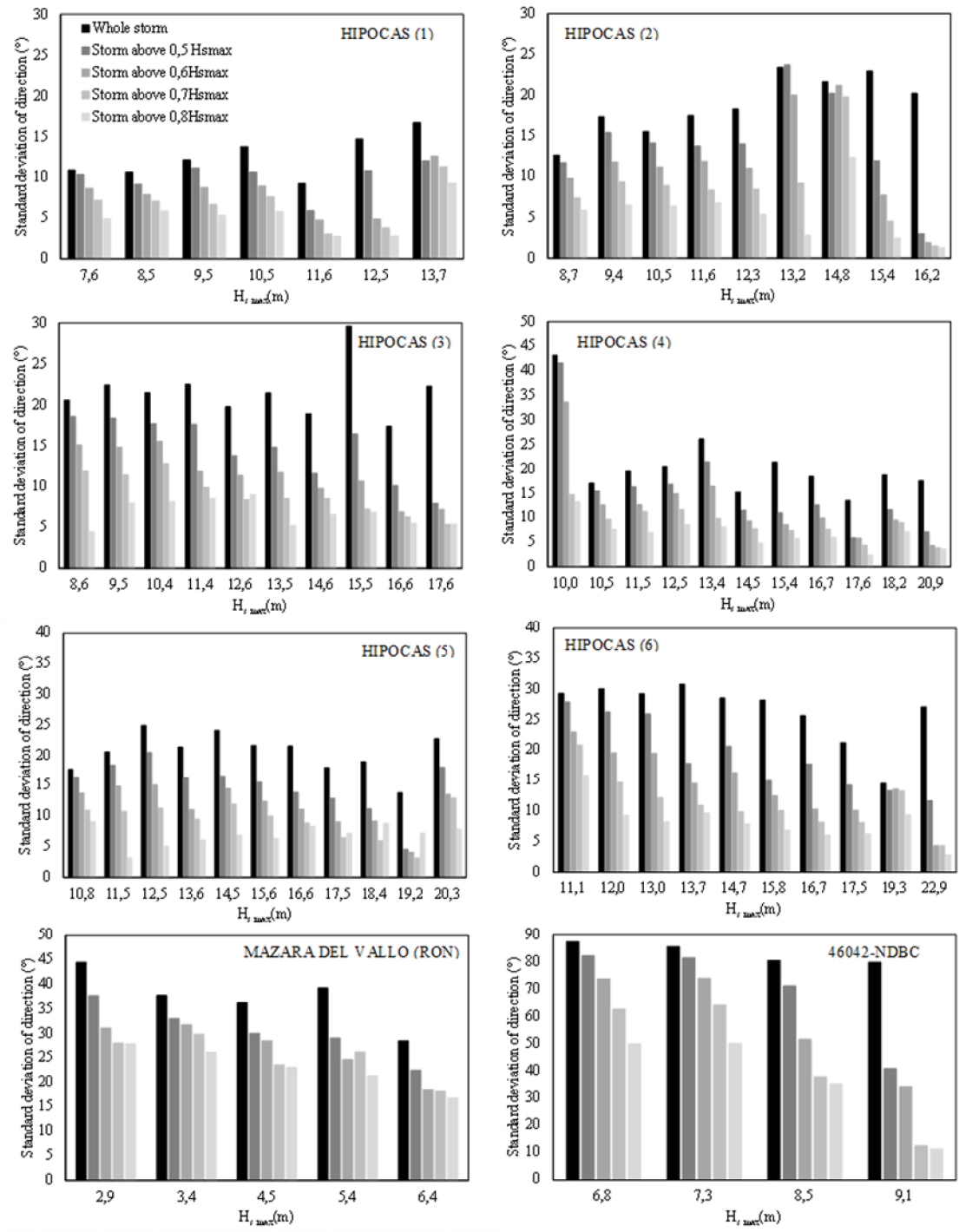


**Figure. 5.7 ï** Average standard deviation of wave direction calculated above a fixed threshold of significant wave height $H_s$ (from 0,5 $H_{smax}$ to 0,8 $H_{smax}$) versus average maximum significant wave height $\overline{H}_{s\,max}$ , for the storms with $H_{smax} \geq 2h_{crit}$.

to a given directional sector $(\vartheta_i \pm \Delta\vartheta)$. The direction $\vartheta_i$ is fixed as the wave direction from which the strongest storm occurs and for the width $\Delta\vartheta$ values of 10°, 20°, 30° are considered. Tables 5.2 and 5.3 show the number of storms classified by means of 5.2(i) and 5.2(ii) as directional storms in the directional sector $(\vartheta_i \pm \Delta\vartheta)$ for each of the main directions $\vartheta_i$ identified and for each considered with $\Delta\vartheta$ and for $h$'=0,5$H_{smax}$. The number of directional storms pertaining to a given directional sector $(\vartheta_i \pm \Delta\vartheta)$ increases for increasing values of the width $\Delta\vartheta$. Furthermore definitions 5.2(i) and 5.2(ii) tend to give the same result if widths of 30° or more are considered.

| | | | | |
|---|---|---|---|---|
| HIPOCAS(1) | $\vartheta_1$=305° | $\Delta\vartheta$=10° | $\Delta\vartheta$=20° | $\Delta\vartheta$=30° |
| | (i) | 52 | 97 | 121 |
| | (ii) | 66 | 99 | 121 |
| HIPOCAS(2) | $\vartheta_1$=110° | $\Delta\vartheta$=10° | $\Delta\vartheta$=20° | $\Delta\vartheta$=30° |
| | (i) | 42 | 64 | 87 |
| | (ii) | 35 | 69 | 94 |
| HIPOCAS(3) | $\vartheta_1$=110° | $\Delta\vartheta$=10° | $\Delta\vartheta$=20° | $\Delta\vartheta$=30° |
| | (i) | 59 | 90 | 118 |
| | (ii) | 55 | 98 | 124 |
| HIPOCAS(4) | $\vartheta_1$=110° | $\Delta\vartheta$=10° | $\Delta\vartheta$=20° | $\Delta\vartheta$=30° |
| | (i) | 73 | 120 | 156 |
| | (ii) | 76 | 138 | 172 |
| | $\vartheta_2$=300° | $\Delta\vartheta$=10° | $\Delta\vartheta$=20° | $\Delta\vartheta$=30° |
| | (i) | 1 | 1 | 2 |
| | (ii) | 1 | 1 | 2 |
| HIPOCAS(5) | $\vartheta_1$=260° | $\Delta\vartheta$=10° | $\Delta\vartheta$=20° | $\Delta\vartheta$=30° |
| | (i) | 81 | 156 | 196 |
| | (ii) | 104 | 180 | 215 |
| | $\vartheta_2$=30° | $\Delta\vartheta$=10° | $\Delta\vartheta$=20° | $\Delta\vartheta$=30° |
| | (i) | 3 | 5 | 7 |
| | (ii) | 2 | 4 | 7 |
| HIPOCAS(6) | $\vartheta_1$=80° | $\Delta\vartheta$=10° | $\Delta\vartheta$=20° | $\Delta\vartheta$=30° |
| | (i) | 80 | 132 | 169 |
| | (ii) | 82 | 143 | 168 |
| | $\vartheta_2$=190° | $\Delta\vartheta$=10° | $\Delta\vartheta$=20° | $\Delta\vartheta$=30° |
| | (i) | 10 | 13 | 15 |
| | (ii) | 8 | 12 | 14 |
| | $\vartheta_3$=360° | $\Delta\vartheta$=10° | $\Delta\vartheta$=20° | $\Delta\vartheta$=30° |
| | (i) | 1 | 1 | 3 |
| | (ii) | 0 | 3 | 10 |

**Table. 5.2 ï** Number of directional storms pertaining to directional sector $\vartheta_{i=1,2,3} \pm \Delta\vartheta$, classified by means of criteria 2.1 (i) and 2.1 (ii) at each location from HIPOCAS.

It is worth noting that the main purpose of the analysis proposed here is related to the introduction of a physically based approach which enables us to associate each storm to a given directional sector. Let us consider the storms with maximum significant wave height $H_{smax} \geq 2h_{crit}$ (see Table 5.1), by applying definition 5.2(i) or 5.2(ii) with a width $\Delta\vartheta$ of 30° it is possible to classify more than 80% of the storms as directional storms at both HIPOCAS (1) and HIPOCAS (6), more than 70% at Mazara Del Vallo RON and more than 60% at 46042-NDBC. The lower percentages for buoys data may be related to the greater variability in the data probably due to instruments malfunction. Finally to test the validity of the criterion the maximum expected wave $\overline{H}_{max}$ heights calculated for the whole storm (storm selected without any condition on wave direction) and for directional storm are calculated are calculated and compared (See Figures 5.8 and 5.9). Results show that if a width $\Delta\vartheta$ of 30° is considered the maximum expected wave height of the whole storm and of the directional storm tend to converge.

| MAZARA (RON) | $\vartheta_1$=280° | $\Delta\vartheta$=10° | $\Delta\vartheta$=20° | $\Delta\vartheta$=30° |
|---|---|---|---|---|
| | (i) | 107 | 126 | 143 |
| | (ii) | 95 | 116 | 146 |
| | $\vartheta_2$=140° | $\Delta\vartheta$=10° | $\Delta\vartheta$=20° | $\Delta\vartheta$=30° |
| | (i) | 28 | 49 | 50 |
| | (ii) | 28 | 39 | 41 |
| 46042-NDBC | $\vartheta_1$=320° | $\Delta\vartheta$=10° | $\Delta\vartheta$=20° | $\Delta\vartheta$=30° |
| | (i) | 7 | 11 | 11 |
| | (ii) | 3 | 4 | 6 |
| | $\vartheta_2$=160° | $\Delta\vartheta$=10° | $\Delta\vartheta$=20° | $\Delta\vartheta$=30° |
| | (i) | 2 | 7 | 8 |
| | (ii) | 0 | 1 | 1 |
| | $\vartheta_3$=10° | $\Delta\vartheta$=10° | $\Delta\vartheta$=20° | $\Delta\vartheta$=30° |
| | (i) | 3 | 11 | 11 |
| | (ii) | 0 | 4 | 6 |

**Table. 5.3 ï** Number of directional storms pertaining to directional sector $\vartheta_{i=1,2,3} \pm \Delta\vartheta$, classified by means of criteria 5.2 (i) and 5.2. (ii) at Mazara del Vallo (RON) and at 46042 NDBC.

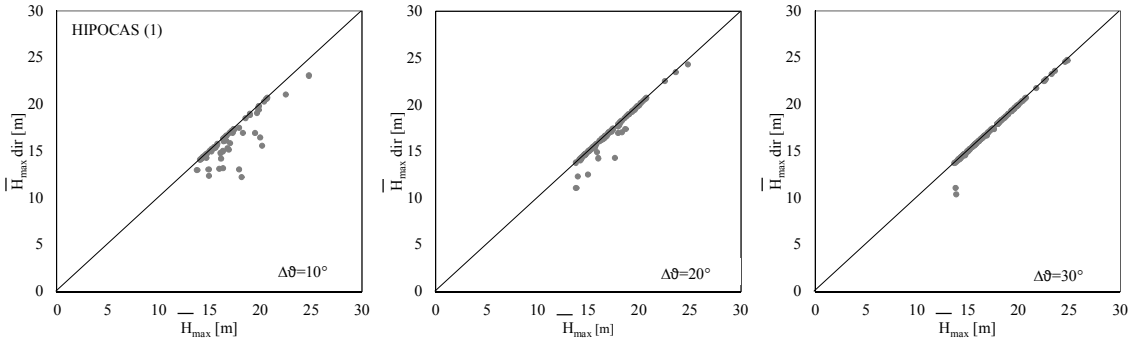


**Figure. 5.8 ï** Maximum expected wave height $\overline{H}_{\max}$ for directional storms pertaining to the directional sector $\vartheta_1 \pm \Delta\vartheta$ versus maximum expected wave height $\overline{H}_{\max}$ for storm selected without condition about wave direction, for the storms with $H_{smax} \geq 2h_{crit}$ at HIPOCAS (1).

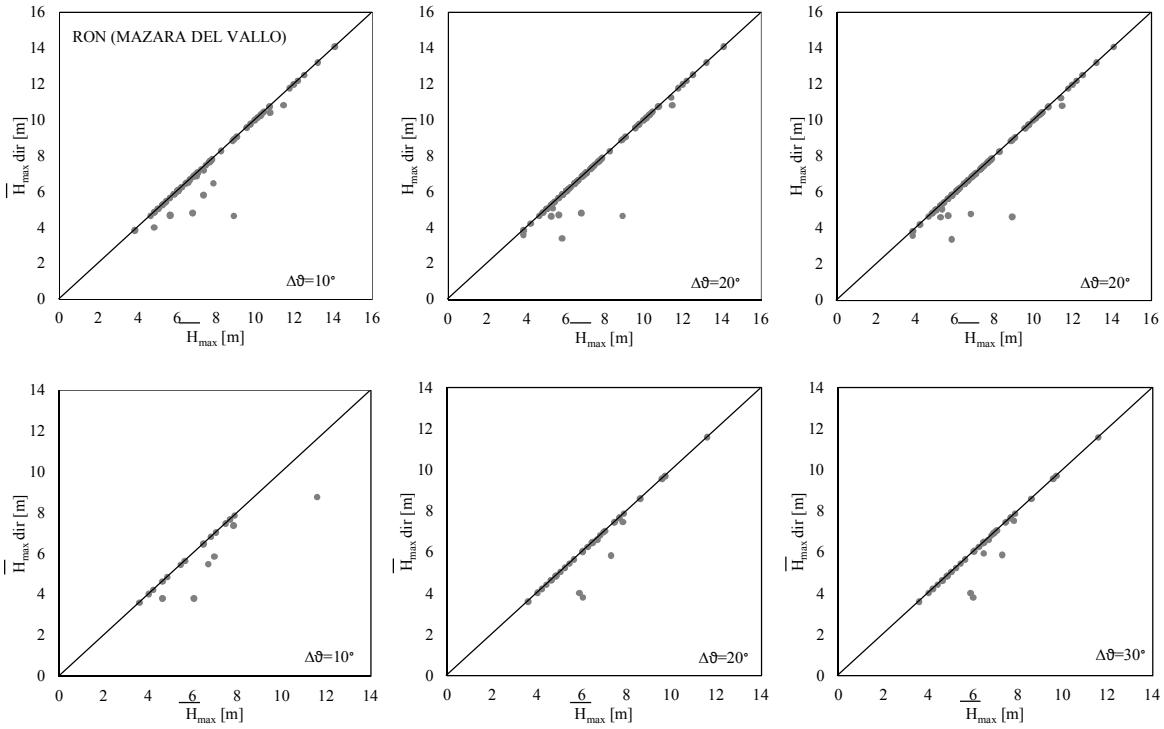


**Figure. 5.9 ï** Maximum expected wave height $\overline{H}_{\max}$ for directional storms pertaining to the directional sectors $\vartheta_1 \pm \Delta\vartheta$ (top) and $\vartheta_2 \pm \Delta\vartheta$ (bottom) versus maximum expected wave height $\overline{H}_{\max}$ for storm selected without condition about wave direction, for the storms with $H_{smax} \geq 2h_{crit}$ at Mazara Del Vallo (RON).

## 5.5. conclusions

The analysis proposed in the chapter has investigated the variability of wave direction during sea storms, showing how it is increased for lower sea states (storm queues) and is reduced by considering the wave direction associated to sea states above increasing thresholds of significant wave height (storm peak). The comparison between average wave direction during storm and direction at $H_{smax}$ has revealed that for most of the storm these two directions are quite similar. A definition of directional sea storm pertaining to a given directional sector is introduced. It has been found as the number of directional storms pertaining to a given directional seector increases for increasing values of the width of the directional sector. Finally it has been proved that an appropriate amplitude for the directional sectors may be of 60°(width $\Delta\vartheta$ of 30°) because it enables to classify as direcional storm a quite great part of the storm set giving the same maximum expected wave height for the whole storm and the directional storm.

# Chapter 6 ï Long-term statistics of ocean storms starting from time series of partitioned sea states

*This chapter deals with the long-term statistic of ocean storms carried out starting from time series of partitioned sea states. Data from HOMERE database (see section 1.5) are used as input. The main focus of the study presented here is to evaluate the variability of return values of significant wave height due to having neglected the contribution of swell components to the significant wave height data. In particular return values of significant wave height corresponding to return periods of 5, 10, 20, 50, 100 years are calculated by applying the Equivalent triangular Storm (ETS) model to the time series of total significant wave height (contribution of both wind and swell components) first and then to the wind sea only. Three different sites with different characteristics are considered: two wind sea dominated and one with comparable wind and swell seas. Results show how in locations dominated by the wind sea the swell component may by neglected in long-term predictions, while for locations with swell and wind comparable seas neglecting swell significant differences in return values may be appreciated.*

## 6.1.Data analysis

The analysis proposed in this chapter is carried out by considering time series of partitioned sea states, separated wind and swell significant wave heights, at three locations among HOMERE database (see Figure 6.1). The analysis is performed by processing first total significant wave height $H_{st}$ time series (combined wind and swell components) and then only wind significant wave height $H_{sw}$ in order to evaluate return values variability neglecting swell components. Three locations are considered for the application (see Figure 6.1). At each site first the average significant wave heights for total, wind and swell components are calculated (Table 6.1). The calculation of the average total significant wave height is useful to determine the threshold $h_{crit}$ used for the storms identification. Instead, the average wind and swell significant wave heights are compared to each other in order to understand if the considered site

is wind or swell dominated, or it is characterized by comparable wind and swell seas. Results show that both HOMERE (1) and HOMERE(2) are wind dominated while HOMERE(3) has comparable wind and swell seas. Storms are identified starting from total significant wave height time series by means of Boccotti's definition given in section (1.3).

| **Location** | $\overline{H}_{s\,tot}$ (m) | $h_{crit}$ (m) | $\overline{H}_{s\,w}$ (m) | $\overline{H}_{s\,s}$ (m) | $H_{s\,max\,tot}$ (m) | $H_{s\,max\,w}$ (m) | $H_{s\,max\,s}$ (m) |
|---|---|---|---|---|---|---|---|
| **HOMERE(1)** | 1,01 | 1,65 | 0,97 | 0,38 | 7,998 | 7,998 | 4,426 |
| **HOMERE(2)** | 1,55 | 2,32 | 1,35 | 0,55 | 8,670 | 8,670 | 5,873 |
| **HOMERE(3)** | 2,65 | 3,98 | 1,79 | 1,63 | 9,875 | 9,875 | 6,431 |

**Table. 6.1 ï**. Average total significant wave height, critical threshold, average wind sea significant wave height, average swell sea significant wave height, maximum total, wind sea and swell sea significant wave heights.

Then for each identified storm the sequence of the wind significant wave height during the given storm is also considered and the ETS model is applied to both storm histories (see Figure 6.2) to calculate return values of significant wave height $h(R)$ for return periods $R$ of 5, 10, 20, 50, 100 years. The analysis is performed by means of the following steps:

- determination of parameters of the distribution $P(H_s>h)$ of both total and wind significant wave heights (Figure 6.3) fitting the data with the two-parameters Weibull distribution obtained from Equation (1.10) with $h_l=0$;
- calculation of ETSs starting from total and wind actual storm histories;
- determination of base-heights regression functions for ETSs both for total and wind sea;
- calculation of return values $h(R)$ for $R$=5, 10, 20, 50, 100 years first by considering the distribution of significant wave height and the base height regression estimated starting from total significant wave height and then by considering those obtained from wind significant wave height time series.
- comparison of the obtained return values for the evaluation of return values variability due to having neglected swell components.

The parameters of the distribution of both total and wind sea significant wave height are determined following the procedure explained in section (1.3.2). The representation in the Weibull plot is given in Figure 6.3. The related parameters are summarised in Table 6.2.

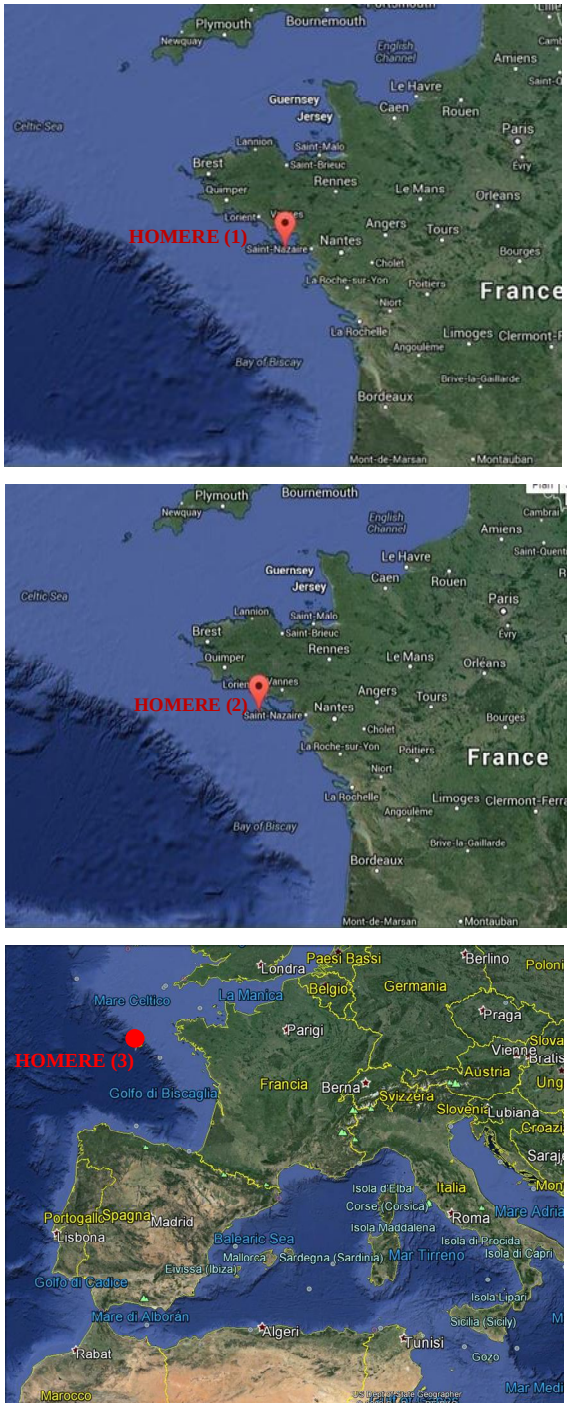


**Figure. 6.1 ï** Locations of the considered sites among HOMERE database.

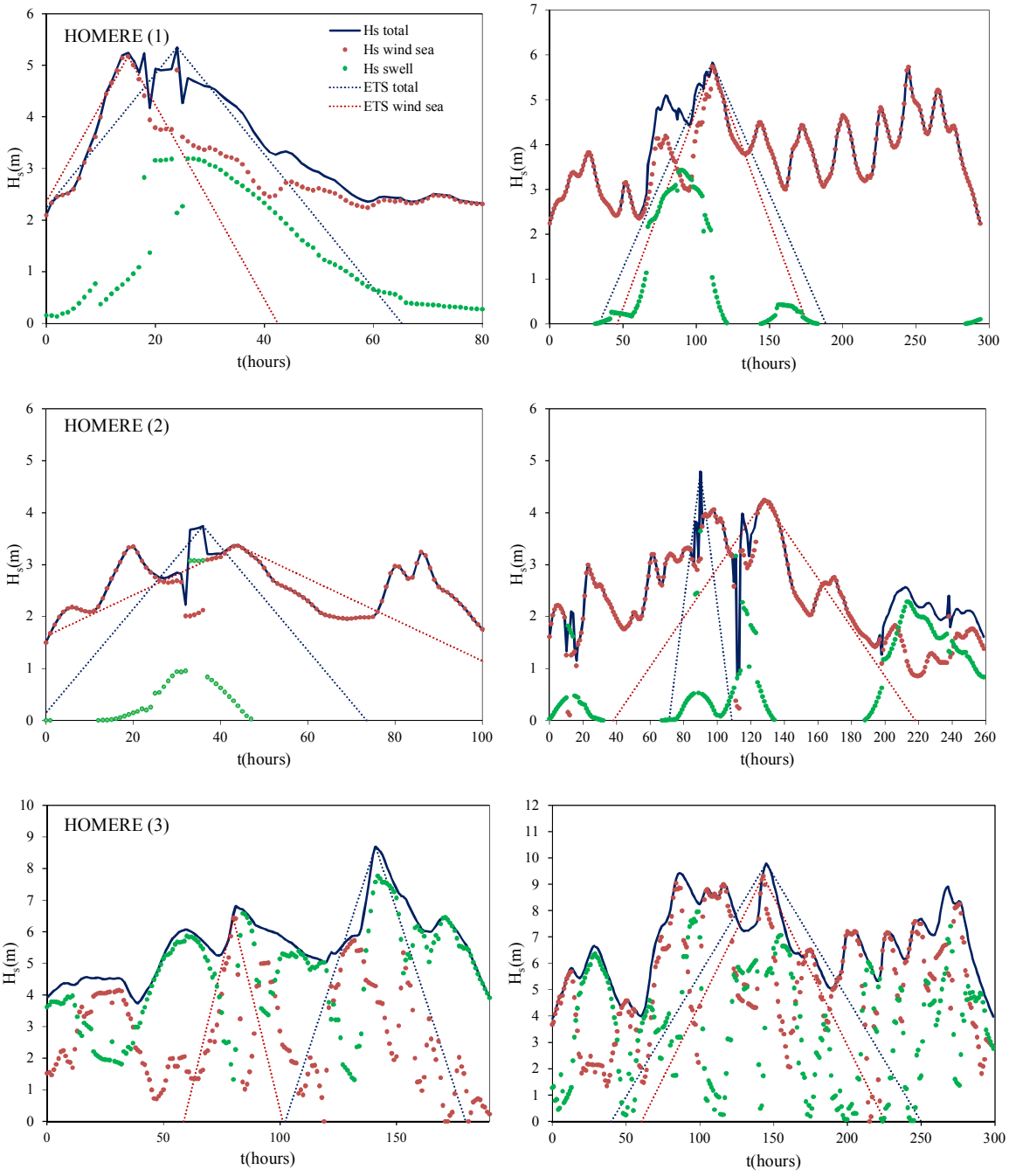


**Figure. 6.2 ï** Some actual storms, total, wind sea and swell sea significant wave heights during the storms, associated ETSs calculated with $H_{st}$ and $H_{sw}$.

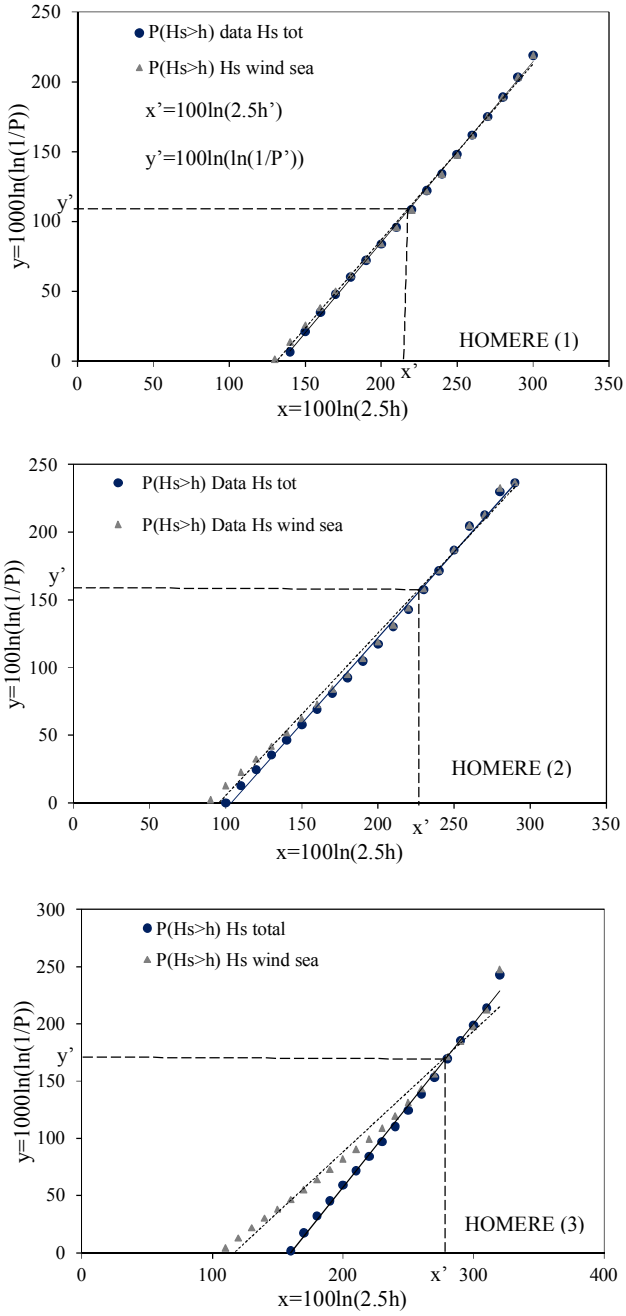


**Figure. 6.3ï** Distribution $P(H_s>h)$ total and wind sea significant wave heights.

| Location | $u_{total}$ | $w_{total}$ (m) | $u_{wind}$ | $w_{wind}$ (m) |
|---|---|---|---|---|
| **HOMERE(1)** | 1,297 | 1,535 | 1,260 | 1,482 |
| **HOMERE(2)** | 1,265 | 1,126 | 1,198 | 1,038 |
| **HOMERE(3)** | 1,460 | 2,662 | 1,184 | 1,942 |

**Table. 6.2 ï** . Parameters of $P(H_s>h)$ for total and wind sea significant wave heights.

From Figure 6.3 it is possible to note that at each considered site the distributions of wind sea and total sea intersect each other identifying a threshold of probability $P$' which defines two regions where the distributions have different behaviours. For $P$ greater than $P$' considering only wind sea data the return values of significant wave height are underestimated, while for $P$ smaller than $P$' are overestimated. This effect is related to the fact that in the less intense events swell components are strong, but the extreme events are due to wind sea only. This leads to have the parameter $u$ of the distribution of total significant wave height smaller than that of wind sea and because of that the two distributions intercept each other. Once the distributions of total and wind seas significant wave height are known, to apply the ETS model for the calculation of return values $h(R)$, the base-heights regression functions of both total and wind seas have to be determined. In order to do that first actual storm are identified from time series of total significant wave height $H_{st}$ and then for each storm the ETS model is applied to both wind and total seas storm histories. Figure 6.4 shows a comparison between the parameters $a$ and $b$ of ETSs calculated by means of total and wind seas time series. In the left panel is shown the comparison of the intensities $a$, while on the right of the bases $b$. It is worth noting that at HOMERE (1) and HOMERE (2) it is possible to identify a threshold of $H_s$ above which the intensities of the storms are due only to the wind sea. Considering lower threshold storm peaks have strong swell components, and because of that neglecting swells a certain variability of both intensities $a$ and durations $b$ is observed. The variability of $b$, is related to the fact that its value is strongly dependent on the storm structure at storm peak which is affected to significant variation neglecting swells. Concerning the site HOMERE (3) it is not possible to identify a threshold above which swells may be neglected, apart for the extreme storms. Then, in site like this, characterized by comparable wind and swell seas, neglecting swells the ETSs are strongly modified.

Starting from the ETSs sequences calculated using total and wind sea time series the base-heights regression functions are determined. Figure 6.5 shows the linear base-heights regression functions for total (left) and wind (right) seas. The parameters of the regression are summarised in Table 6.3. No significant changes in the base-heights regression functions may be appreciated at HOMERE (1) and HOMERE (2) , unlike for HOMERE (3). Finally return period $R(H_s>h)$ and mean persistence $D_m(h)$ are calculated for both total and wind seas (Figure 6.6).

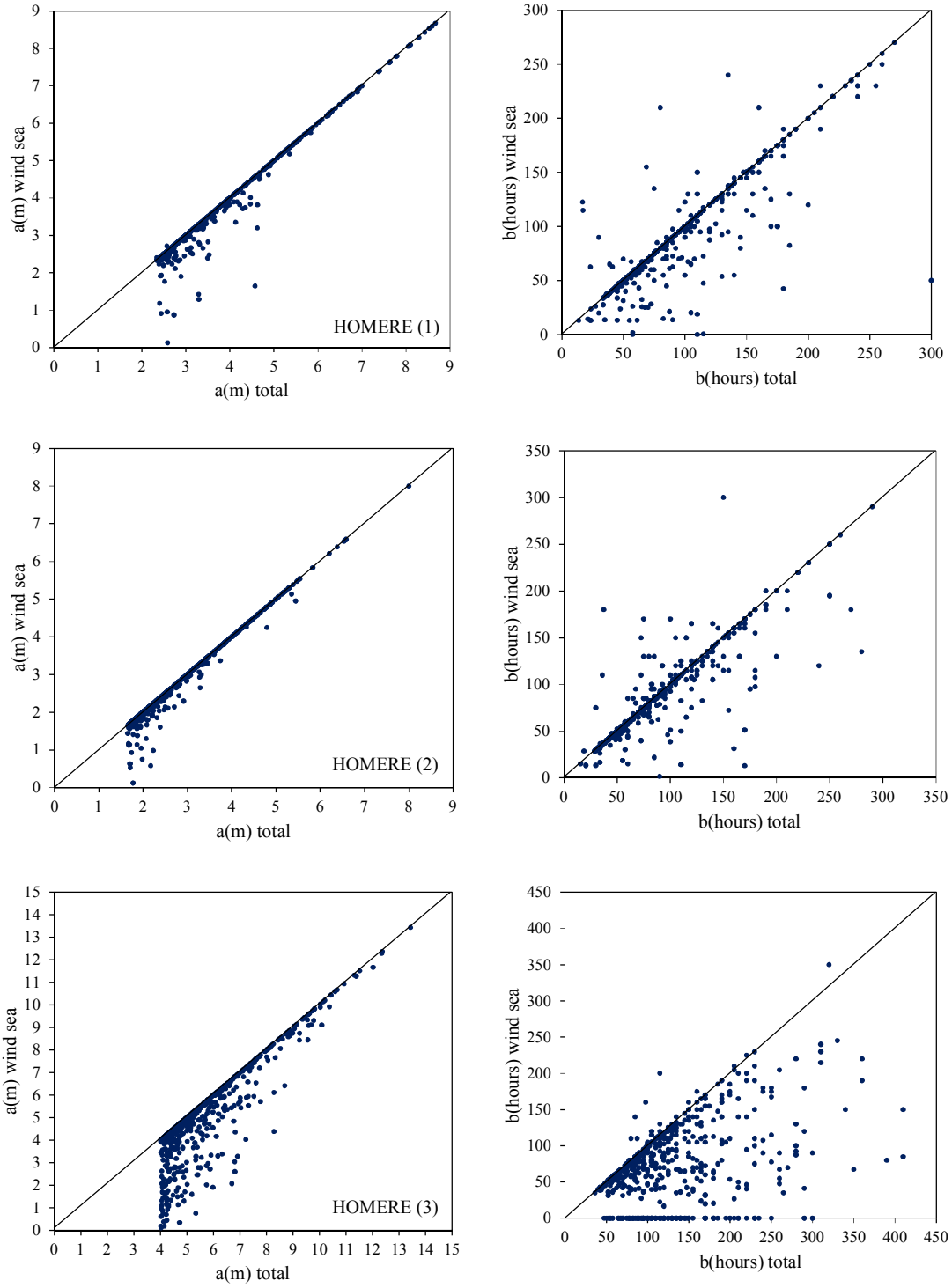


**Figure. 6.4 ï** Parameters of ETSs calculated by means of wind sea significant wave height versus parameters of ETSs calculated for total significant wave height: intensity *a* (left), duration *b* (right).

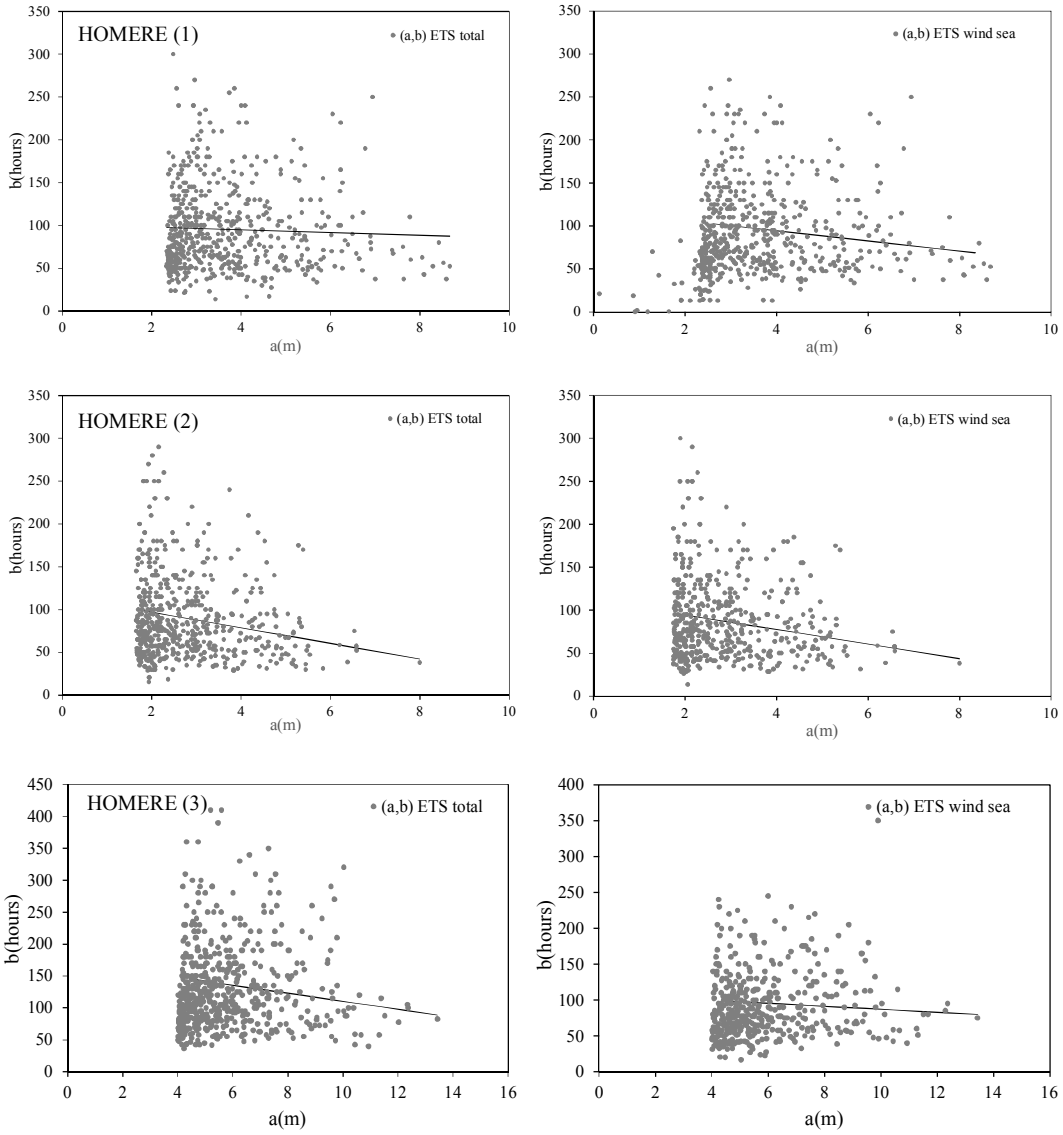


**Figure. 6.5 ï** Base-height regressions for ETSs: for total significant wave height (left), for wind sea significant wave height (right).

| **Location** | $K_{1\ total}$ ($m^{-1}$) | $K_{2\ total}$ (hours) | $K_{1\ wind}$ ($m^{-1}$) | $K_{2\ wind}$ (hours) |
|---|---|---|---|---|
| **HOMERE(1)** | -6,567 | 123,010 | -5,925 | 118,320 |
| **HOMERE(2)** | -9,158 | 115,520 | -8,539 | 111,730 |
| **HOMERE(3)** | -6,276 | 173,220 | -2,098 | 108,140 |

**Table. 6.3 ï** . Parameters of bas- height regression for ETSs calculated from total and wind sea significant wave heights.

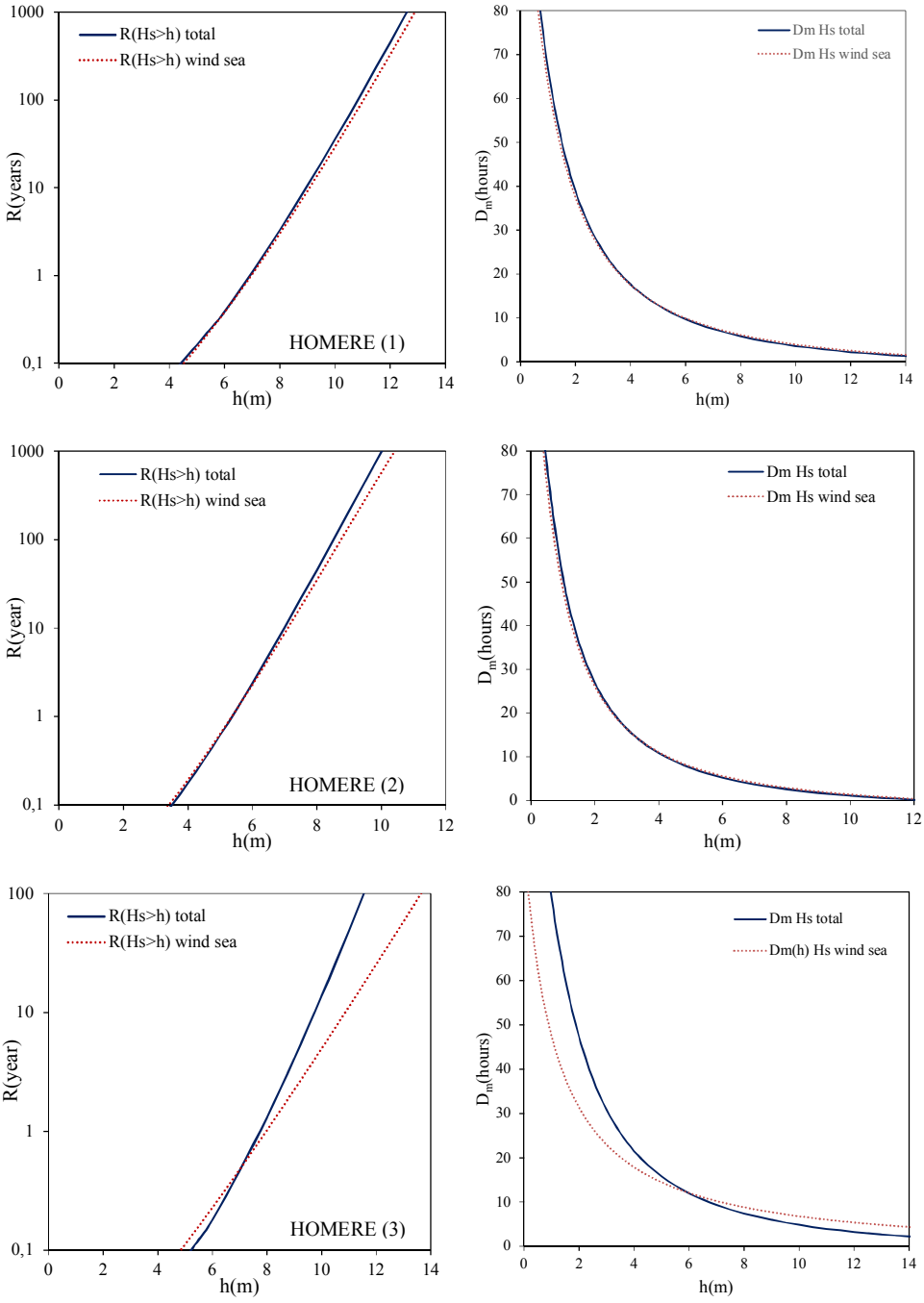


**Figure. 6.6 ï** Base-height regressions for ETSs: for total significant wave height (left), for wind sea significant wave height (right).

From a comparison of both return periods and mean persistence it is evident that they follow the same behaviour of the probability distributions. Concerning the return period it is possible to identify a value of $R$ above which return values of significant wave height are overestimated considering only wind sea contribution to $H_s$ data. In Tables 6.4 and 6.5 are given return values $h(R)$ for $R$=5, 10, 20, 50, 100 years calculated by means of total and wind seas time series respectively. From a comparison of the results it is clear that at the considered levels of return period $R$, accounting only wind sea contribution return values $h(R)$ are overestimated respect to the case accounting the total significant wave height (wind and swell seas). The maximum differences are less than 3% at HOMERE (1) and HOMERE (2) which are wind sea dominated locations, while it reaches the 7,8 % at HOMERE (3), which is a site characterized by comparable wind and swell seas.

| **Location** | h(R=5years) [m] | h(R=10years) [m] | h(R=20years) [m] | h(R=50years) [m] | h(R=100years) [m] |
|---|---|---|---|---|---|
| **HOMERE(1)** | 8,36 | 8,95 | 9,53 | 10,27 | 10,82 |
| **HOMERE(2)** | 6,51 | 6,99 | 7,46 | 8,06 | 8,51 |
| **HOMERE(3)** | 11,72 | 12,47 | 13,2 | 14,12 | 14,8 |

**Table. 6.4 ï** Return values of significant wave height $h(R)$ calculate by applying the ETS model to total significant wave height time series.

| **Location** | h(R=5years) [m] | h(R=10years) [m] | h(R=20years) [m] | h(R=50years) [m] | h(R=100years) [m] |
|---|---|---|---|---|---|
| **HOMERE(1)** | 8,46 | 9,07 | 9,67 | 10,45 | 11,02 |
| **HOMERE(2)** | 6,58 | 7,09 | 7,6 | 8,26 | 8,75 |
| **HOMERE(3)** | 12,06 | 12,99 | 13,90 | 15,07 | 15,95 |

**Table. 6.5 ï** Return values of significant wave height $h(R)$ calculate by applying the ETS model to wind sea significant wave height time series.

## 6.2. Conclusions

In the chapter the long-term analysis of ocean storms is proposed starting from time series of partitioned sea states. The analysis has been carried out by applying the ETS model both to the total significant wave height (combined wind and swell contributions) and to the wind significant wave height time series, in order to evaluate return values variability if swell components are neglected. Results have showed how different behaviours may be observed comparing locations characterized by comparable wind and swell components with locations wind sea dominated. In particular, if the considered site is wind sea dominated it is possible to identify a threshold of significant wave height $h$' above which the contribution of swells to the storm intensity is negligible. Instead, for locations with comparable wind and swell sea, only the strongest sea storms are wind dominated. In both cases neglecting swell contributions and determining the distribution of the significant wave height accounting only wind sea it is possible to identify a threshold of probability $P$' to which corresponds the equality of the distributions of total and wind significant wave heights. For probability $P>P$' neglecting swell significant wave height are underestimated, while for $P<P$' are overestimated. The above results involve differences in return values if the ETS model is applied to the wind significant wave height time series. These differences are quite limited if the considered site is wind sea dominated and could be relevant for locations with comparable wind and swell sea.

THIS PAGE INTENTIONALLY LEFT BLANK

# Chapter 7 ï Wave climate analysis for the design of wave energy harvesters in the Mediterranean Sea

*The objective of the work proposed in this chapter is to provide a synthetic tool for determining expeditiously the wave climate conditions in several areas of the Mediterranean Sea. In the open literature, several authors have already conducted this specific analysis also for the area examined here. However, the need of discussing aspects strictly related to the design of wave energy harvesters is still relevant. Therefore, considering the variety of devices and the amount of information needed for conducting an energy-wise optimization and a structural reliability assessment, a holistic view on the topic is provided. Specifically, the work elucidates the theoretical aspects involved in the estimation of wave energy statistics and in the calculation of relevant return values. Next, it provides synthetic data representing the mean wave power and the return value of extreme events in several coastal areas of the Mediterranean Sea. In this regard, this work complements information available in the open literature by discussing the influence of the directional pattern of the sea states in the determination of sea state statistics as well as in the design of a wave energy harvester.*

## 7.1. Introduction

The optimized design of any wave energy harvester is based on the quantitative description of the wave climate at a certain location. Indeed, structural safety, as well as energy production, relies on the calculation of relevant statistical parameters, such as wave height of given return period, average annual wave power, etc. Thus, the remarkable number of contributions given in the field of wave resource assessment, with the construction of wave atlases, is not surprising. From a methodological perspective, wave atlases are constructed by utilizing either recorded or artificially generated wave data. The first category involves the utilization of buoy or of satellite data. The second one uses numerical codes, such as WAM models *(T.W. Group, 1988)*, for

simulating the wave field generation and evolution by using wind field information as input. Depending on data quality and on numerical code peculiarities, wave atlases were developed at different spatial scales. Global estimates were proposed, for instance, by *Cornett (2008)*, *Barstow, et al. (2009)*, *Mørk, et al. (2010)* and *Arinaga and Cheung (2012)*. The key characteristic of these analyses is the possibility of identifying wide areas of interest for the realization of a wave energy harvester. Obviously, the coarse scale used in these global analyses does not allow the complete design of a wave energy harvester. Nevertheless, it is useful for defining locations where fostering the realization of wave energy devices. Detailed investigations are restricted to well defined areas and involve the use of high-resolution numerical codes. This aspect is quite relevant in closed areas, such as the Mediterranean Sea, where the spatial variability is not compatible with the resolution associated with classical measurement techniques *(Liberti et al. 2013)*. Several authors proposed a holistic view on the wave energy status by focusing on certain areas. For instance, *Liberti, et al. (2013)* investigated wave energy availability in the Mediterranean Sea with an emphasis on the Italian area; *Ayat (2013)* developed a wave power atlas for the Eastern Mediterranean Sea and the Aegean Sea; a similar analysis was proposed by *Aydoğan, et al. (2013)* for the Black Sea and by *Sierra, et al. (2014)* in Spain. The mentioned analyses are necessary for an energy-wise optimization of the device. However, an extreme value analysis must be pursued in parallel for predicting extreme actions on the device. So that, a reliability assessment can be conducted by considering certain extreme events. In this regard, the process invokes concepts developed in the context of classical coastal and marine engineering. The common procedure involves an analysis at short time scale (~hours) and at long time scale (~years). This distinction accommodates convenient representations of the wave motion. Specifically, the short-term analysis is pursued by invoking a spectral representation of the free surface displacement, which is connected to a stationary representation of the process *(Ochi, 2005)*. The long-term statistics involves the non-stationary character of the free surface displacement, which is treated by accumulating the statistical information of the process in a few synthetic parameters (commonly, significant wave height, peak spectral period, mean wave direction) described via simplified models *(Goda, 2010)*. In this context, recently proposed models for extreme value analysis are the Equivalent Triangular Storm (ETS) model and the Equivalent Power Storm (EPS) model *(Arena and Pavone 2006; Fedele and Arena, 2010)*. These models found on a theoretical representation of real sea storms, which accommodates the derivation of closed form solutions of relevant return values.

To conduct a joint analysis of extreme waves and of wave climate along the coasts of the Mediterranean Sea is the objective of this work. Specifically, the chapter presents a holistic

view on the preliminary wave related steps involved in the design of a wave energy harvester. The findings of this analysis are useful for designing a device as it provides the crucial information for optimizing the energetic performance as well as for conducting a reliability assessment of a device. In this regard, it is worth mentioning that the variety of devices developed in the last decades requires a more detailed quantification of the wave climate. Indeed, some devices can be designed by considering only the energetic characteristics of the sea states, but several are highly influenced by the mean wave direction *(see Falcão, 2010*) for a review of the available technologies). Therefore, the work considers, in addition, the directional features of the recorded sea states, as it is relevant in the design of several wave energy devices. The analysis utilizes data generated by a WAM numerical model. Thus, a reliability assessment of this model is conducted by restricting the attention to the directional pattern of the sea states. Then, this work elucidates the key characteristics of the theoretical model used in the successive analysis. Next, the results of the analysis are disseminated by investigating both the mean wave power (in conjunction with its "directional" distribution) and the return period of significant wave height (with its "directional" distribution, as well).

## 7.2. Wave data: reliability assessment of the used WAM model with emphasis on mean wave directions.

Wave simulations have been performed using a parallel version of WAM wave model Cycle 4.5.3 *(Günther and Behrens, 2011)*. An extensive validation of the model both against buoys of the Italian Buoy Network (Rete Ondametrica Nazionale, RON) and against satellite data has been already presented in *(Liberti et al., 2013)*. Here model results are compared with buoy data in two of the most energetic sites in the coasts of Central Mediterranean Sea (from Italian Buoy Network): Alghero (West coast of Sardinia Island - buoy coordinates: 40.548°N, 8.107°E) and Mazara del Vallo (Sicily Channel - buoy coordinates: 37.525°N, 12.533°E). Buoy data have been compared with values extracted from the nearest computational model point. Only simultaneous data have been considered, buoy records where the peak spectral period $T_p$ fell in the infra-gravity waves range, above 20 s, have been excluded from the analysis.

Tables 7.1 and 7.2 show the principal statistics computed between buoys and model results for significant wave heights and circular statistics for mean wave directions, computed as described by *Mardia and Jupp (2000)*. In particular, Table 7.1 includes values of the bias between model and measures, root mean square error (rmse), slope of the best fit line passing

through the origin and scatter index (si), and Table 7.2 the directional bias (bias°) and the directional variance (var). The statistics in these two sites give quite good results, with the slope close to the unity and the bias of the order of 1 cm. Figures 7.1 and 7.2 show histograms with the relative frequency of occurrence of $H_s$ divided in bins of 0.2 m for buoy and model data. In both sites the measured distribution is well reproduced and the main difference observed is the overestimation of the number of events with $H_s$ in the lowest range (0-0.2 m).

| **Buoys** | **Bias (m)** | **Rmse (m)** | **Slope** | **si** |
|---|---|---|---|---|
| Alghero | -0.005 | 0.311 | 0.985 | 0.278 |
| Mazara del Vallo | 0.013 | 0.257 | 1.022 | 0.253 |

**Table. 7.1 ï** Main statistics of the significant wave height between buoy and model.

| Buoys | Bias (°) | var |
|---|---|---|
| Alghero | 4.5 | 0.036 |
| Mazara del Vallo | 11.0 | 0.057 |

**Table. 7.2ï** Main statistics of the mean wave direction between buoy and model.

A further validation focusing on the sea state directional characteristics is accomplished, as this aspect is relevant for near-shore and on-shore devices.

Figures 7.3 and 7.4 show polar plots associated with buoy and model data at Alghero and Mazara del Vallo, respectively. Data are divided in classes of significant wave heights with intervals of 1m; calms are identified as significant heights less than 0.5m. In both sites the prevailing propagation is toward ESE as both places are influenced by the north-westerly winds blowing over most of the western Mediterranean. The wave direction of propagation at Alghero is very well reproduced as shown also by values in Table 7.2. At Mazara del Vallo the most frequent class in model results appears to be slightly rotated northward respect to observations, the circular bias *(see Mørk et al., 2010)* is 11° as shown in the table.

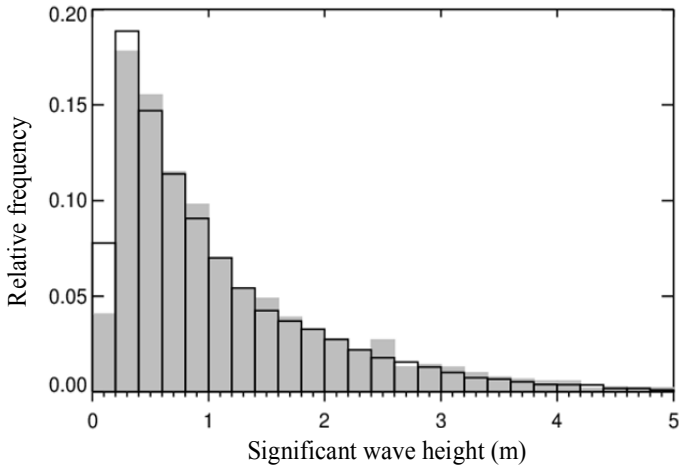


**Figure. 7.1 ï** Histogram with the relative frequency of significant wave heights in bins of 0.2 m at coordinates corresponding to the buoy of Alghero. Filled grey relates to buoy data, black line to model data.

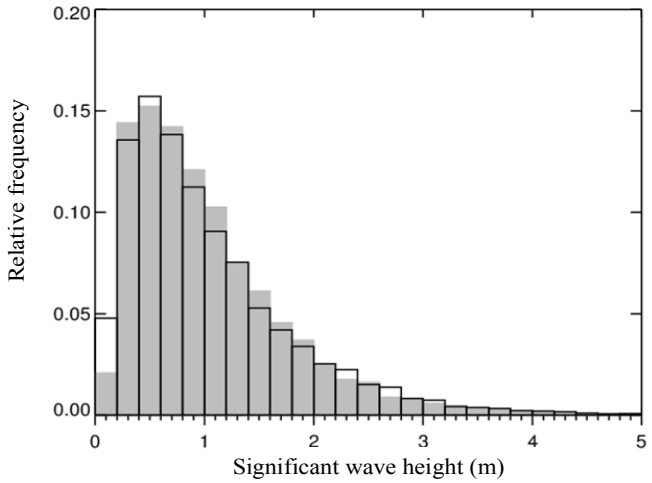


**Figure. 7.2ï** Histogram with the relative frequency of significant wave heights in bins of 0.2 m at coordinates corresponding to the buoy of Mazara del Vallo. Filled grey relates to buoy data, black line to model data.

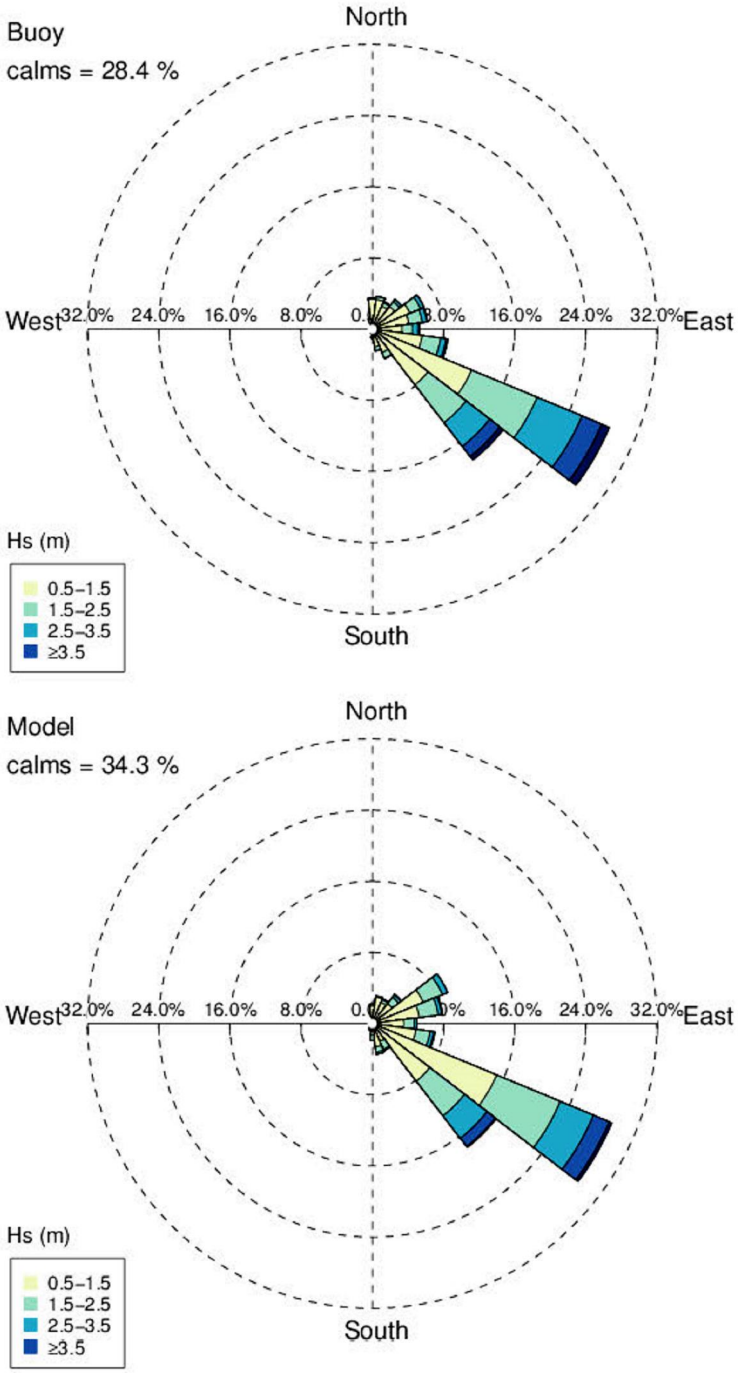


**Figure. 7.3 ï** Polar plot of wave climate at the coordinates corresponding to the buoy of Alghero. Upper panel climatology derived by buoy data, lower panel derived from the model simulations. Directional bins of 15°.

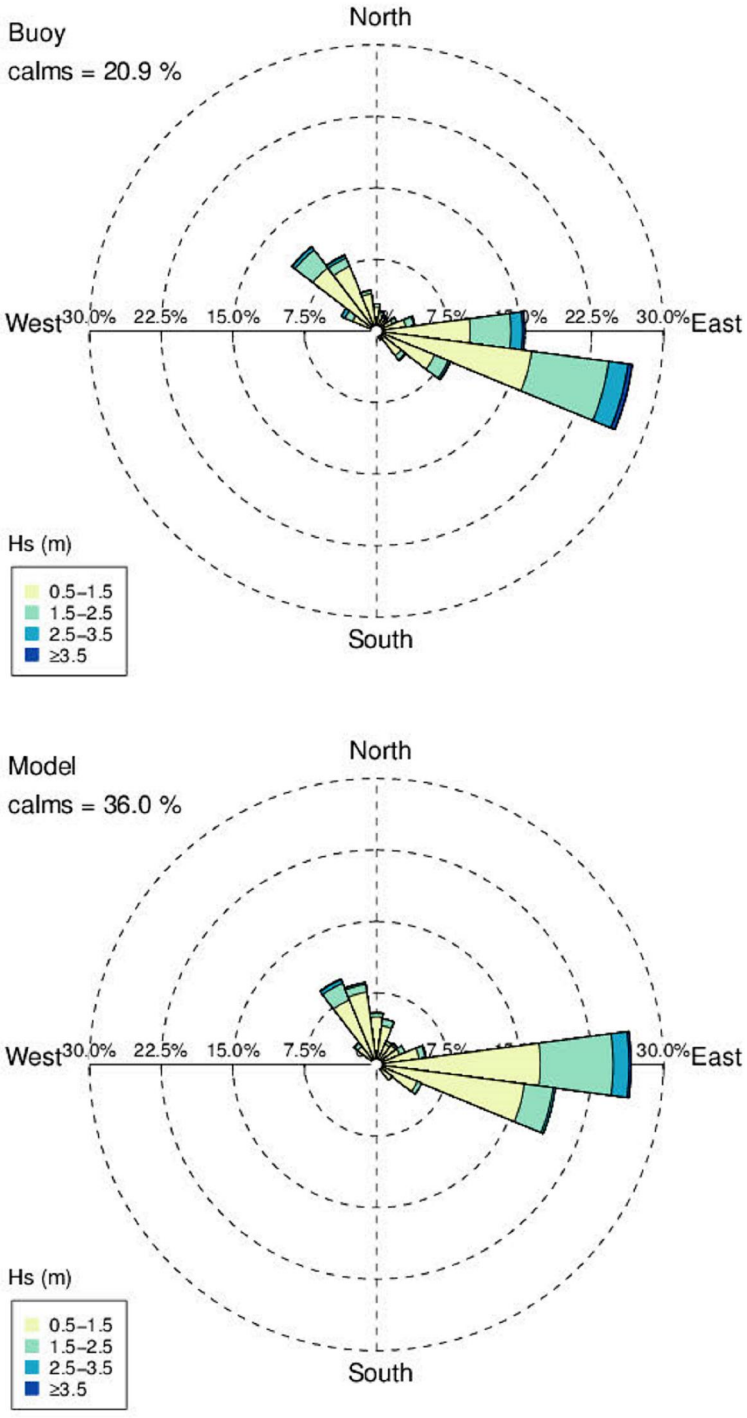


**Figure. 7.4 ï** Polar plot of wave climate at the coordinates corresponding to the buoy of Mazara del Vallo. Upper panel climatology derived by buoy data, lower panel derived from the model simulations. Directional bins of 15°.

### 7.3 Synthetic equation of the wave power and of the mean wave power

Consider an undisturbed wave field of significant wave height $H_s$, frequency spectrum $E(\omega)$ ($\omega$ being the angular frequency) and peak spectral period $T_p$ ($=2\pi/\omega_p$; $\omega_p$ being the peak frequency of the spectrum). For this sea state, the wave power per unit width is calculated by the equation *(see Boccotti, 2000)*

$$\Phi = \rho g \int_0^\infty c_g(\omega) E(\omega) \mathrm{d}\omega, \tag{7.1}$$

where $\rho$ denotes the water density, $g$ is the acceleration due to gravity and $c_g$ is the group velocity. In deep water, $c_g$ equates half wave celerity in deep water. Thus, Equation (7.1) reduces to the equation

$$\Phi = \frac{\rho g^2}{2} \int_0^\infty \omega^{-1} E(\omega) \mathrm{d}\omega. \tag{7.2}$$

Equation (7.2) can be related explicitly to the statistical characteristics of the sea state via the associated spectral moments $m_j$, which are defined by the equation *(see Ochi, 2005)*

$$m_j = \int_0^\infty \omega^j E(\omega)\, \mathrm{d}\omega. \tag{7.3}$$

Specifically, by observing that the significant wave height is related to the zero$^{th}$ order moment $m_0$,

$$H_s = 4\sqrt{m_0}, \tag{7.4}$$

that the mean wave period $T_m$ can be calculated via the zero$^{th}$ and the second-order moments,

$$T_m = 2\pi\sqrt{m_0 / m_2}, \tag{7.5}$$

and that an energy period $T_e$ can be defined by the equation *(see Cruz, 2008)*

$$T_e = 2\pi\, m_{-1} / m_0. \tag{7.6}$$

It is seen that Equation (7.2) can be manipulated by selecting a priori a certain spectral shape. For instance, consider the classical JONSWAP spectral model proposed by *Hasselmann, et al. (1973)*. Introducing the dimensionless frequency $w=\omega/\omega_p$, it may be written in the form

$$E(\omega) = \alpha_{PH} g^2 \omega_p^{-5} w^{-5} \exp(-1.25 w^{-4}) \exp\left\{\ln\gamma \exp\left[-\frac{(w-1)^2}{2\sigma^2}\right]\right\}, \tag{7.7}$$

where $\alpha_{PH}$ is the Phillip's parameter and $\gamma$ and $\sigma$ are the shape parameters of the spectrum. The parameter $\alpha_{PH}$ varies between 0.008 and 0.02 for wind waves and $\gamma$ varies over the interval 1 - 7, being equal to 3.3 and 1 for the mean JONSWAP and the *Pierson-Moskowitz (PM) spectrum (1964)*, respectively. Such a formulation allows defining the dimensionless spectral moments

$$m_{w_j} = \int_0^\infty w^{-5+j} \exp(-1.25 w^{-4}) \exp\left\{\ln\gamma \exp\left[-\frac{(w-1)^2}{2\sigma^2}\right]\right\} dw, \tag{7.8}$$

which are related to the spectral moments (7.3) by the equation

$$m_j = \alpha_{PH} g^2 \omega_p^{-4+j} m_{w_j}. \tag{7.9}$$

So that, the mean wave period $T_m$ and the energy period $T_e$ may be expressed in function of the peak period $T_p$, respectively, through the following conditions,

$$T_m = \alpha_{f_1} T_p, \tag{7.10}$$

$$T_e = \alpha_{f_2} T_p, \tag{7.11}$$

being

$$\alpha_{f_1} = \sqrt{m_{w_0} / m_{w_2}} \,. \tag{7.12}$$

and

$$\alpha_{f_2} = m_{w_{-1}} / m_{w_0} \,. \tag{7.13}$$

For example, $\alpha_{f1}$=0.81, $\alpha_{f2}$=0.91 for the mean JONSWAP spectrum and $\alpha_{f1}$=0.75, $\alpha_{f2}$=0.86 for the PM spectrum. Finally, by combining Equations (7.4), (7.10) and (7.11), the energy power per unit crest length on deep water [Equation (7.2)] may be calculated by the formula

$$\Phi = \frac{\rho g^2}{64\pi} \gamma_f H_s^2 T_m \,. \tag{7.14}$$

The parameter $\gamma_f$ is spectrum dependent, and is given by the equation

$$\gamma_f = \alpha_{f_2} / \alpha_{f_1} \,. \tag{7.15}$$

Typical values are $\gamma_f = 1.12$ for the mean JONSWAP spectrum and $\gamma_f = 1.15$ for the PM spectrum.

Obviously, Equation (7.14) does not compute the statistical distribution of the significant wave height and of the mean period. Therefore, Equation (7.14) is associated with an adequate probability distribution of the significant wave height for estimating the mean incident wave power. Specifically, the mean wave power per unit width at a certain location is calculated by the equation

$$\overline{\Phi} = \int_0^\infty \Phi(h)\, p(H_s = h) \mathrm{d}h \tag{7.16}$$

where $p(H_s=h)$ is the probability density function of the significant wave height, which is specified in the next section. Further, to account for the directional distribution of the sea states, Equation (7.14) can be exploited for obtaining the mean wave power associated with a given sector of wave propagation. Denoting $\Delta\delta$ the given sector, the mean wave power per unit width for given values of wave direction is

$$\overline{\Phi}_{\theta} = \int_{0}^{\infty} \Phi(h)\, p(H_s = h; \Delta\theta) \mathrm{d}h \,, \tag{7.17}$$

where $p(H_s=h;\Delta\boldsymbol{\theta})$ is the "directional" probability density function, that is the probability distribution of the significant wave height extracted from a subset of sea states with wave directions belonging to the sector $\Delta\boldsymbol{\theta}$. This function is defined more precisely in the next section.

The attractive feature of Equations (7.16) and (7.17) is the fact that they do not require time-consuming calculations in frequency domain, as they postulate the agreement between the theoretical JONSWAP spectrum and the "real" one. Even if this assumption is quite restrictive, section 7.4.1 will show that it can be adopted for the purpose of estimating the mean wave power without losing significant information even in case of bimodal seas.

## 7.4 Data analysis

A data analysis is pursued for a certain number of locations in the Mediterranean Sea. The locations are selected by considering only zones in the vicinity of coastal areas, as these are the most likely to host a wave energy harvester. The proposed map covers approximately the entire Mediterranean Sea. However, some areas with a low energetic contribution are not investigated, because of the restricted interest in wave energy applications.

Figure 7.5 shows point locations, while Table 7.3 shows the specific coordinates. In the following, wave energy potential, extreme waves and sea state directional features pertaining to these locations are disseminated. However, a preliminary analysis is proposed regarding the formulae derived in section 7.3, in order to assess their reliability.

### 7.4.1 Reliability of Equation (7.14)

The data analyses involve the calculation of the mean wave power at each location via Equation (7.14). Thus, before conducting the analyses, this section shows that the estimations conducted by the proposed method are reliable. That is, the discrepancies between the results provided by adopted method and by a more rigorous approach are small.

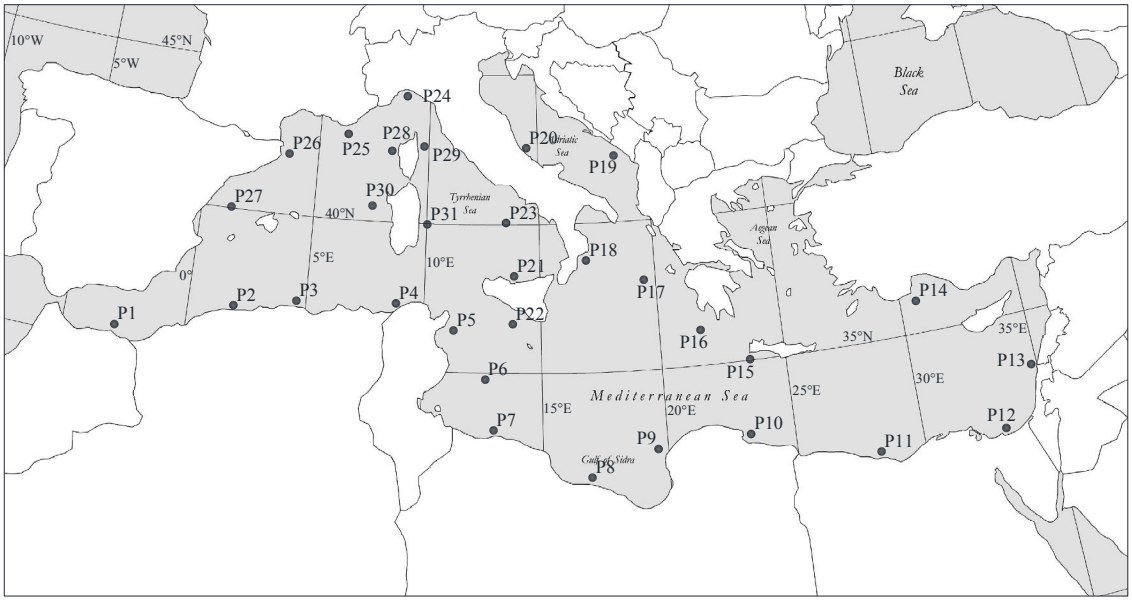


**Figure. 7.5 ï** Map of the Mediterranean Sea and locations of the investigated areas.

The crucial limit of the formula (7.14) is the assumption of unimodal frequency spectrum. Indeed, by restricting the attention to a JONSWAP like frequency spectrum, the contribution of bimodal sea states is neglected. This element could be crucial in locations with several bimodal sea states per years. However, numerical evidence proves that this is not relevant for the calculation of the mean wave power associated with each sea state. Specifically, consider locations P9, P16 and P17. The wave power considering the contribution of the bimodal seas is calculated and compared to the one estimated via Equation (7.14) (see Figure 7.6). In this regard, note that the calculation via the simplified formula is pursued by considering a significant wave height calculated from the significant wave height values pertaining to each component of the bimodal sea, while the peak period is the period associated with the peak of the frequency spectrum over the entire frequency domain. It is seen that the calculations provide in all cases results in quite good agreement. The mean error implied by the proposed method is calculated by the equation

$$\varepsilon = \frac{1}{N-1}\sqrt{\sum_{i=1}^{N}[\Phi_i(H_s,T_m)-\Phi_i(H_{sw},H_{ss},T_{mw},T_{ms})]^2}\ , \tag{7.18}$$

$N$ being the number of sea states, $\Phi_i(H_s,T_m)$ is the wave power calculated considering the unimodal frequency spectrum and $\Phi_i(H_{sw},H_{ss},T_{mw},T_{ms})$ is the wave power calculated via the bimodal frequency spectrum.

| Marker | Latitude | Longitude | Depth [m] | Distance [km] |
|---|---|---|---|---|
| P1 | 35,70000 | -3,00000 | 866 | 29,1 |
| P2 | 36,95000 | 2,00000 | 2680 | 41,8 |
| P3 | 36,95000 | 4,37500 | 559 | 6,5 |
| P4 | 37,20000 | 8,50000 | 133 | 30 |
| P5 | 36,38750 | 11,56250 | 224 | 65 |
| P6 | 34,70000 | 12,75000 | 120 | 160 |
| P7 | 33,26250 | 13,18750 | 237 | 40 |
| P8 | 31,38750 | 17,18750 | 139 | 28,5 |
| P9 | 32,45000 | 20,00000 | 257 | 27 |
| P10 | 31,95000 | 25,50000 | 806 | 45 |
| P11 | 31,45000 | 28,50000 | 1382 | 40 |
| P12 | 31,57500 | 33,18750 | 244 | 38 |
| P13 | 33,45000 | 34,75000 | 1516 | 47 |
| P14 | 35,95000 | 30,75000 | 2595 | 44 |
| P15 | 35,13750 | 23,25000 | 3557 | 30 |
| P16 | 36,20000 | 21,68750 | 3467 | 69 |
| P17 | 38,20000 | 19,56250 | 3513 | 70 |
| P18 | 38,45000 | 17,00000 | 1424 | 36 |
| P19 | 42,20000 | 17,50000 | 1118 | 68 |
| P20 | 42,38750 | 14,75000 | 98 | 24,5 |
| P21 | 38,20000 | 14,06250 | 1290 | 18,4 |
| P22 | 36,57500 | 13,68750 | 609 | 42,2 |
| P23 | 40,26250 | 13,50000 | 1902 | 94 |
| P24 | 43,95000 | 9,00000 | 880 | 43 |
| P25 | 42,57500 | 6,25000 | 2547 | 52 |
| P26 | 41,95000 | 3,50000 | 339 | 22,5 |
| P27 | 40,07500 | 1,00000 | 113 | 61 |
| P28 | 42,20000 | 8,00000 | 2795 | 46,5 |
| P29 | 42,20000 | 10,00000 | 359 | 36,5 |
| P30 | 40,45000 | 7,50000 | 2624 | 59 |
| P31 | 39,95000 | 10,00000 | 1548 | 25,5 |

**Table. 7.3 ï** Coordinates of the investigated points, water depth and distance from the shoreline.

| | Location | | |
|---|---|---|---|
| | P9 | P16 | P17 |
| **Ú**(KW/m) | 3,75E-06 | 2,57E-05 | 1,27E-05 |

**Table. 7.4 ï** Error ε calculated via Equation (7.18) at points P9, P16 and P17.

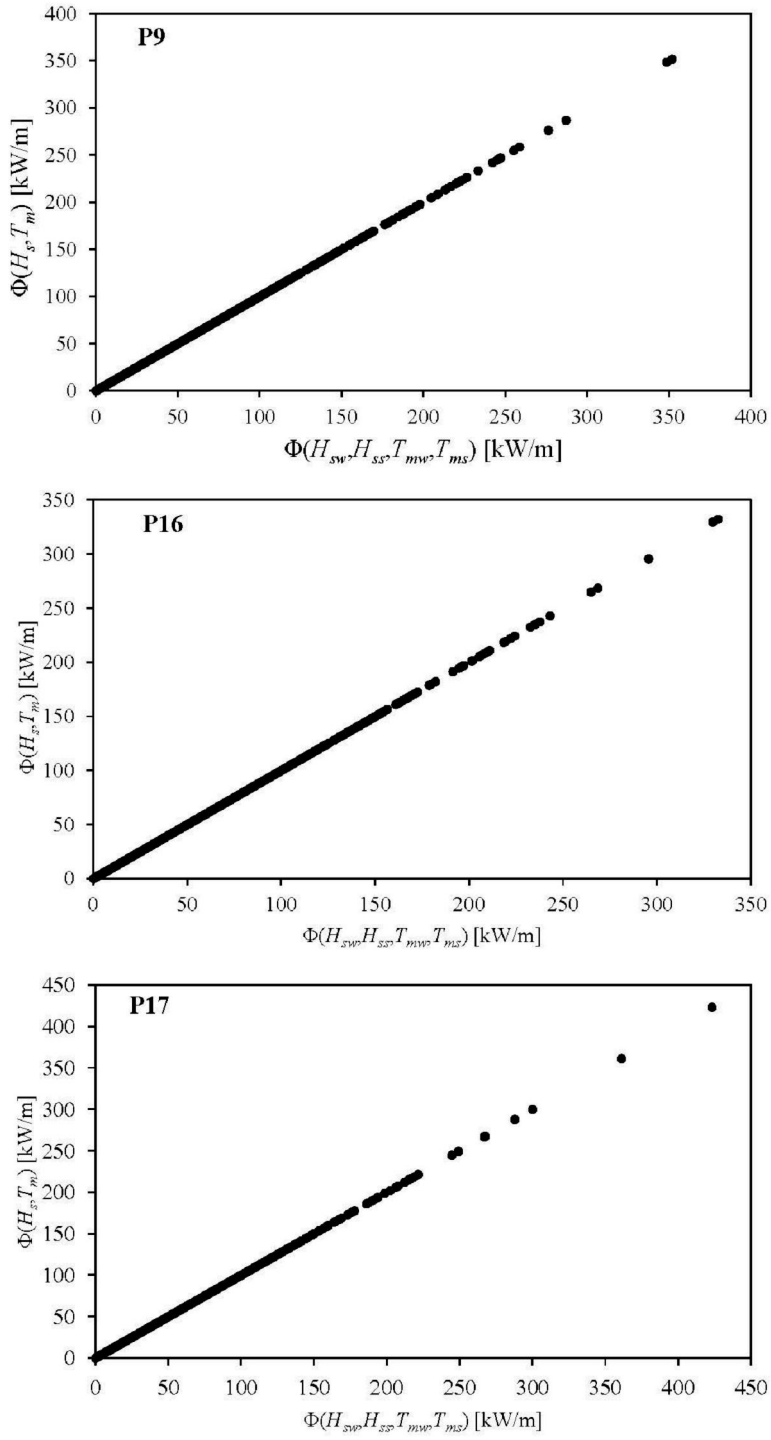


**Figure. 7.6 ï** Comparison between the wave power calculated via Equation (7.14) [$\bar{\boldsymbol{u}}\,(H_s,T_m)$] and the wave power calculated considering the bimodal sea states occurring at locations P9, P16 and P17 [$\bar{\boldsymbol{u}}\,(H_{sw},H_{ss},T_{mw},T_{ms})$].

### 7.4.2 Wave power

For a given recorded sea state time history, the mean wave power is given by Equation (7.17). The computation has been pursued by considering that all data are in deep waters. As mentioned previously, the directional pattern of the wave climate is relevant in the design of several energy harvesters. Therefore, the wave power is investigated by considering the directional distribution of the sea states. Specifically, the estimated time histories allow calculating the mean wave power associated with a certain sector of wave propagation. In this analysis, the width of each sector is 20°. The Figures 7.7-7.9 show the wave power of each record (points) and the mean wave power associated with sea states propagating to a certain direction. They provide a holistic view on the energy characteristic of the sites. Indeed, given a certain location, the characteristics of the wave energy harvester, and the orientation of the shoreline with respect to the North direction, a preliminary investigation on the energy-wise performance of the device can be pursued. Obviously, these results are relevant also for devices in a coastal area, as they can be coupled to a classical wave propagation model for determining the wave field in the vicinity of the shoreline. In this regard, it is worth-mentioning that if the wave direction corresponding to the largest amount of wave energy is almost orthogonal to the shoreline, the total amount of wave energy is expected to be slightly smaller than offshore. Vice versa, a large angle between the shoreline orthogonal and the wave direction implies a larger reduction of wave energy due to refraction effects.

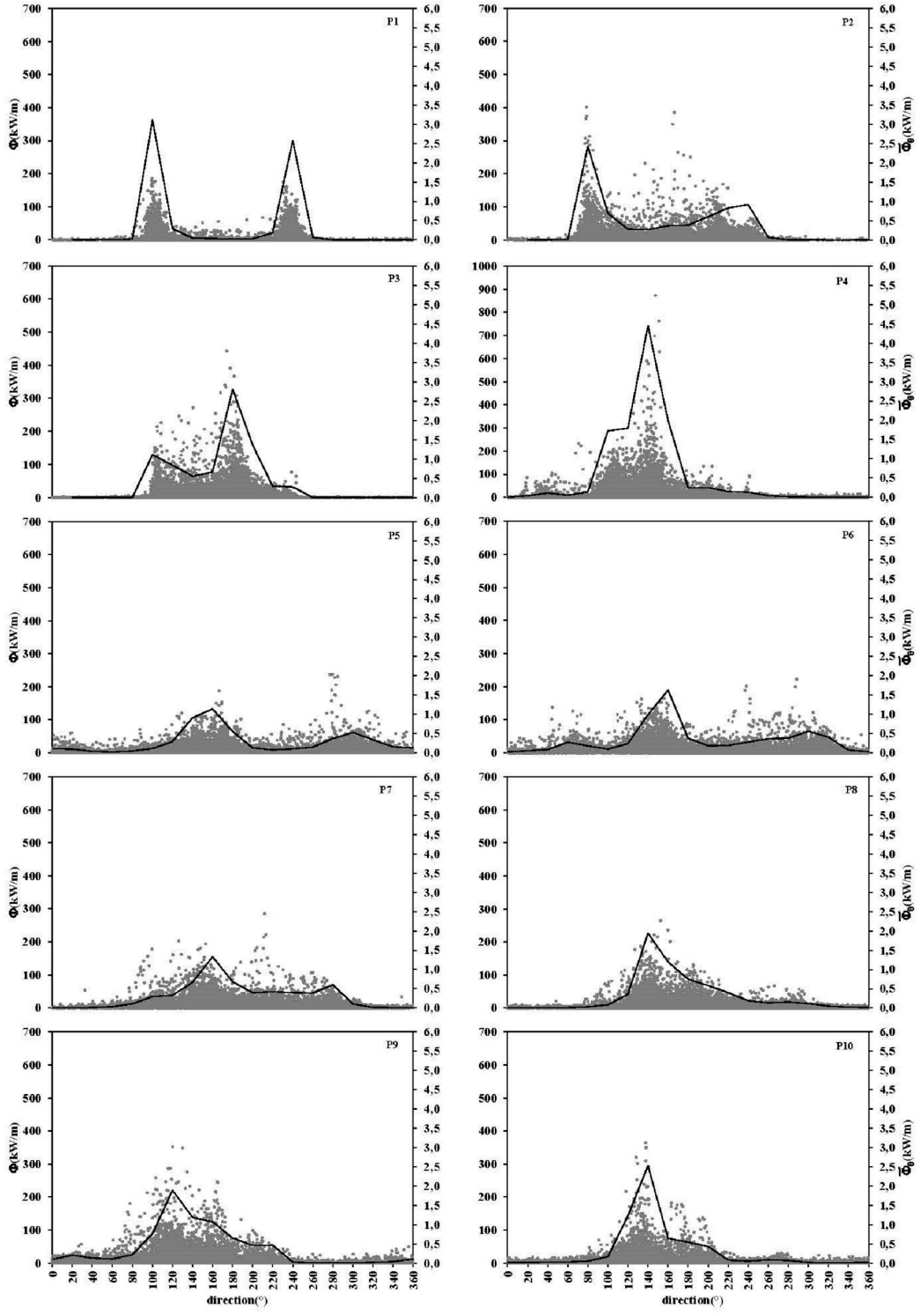


**Figure. 7.7 ï** Wave power calculated for sea states generated at locations P1 - P10 (points) and mean wave power calculated for a certain directional sector. The left vertical axis pertains to the wave power; the right vertical axis pertains to the mean wave power; the horizontal axis shows the wave direction.

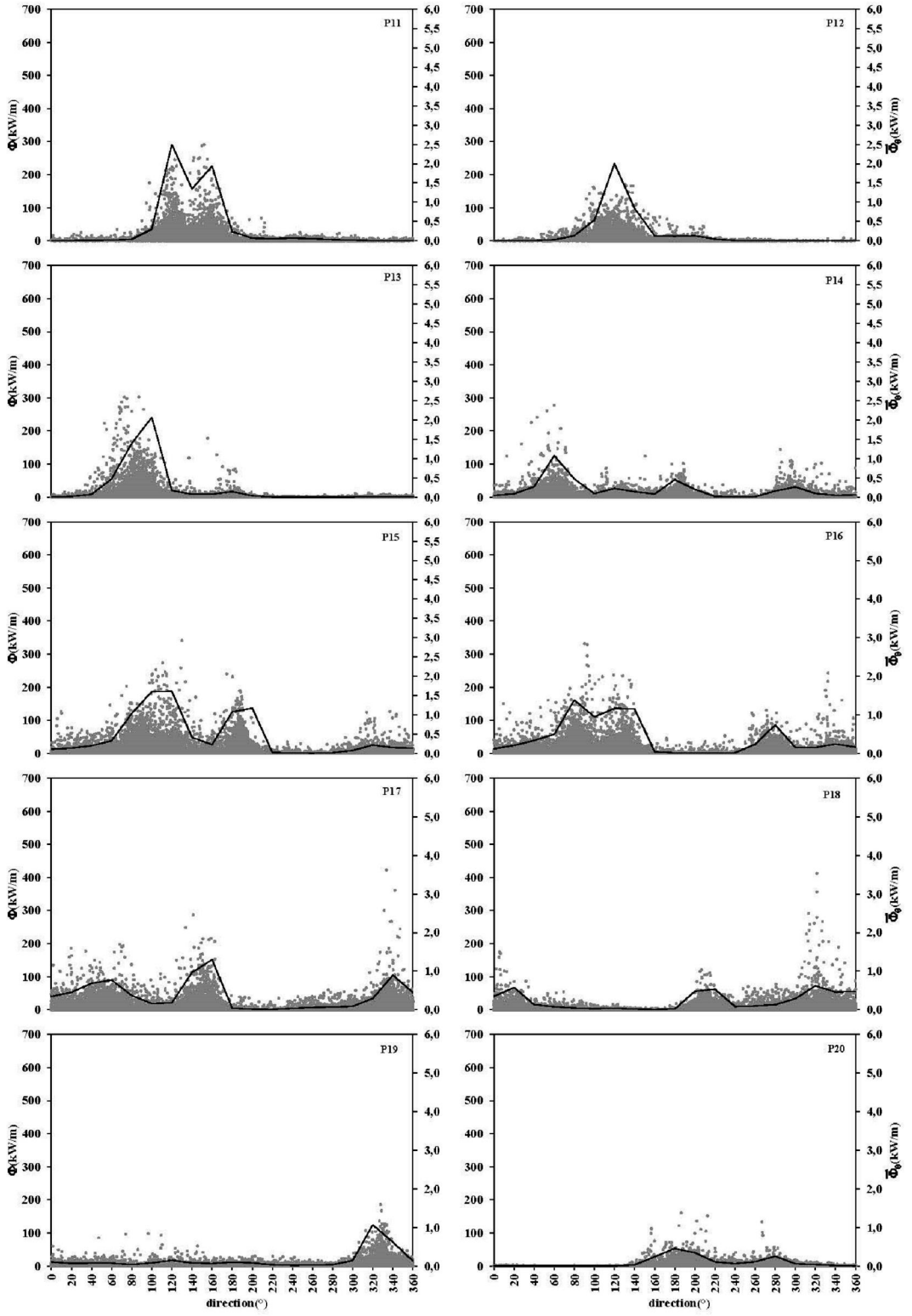


**Figure. 7.8 ï** Wave power calculated for sea states generated at locations P11 – P20 (points) and mean wave power calculated for a certain directional sector. The left vertical axis pertains to the wave power; the right vertical axis pertains to the mean wave power; the horizontal axis shows the wave direction.

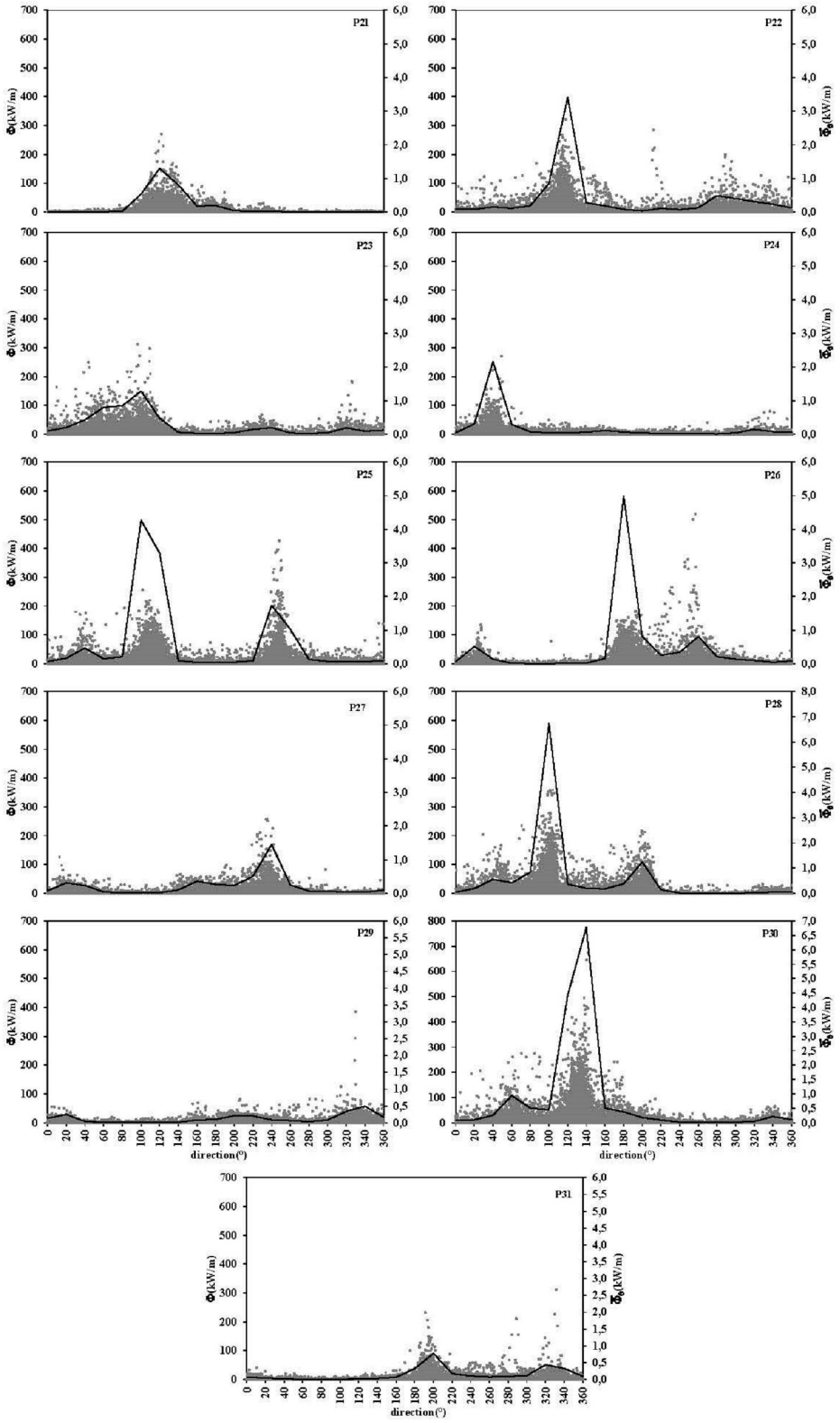


**Figure. 7.9 ï** Wave power calculated for sea states generated at locations P21 – P31 (points) and mean wave power calculated for a certain directional sector. The left vertical axis pertains to the wave power; the right vertical axis pertains to the mean wave power; the horizontal axis shows the wave direction.

### 7.4.3 Extreme values analysis

A structural reliability assessment involves an analysis of the device dynamics in extreme conditions. Indeed, the long-term performance of the device is affected by the occurrence of extreme events naturally occurring at a certain location. During the design stage, the crucial issue is to determine the most probable "extreme wave" (significant wave height, individual crest-to-trough wave height, etc.) occurring during the lifetime of the device. For the purpose, the ETS method is suggested. The theoretical background was discussed in section 1.4 in conjunction with the concept of replacing real storms with ETSs. Figure 7.10 shows several examples, extracted from the WAM data, of real sea storms and of associated ETSs. It is seen that the ETSs are capable of describing roughly the time variation of the real storms. However, this aspect is not relevant as the related statistics are quite close to each other.

For implementing the methodology, the short-term probability distribution must be determined. For the purpose, Table 7.5 shows the parameters of distribution given by Equation (1.10) ($h_l$=0) and Figure 7.11 plots the omnidirectional distributions in conjunction with the directional distributions (1.11) ($h_l$=0). Figure 7.11 pertains only to the locations with, at least, a double peak in the energy distribution over direction and it is useful not only for calculating the extreme values, but also for complementing the information of Figures 7.7-7.9. Indeed, it is seen that the most energetic directions are quite close to the omnidirectional distribution (see for instance the Sardinia case, P30). In some contexts, this characteristic is less evident. For instance off Greece (P17) there are three different peaks, which are energy-wise equivalent. In this case, the directional distributions are quite close to each other and do not allow determining a "main" direction of wave propagation.

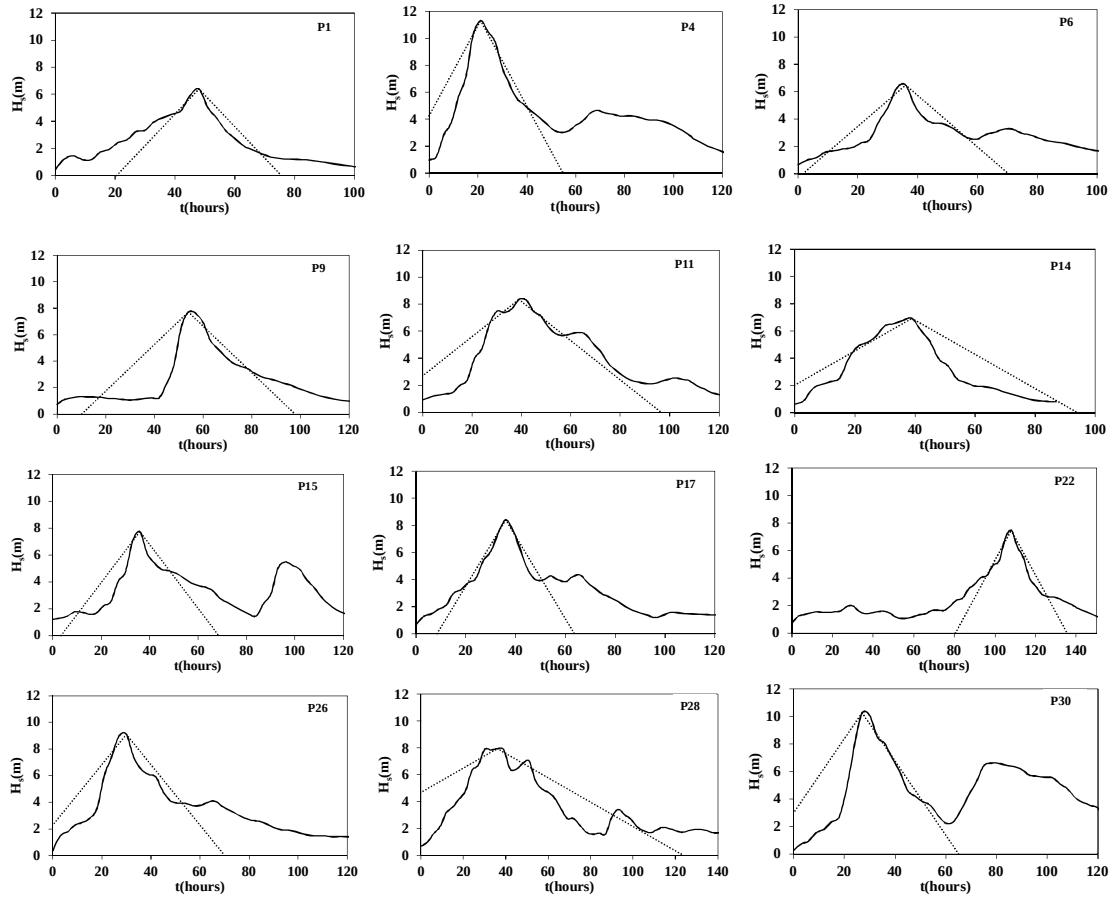


**Figure. 7.10 ï** Comparison between actual sea storms (continuous lines) and ETSs (dotted line) recorded at the locations shown in the legends.

Figure 7.12 shows the return period given by Equation (1.19). This representation is relevant for devices that work irrespective of the direction of wave propagation. The return period is shown for all the case studies and, in addition, Table 7.3 shows significant wave height values of a given return period. Obviously, these elements are necessary for identifying "operational" and "extreme" sea states, but are not complete for designing an angle-dependent device. In this context, the directional return period (1.21) is more appropriate. Figure 7.13 shows the directional return period for the same locations investigated in Figure 7.11. From a design perspective, the crucial element of these representations is that the significant wave height of a given return period is smaller in the directional case. Thus, it implies that the design sea state is less severe than a conventional omnidirectional case.

| Location | $\overline{H_s}$ [m] | $H_{smax}$[m] | u | w [m] | $k_1$ [h] | $k_2$ [$m^{-1}$] | $\overline{\Phi}$ [KW/m] | h(5yr) [m] | h(10yr) [m] | h(20yr) [m] | h(50yr) [m] | h(100yr) [m] |
|---|---|---|---|---|---|---|---|---|---|---|---|---|
| P1 | 1,09 | 6,39 | 1,274 | 1,149 | 80,86 | 1,22 | 6,3 | 6,1 | 6,5 | 6,9 | 7,4 | 7,8 |
| P2 | 1,10 | 8,20 | 1,06 | 0,960 | 85,03 | 0,37 | 6,8 | 7,2 | 7,8 | 8,4 | 9,2 | 9,7 |
| P3 | 1,07 | 8,42 | 1,071 | 0,979 | 82,24 | 1,07 | 7,9 | 6,9 | 7,5 | 8,1 | 8,9 | 9,4 |
| P4 | 1,22 | 11,34 | 1,057 | 1,162 | 104,59 | -0,37 | 11,1 | 8,8 | 9,5 | 10,3 | 11,3 | 12,0 |
| P5 | 1,01 | 6,69 | 1,187 | 0,968 | 94,39 | 0,02 | 5,2 | 5,9 | 6,3 | 6,8 | 7,3 | 7,8 |
| P6 | 1,10 | 6,48 | 1,276 | 1,120 | 83,04 | 0,59 | 6,4 | 6 | 6,4 | 6,8 | 7,4 | 7,7 |
| P7 | 1,06 | 7,11 | 1,177 | 0,978 | 81,19 | 0,77 | 5,8 | 6 | 6,4 | 6,9 | 7,4 | 7,8 |
| P8 | 1,06 | 6,90 | 1,128 | 1,071 | 90,04 | 0,60 | 6,1 | 6,9 | 7,5 | 8,1 | 8,8 | 9,3 |
| P9 | 1,13 | 7,71 | 1,129 | 1,033 | 88,73 | 0,89 | 7,4 | 6,7 | 7,2 | 7,7 | 8,4 | 8,9 |
| P10 | 1,08 | 7,71 | 1,022 | 0,840 | 104,79 | 0,29 | 6,1 | 6,5 | 7,1 | 7,7 | 8,5 | 9,1 |
| P11 | 1,12 | 8,35 | 1 | 0,919 | 189,95 | -0,07 | 7,5 | 7 | 7,7 | 8,4 | 9,2 | 9,9 |
| P12 | 0,91 | 5,71 | 1,054 | 0,738 | 106,49 | 0,01 | 4,0 | 5,5 | 6 | 6,5 | 7,1 | 7,5 |
| P13 | 0,88 | 7,10 | 0,904 | 0,655 | 106,01 | -0,23 | 4,6 | 6,8 | 7,5 | 8,2 | 9,2 | 9,9 |
| P14 | 0,84 | 6,92 | 1,039 | 0,755 | 77,90 | 0,68 | 4,3 | 5,8 | 6,3 | 6,8 | 7,5 | 7,9 |
| P15 | 1,25 | 7,73 | 1,249 | 1,216 | 161,10 | -0,06 | 8,5 | 6,7 | 7,2 | 7,7 | 8,3 | 8,8 |
| P16 | 1,15 | 7,48 | 1,194 | 1,140 | 103,16 | -0,09 | 7,5 | 6,8 | 7,4 | 7,9 | 8,5 | 9,0 |
| P17 | 1,08 | 8,41 | 1,166 | 1,090 | 91,59 | 0,00 | 6,9 | 6,9 | 7,4 | 7,9 | 8,6 | 9,1 |
| P18 | 0,84 | 8,21 | 1,012 | 0,763 | 90,83 | 0,00 | 4,1 | 6,3 | 6,8 | 7,4 | 8,1 | 8,7 |
| P19 | 0,75 | 6,06 | 1,076 | 0,728 | 74,28 | 0,44 | 2,9 | 5,3 | 5,8 | 6,2 | 6,8 | 7,2 |
| P20 | 0,57 | 5,75 | 0,949 | 0,503 | 83,93 | -0,09 | 1,8 | 4,8 | 5,3 | 5,7 | 6,3 | 6,8 |
| P21 | 0,67 | 6,76 | 0,95 | 0,618 | 101,93 | -0,42 | 3,2 | 5,9 | 6,4 | 7 | 7,8 | 8,3 |
| P22 | 1,09 | 7,46 | 1,16 | 1,094 | 99,17 | -0,29 | 8,2 | 7 | 7,5 | 8,1 | 8,7 | 9,3 |
| P23 | 0,89 | 7,38 | 1,061 | 0,880 | 87,57 | 0,00 | 5,1 | 6,6 | 7,2 | 7,8 | 8,5 | 9,0 |
| P24 | 0,77 | 7,02 | 1,005 | 0,690 | 87,67 | -0,33 | 3,6 | 5,9 | 6,4 | 7 | 7,6 | 8,2 |
| P25 | 1,39 | 8,69 | 1,545 | 2,024 | 73,02 | 2,30 | 11,0 | 8 | 8,5 | 8,9 | 9,5 | 9,9 |
| P26 | 1,23 | 12,52 | 1,27 | 1,320 | 73,21 | 2,64 | 8,7 | 6,8 | 7,2 | 7,7 | 8,3 | 8,7 |
| P27 | 0,86 | 6,58 | 1,052 | 0,782 | 72,87 | 1,01 | 4,1 | 5,8 | 6,3 | 6,8 | 7,4 | 7,9 |
| P28 | 1,25 | 7,93 | 1,198 | 0,736 | 92,46 | 0,01 | 11,4 | 4,4 | 4,8 | 5,1 | 5,5 | 5,8 |
| P29 | 0,65 | 8,27 | 0,9 | 0,503 | 80,41 | 0,22 | 2,2 | 5,3 | 5,8 | 6,4 | 7,1 | 7,6 |
| P30 | 1,40 | 10,27 | 1,176 | 1,499 | 100,11 | 0,25 | 15,1 | 9,2 | 9,9 | 10,6 | 11,5 | 12,1 |
| P31 | 0,68 | 7,47 | 0,924 | 0,580 | 81,70 | 0,46 | 2,8 | 5,7 | 6,2 | 6,8 | 7,5 | 8,1 |

**Table. 7.5 ï** Average significant wave height $\overline{H}_s$ , maximum significant wave height $H_{smax}$, parameters of the Weibull distribution (1.10) ($h_l$=0) and of the base – height regression (1.16), mean wave power per unit length , and return values of the significant wave height h(R) calculated at the considered locations.

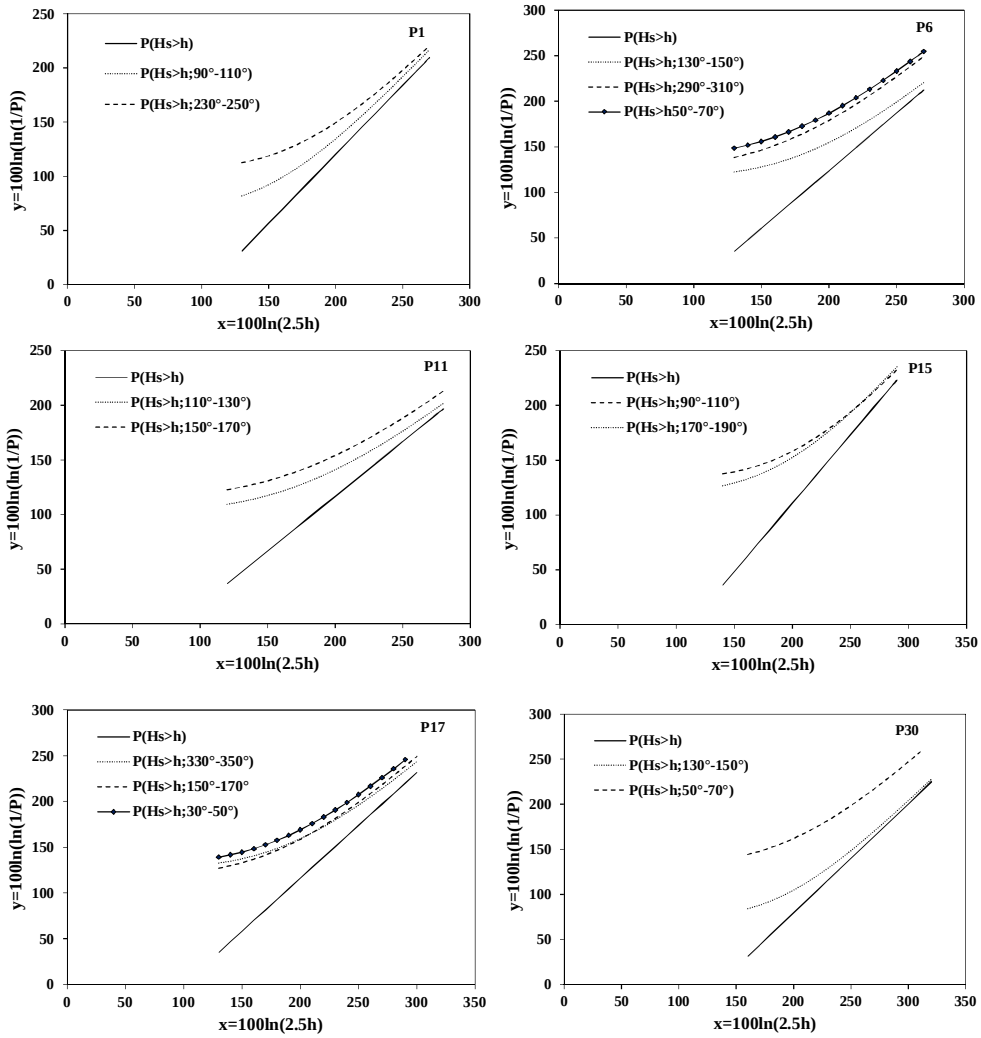


**Figure. 7.11 ï** Omnidirectional distribution and directional distribution of significant wave height estimated from the wave data generated artificially at the locations shown in the legends.

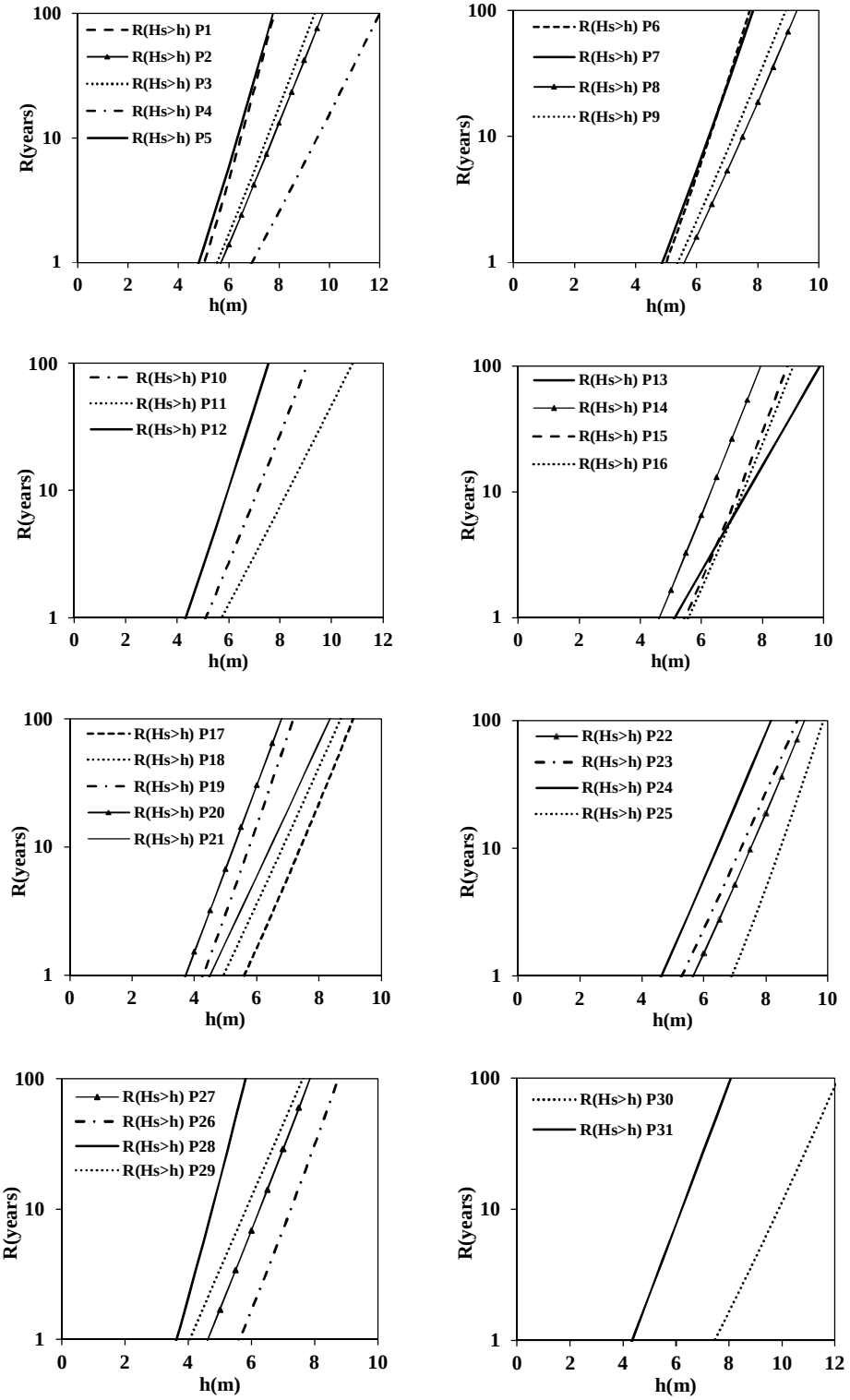


**Figure. 7.12ï** Omnidirectional return period of significant wave height calculated at all the locations.

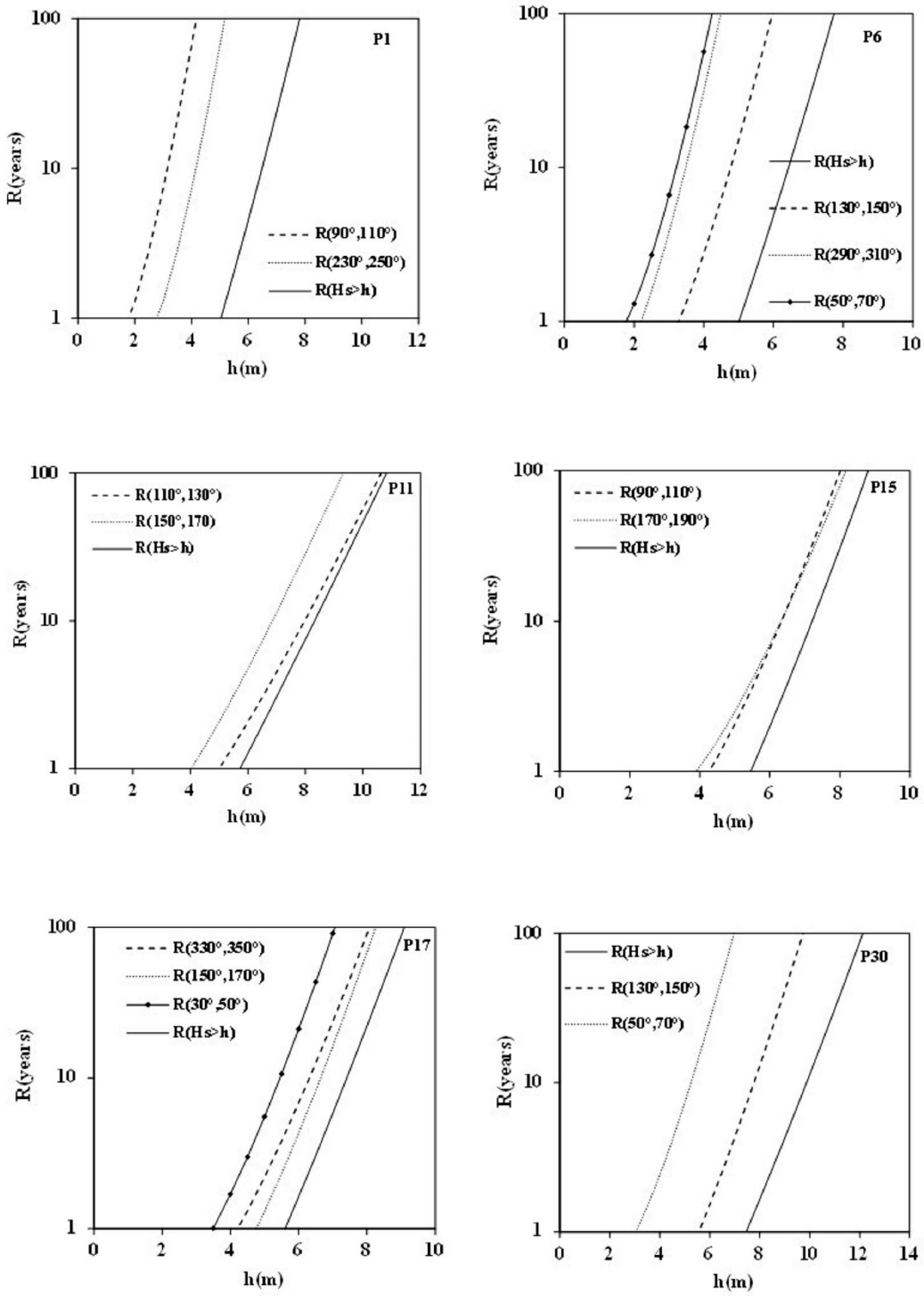


**Figure. 7.13 ï** Directional return period of significant wave height calculated at the locations shown in the legend.

## 7.5 Discussion

The results shown in section 7.4 confirm the outputs of previous studies *(Liberti et al., 2013)*. Indeed, the highest wave energy potential is in the North-West of the Mediterranean Sea. At this location, the results show that the mean wave power is up to 15.1kW/m in Alghero (P30). However, it is seen that there are several areas that can be eligible for placing a wave energy harvester. Specifically, Tunisia (P4) has a mean wave power of 11.1kW/m, the area of Crete (P15) has a mean wave power of 8.5kW/m. In Sicily (P22) there is a mean wave power of 8.2kW/m, and in Greece (P16, P17) the mean wave power is about 7.3kW/m. These considerations are relevant in a preliminary design stage, but they must be complemented by proper considerations on the directional pattern of the sea states. Indeed, it is well known that the direction associated with the maximum wave power is fundamental in the design of several devices. In addition, further considerations are mandatory when a second maximum occurs at a different wave direction. Consider for instance the directional wave power in Morocco (P1) (Figure 7.7). In this context, it is seen that two maxima occur at 100° and at 240°. During the design process of an angle-dependent device, this feature poses a crucial issue: it is quite complex to harvest the total amount of energy. Indeed, in this situation the device can be optimized for harvesting energy propagating from, say, 100°, but it cannot exploit the energy propagating from the other direction. However, at the design stage in a coastal area, this information must be connected with a bathymetric analysis in order to assess the convenience of realizing a wave energy device. As the useful amount of energy can be drastically reduced with respect to the offshore available energy.

In terms of available wave power, it is worth-mentioning the fact that in a European context the Mediterranean Sea is not energy-wise rich. Indeed, the areas exposed to oceanic waves have larger mean wave power values. Consider the case of the Azores Islands investigated by Rusu and *Guedes Soares (2012)*. In this context, the average wave power can be up to 75.5kW/m. The difference is certainly relevant, as it is about 5 times larger than largest values calculated in the Mediterranean Sea. A similar result can be obtained by considering for instance the location investigated by *Rusu and Guedes Soares (2012)*, the Madeira Islands, where the average wave power is up to 65.4kW/m. The wave energy resource in the Atlantic European coasts was investigated also by *Guedes Soares, et al. (2014)*. They estimated seasonal parameters (specifically, winter and summer periods) and showed that the winter mean wave power is almost 100kW/m in Ireland, 21.66kW/m in UK and 52.45kW/m in France.

In many respects, these comparisons could depict a quite inconvenient framework for the wave energy devices in the Mediterranean Sea. Indeed, it may be argued that, the potentially exploitable energy does not compensate the effort for constructing and for maintaining a wave power plant. In this regard, a cost-benefit analysis is crucial. Irrespective of the specific problems investigated in this context, two points are emphasized herein. First, it is relevant to consider the fact that a variety of devices have been conceived and some of them work well in the Mediterranean Sea *(e.g., the REWEC3 plant: Boccotti, 2007, 2012; Malara and Arena, 2013; Arena et al., 2013)*. Further, hybrid solutions combining, for instance, wave energy and wind energy harvesters are attractive in the Mediterranean context, as well. Second, the extreme waves associated with the Mediterranean Sea are certainly smaller than the ones typically occurring at an ocean sea (for a certain return period). This implies reduced manufacturing/material costs, as the structural reliability is assessed in conjunction with severe, but feasible, environmental conditions. A comparison between the calculated return values and the mean wave powers shows that a direct correspondence cannot be identified. Indeed, a high return value is not associated, in general, with a high mean wave power. In Sardinia (P30), the largest return values and the largest mean wave power have been calculated. However, a comparison with other locations shows a variety of situations. For instance, consider the data of Tunisia (P4). In this context, the return values are quite close to the Sardinia ones, but the mean wave power is markedly smaller. A location with energy content similar to the one of Tunisia is in Corsica (P28). However, in this context it is seen that extreme events are quite mild in comparison to the ones in Tunisia. As mentioned previously, these considerations are relevant from a design perspective, as the design process involves an energy-wise optimization of the device, and, at the same time, a structural reliability assessment in extreme conditions. Therefore, by comparing the results of the last two mentioned locations, it is seen that a hypothetical wave energy device installed in Tunisia harvests as much energy as in Corsica, but it is exposed to extreme sea states as severe as in Sardinia.

## 7.6 Conclusions

This chapter has proposed a synthetic view on the wave related elements involved in the design process of a wave energy harvester. The first part of the work has disseminated the theoretical elements involved in the determination of the available wave power and of the extreme events. In this context, a simplified formula for the calculation of the wave power in a given sea state has been derived. This expression has been shown to provide reliable wave power estimates in a variety of sea states by comparing their outcomes with the “real” ones. The

return period of a sea state with a given wave height are been discussed by applying the Equivalent Triangular Storm (ETS) model. The model allows determining closed form solutions for the determination of relevant return values. The second part of the chapter has discussed the wave climate characteristics along the coasts of the Mediterranean Sea. Specifically, it has been identified the most energetic areas of the Mediterranean Sea and the most severe locations in terms of extreme events. In addition, it has been elucidated elements connected to the design of angle-dependent wave energy converters. Specifically, the chapter has shown that both wave energy and return values must be determined by including the influence of direction and of wave propagation. In this regard, it is seen that conventional analyses are irrespective of the wave direction. Thus, they do not provide a complete description of the wave climate and are inadequate for designing angle-dependent wave energy harvesters. The paper has showed that, in these circumstances, a wave energy converter cannot exploit the total amount of wave energy. This is due to the fact that the energy is not concentrated on a restricted directional sector, but is distributed over several directions that cannot be covered simultaneously. Analogously, the extreme events are not well predicted via conventional, angle-independent, techniques. In this context, the use of a directional return period is suggested. Such a return period allows estimating the significant wave height of a given return period and direction of wave propagation. In this regard, the numerical results show that the use of a conventional return period leads to overestimations of significant wave height values.

THIS PAGE INTENTIONALLY LEFT BLANK

# Chapter 8 ï Optimal configuration of an U-OWC wave energy converter

*This chapter deals with the geometric optimization of a REWEC3 (Resonant Wave Energy Converter) or U-OWC device. An U-OWC is similar to a conventional breakwater implemented by a U-shaped duct representing the active part of the plant. The working principles is similar to the one of a classical OWC, but there are not waves entering the plant: an oscillating water column produced by pressure fluctuations on the outer opening of the vertical duct. The main feature of the device is related to the possibility to design the vertical duct in order to tune the eigenperiod of the plant very close to the peak period of the incident waves reaching the natural resonance without any device for phase control. The application proposed in this chapter aims to identify the key geometric parameters which are involved in the identification of optimal geometric configuration intended as the one giving the maximum converted power. Considering a real case study pertaining to applications of the U-OWC in the Mediterranean Sea, the work proposes a parametric analysis for investigating the influence of the geometrical parameters involved in the mathematical description of the plant. The work shows that few parameters are relevant in the design process of U-OWC plants and that the maximum converted power occurs close to resonance, but these conditions do not involve the same geometrical configuration.*

## 8.1 Introduction

The U-OWC wave energy converter (also known as Resonant Wave Energy Converter, REWEC) is a device for converting wave energy into electrical energy. It was developed in the past decade by *Boccotti (2003)* via modifications of conventional OWCs. The key characteristic of the device is the use of a vertical U-duct for connecting the water column to the open wave field. Such a vertical duct allows improving the performance of the plant. Indeed, *Boccotti (2003)* proved by experimental data that such a device is capable of reaching naturally the resonance condition with the incident waves, without the use of phase control devices, and, consequently, of absorbing a larger amount of energy. From the perspective of technological

development, the main steps involved the incorporation of the device into traditional maritime structures. The first model involved a U-OWC incorporated into a submerged breakwater. Nowadays, the most investigated U-OWC configuration is the one employed in conjunction with classical vertical breakwaters. *Boccotti (2007a)* conceived this solution and proposed a comparison with an analogous OWC. In this regard, he showed that the plant has a better performance both in wind-generated sea states and in swell seas. The mathematical modelling of the device was investigated by *Boccotti (2007b)* and validated against experimental data by *Boccotti et al. (2007)*. The relevant characteristic of the proposed model is the introduction of a nonlinear term for describing the oscillating flow into the vertical duct. Indeed, head losses into the duct are not negligible and must be modelled via a drag-type nonlinearity. In this context, the proposed approach for describing the hydrodynamics relies on the determination of a simplified representation of the wave field that is properly determined via an iterative procedure maximizing the ratio between the absorbed wave power and the incident wave power. Despite the fact that this representation is not consistent with the associated boundary value problem, the predicted absorbed energy is in agreement with the experimental data. *Malara and Arena (2013)* developed a consistent representation of the wave field surrounding the U-OWC. Specifically, they proposed an approximate, but consistent, representation of the diffracted and of the radiated wave field via an eigenfunction expansion of the related boundary value problem. In this manner, they determined also infinite added mass and retardation function of the system. *Boccotti (2012)* proposed a holistic view on the U-OWC design. He disseminated the key issues involved in: numerical simulation of the plant dynamics; optimal plant determination; and structural reliability assessment in extreme conditions con-ducted via a Quasi-Deterministic approach *(Boccotti, 2000)*. Considering the need of developing reliable and automated techniques for the optimization of the device, the work proposed in this chapter addresses the problem of identifying the key parameters involved in the optimization of a U-OWC plant. For the purpose, a relevant case study is examined: U-OWC in Alghero, North-West Mediterranean Sea, which is the most energetic site in Mediterranean Sea. Starting from a properly designed plant, a parametric analysis is pursued and the relevant parameters are identified.

## 8.2 Working principles and hydrodynamic modelling of an U-OWC

Figure 8.1 shows a scheme of a U-OWC wave energy converter. The device is composed by a partially closed air chamber, which is connected to the atmosphere via an air duct hosting a turbine. Under the air chamber is located a water column, which is connected to the open wave field via a small vertical U-shaped duct. The working principle of the device is similar to the

one of classical OWCs. Specifically, the sea waves excite the water column by inducing oscillations of the inner free surface that, consequently, compresses and expands the air chamber. Thus, an alternating air flow is generated in the air duct, which is exploited by a turbine (such as a Wells turbine) converting (in conjunction with adequate electrical equipment) wave energy to electrical energy.

From the perspective of dynamic modelling, *Boccotti* (2007b) and *Malara and Arena* (2013) elucidated the crucial elements involved in the description of the plant dynamics. The equation of motion of the water column is

$$\frac{l'}{g}\frac{s''}{s'}\frac{d^2\xi}{dt^2}+\frac{(l''-\xi)}{g}\frac{d^2\xi}{dt^2}=h'-h''-\Delta h_w\,, \tag{8.1}$$

in which

$$h'=\xi_0-\xi+\frac{1}{2g}\left(\frac{d\xi}{dt}\right)^2+\frac{p_a-p_{atm}}{\rho g} \tag{8.2}$$

$$h''=\frac{\Delta p}{\rho g} \tag{8.3}$$

$$\Delta h_w=K_w\frac{u\,|u|}{2g} \tag{8.4}$$

and

$$u=\frac{s''}{s'}\frac{d\xi}{dt} \tag{8.5}$$

where $g$ = acceleration due to gravity; $z$ = air pocket height measured from the top of the air chamber; $z_0$ = distance from the top of the air chamber to the mean water level; $s_d$ = vertical duct width; $s_c$ = inner chamber width; $l_w$ = water column length; $l_d$ = vertical duct length; $p_a$ = air pocket pressure; $p_{atm}$ = atmospheric pressure; $\rho$ = water density; $\Delta p$ = wave pressure at the top of the vertical duct; and $K_w$ = head loss coefficient.

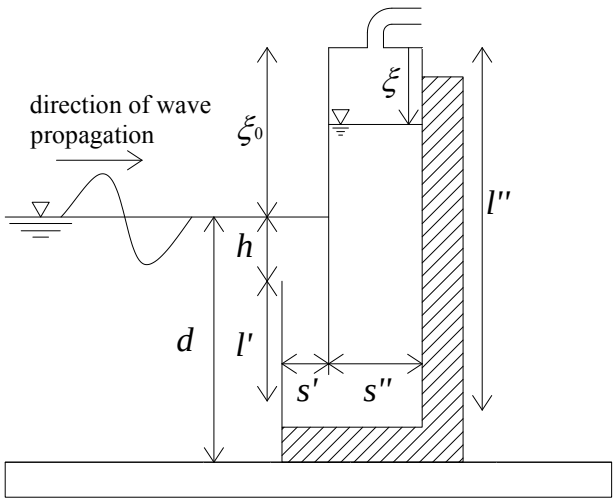


**Figure. 8.1 ï** Cross-section of a U-OWC wave energy converter.

Equation (8.1) is coupled to the equation of the air pocket, that is the equation of state,

$$\frac{p_a}{\rho_a^k} = \frac{p_{atm}}{\rho_{atm}^k} \tag{8.6}$$

$k$ being the exponent of the equation of state, $\rho_{atm}$ the atmospheric density and $\rho_a$ the air pocket density. The numerical integration of Equations (8.1) and (8.6) is accomplished by considering also the air density time variation and the air mass ($M_a$) change due to the flow into the air duct. These quantities are calculated as

$$\rho_a = \frac{M_a}{bs''\xi} \tag{8.7}$$

in which $b$ is the width of a single cell of the plant; and

$$\frac{dM_a}{dt} = -\frac{1}{2}(\rho_a + \rho_{atm})\frac{\pi D^2}{4}u_a \tag{8.8}$$

where $u_a$ is the air flow velocity and is related to the air pressure $p_a$ of the air pocket via the equation

$$l_a \frac{du_a}{dt} = \frac{p_{atm}}{\rho_{atm}}\frac{k}{k-1}\left[\left(\frac{p_a}{p_{atm}}\right)^{1-1/k} - 1\right] - \Delta h_a g \tag{8.9}$$

$\Delta h_a$ being given by

$$\Delta h_a = \left( K_a \frac{u_a^2}{2g} + \Delta h_t \right) \frac{u_a}{|u_a|} \tag{8.10}$$

where $K_a$ is a head loss coefficient and $\Delta h_t$ is turbine dependent. Equations (8.1)–(8.9) are integrated numerically by a finite difference scheme given the initial conditions, at $t = 0$,

$$\xi = \xi_0; \ \frac{d\xi}{dt} = 0; \ M_a = \rho_{atm} bs'' \xi_0 \tag{8.11}$$

and the time history of $\Delta p(t)$.

The time history $\Delta p(t)$ is calculated given the wave pressure of the incident wave field $\Delta p_i(t)$. Specifically, it is estimated as

$$\Delta p = C_d \Delta p_i \tag{8.12}$$

being $C_d$ a diffraction coefficient dependent on the absorption coefficient of the plant $C_a$. That is,

$$C_d = 2 - C_a \tag{8.13}$$

The absorption coefficient $C_a$ is the ratio of the average energy absorbed by the plant over the average incident wave energy. Obviously, $C_a$ depends on the $\Delta p$. Thus, the calculation involves iteration on the diffraction coefficient $C_d$. The procedure converges rapidly by assuming $C_d = 2$ at the first iteration. The time history of the incident wave pressure is synthesized via the spectral method in conjunction with the Fast Fourier Transform (FFT) algorithm. For the purpose, the theoretical spectrum used for the computation is

$$S_{\Delta p}(\omega) = S(\omega) \frac{\cosh^2[k_0(d-q)]}{\cosh^2(k_0 d)}, \tag{8.14}$$

where $d$ is the water depth, $q$ is the submergence of the U-duct opening, $k_0$ is the wavelength estimated by the linear dispersion relation

$$k_0 \tanh(k_0 d) = \frac{\omega^2}{g}, \tag{8.15}$$

and $S(\boldsymbol{\gamma})$ is the spectrum of the free surface displacement.

The performance of the plant is assessed according to three parameters: resonance index; absorption coefficient and production coefficient. The resonance index $R$ is given by the equation:

$$R = 4T_1 / T_2 , \tag{8.16}$$

where $T_2$ is the peak spectral period and $T_1$ is the time lag of the first minimum of the cross-correlation function between the wave pressure $\Delta p$ and the air pocket height $\xi$. Such an index is useful for checking if the plant is able to work in resonance conditions. Indeed, $R$ close to 1 means that it works close to the resonance condition. This parameter is also quite useful for tuning the plant, as it is sensible to the deviations from the resonance condition. If $R$<1, the natural period of the plant is smaller than the peak spectral period, otherwise it is larger than the peak spectral period.

The performance of the plant from the energy-wise perspective is described via the absorption coefficient $A$ and the production coefficient $A_p$. These coefficients are calculated via the equations:

$$A = < P_{abs} > / < P_{inc} > , \tag{8.17}$$

and

$$A_p = < P_{conv} > / < P_{inc} > , \tag{8.18}$$

$P_{abs}$ being the power absorbed by the plant, $P_{conv}$ being the power converter to electrical power, $P_{inc}$ being the incident wave power and <·> denotes averaging over time.

The coefficients (8.17) and (8.18) provide a quantification of the efficacy and efficiency of the U-OWC. Indeed, the absorption coefficient renders a mean estimate of the fraction of incident wave energy captured by the plant, while the production coefficient shows the fraction of incident wave energy converted to electrical energy. Obviously, the effect of the head losses in the vertical duct and of the turbine efficiency imply that

$$A > A_p , \tag{8.19}$$

In the light of a U-OWC design, this distinction is relevant. Indeed, $A$ allows optimizing the performance of the plant in terms of absorption capability, while $A_p$ allows optimizing the synergy of the plant with a certain turbine.

## 8.3 Case study

The parametric analysis is conducted by estimating, from Monte Carlo simulations, the parameters introduced in section 8.2 for a number of U-OWC configurations. The geometrical configurations are selected starting from a U-OWC working in resonance conditions. That is, given the "resonant" U-OWC, the subsequent systems are chosen by modifying one geometrical parameter. In a preliminary stage, a certain sea state is determined for conducting the simulations. In this regard, the objective is to identify the sea state propagating the most relevant fraction of mean annual wave energy. Such a sea state plays the role of a "design" sea state.

### *8.3.*1 Preliminary wave data analysis for the identification of design sea state

A preliminary wave data analysis is pursued to determine a relevant stationary sea state for performing the Monte Carlo simulations. The location under investigation is Alghero (West Sardinia, Italy), shown in Figure 8.2. This is an interesting site as it possesses the largest amount of the mean annual wave energy of the Mediterranean Sea *(Liberti et al. 2013, Vicinanza et al. 2013, Arena et al. 2014)*. The sea state is identified by processing the buoy data provided by the Rete Ondamentrica Nazionale (RON) buoy network. This database provides significant wave height $H_s$ and mean wave period $T_m$ of the recorded sea states. Specifically, the present computation considers data recorded from September 1st, 1989 to April 5th, 2008, which includes 125442 records.

The design sea state is determined considering the average wave power associated with each sea state, which is calculated as *(Arena et al., 2013)*

$$\Phi = \frac{\rho g^2}{64\pi} \gamma_f H_s^2 T_m f \ , \tag{8.20}$$


**Figure. 8.2 ï** Location of Alghero.

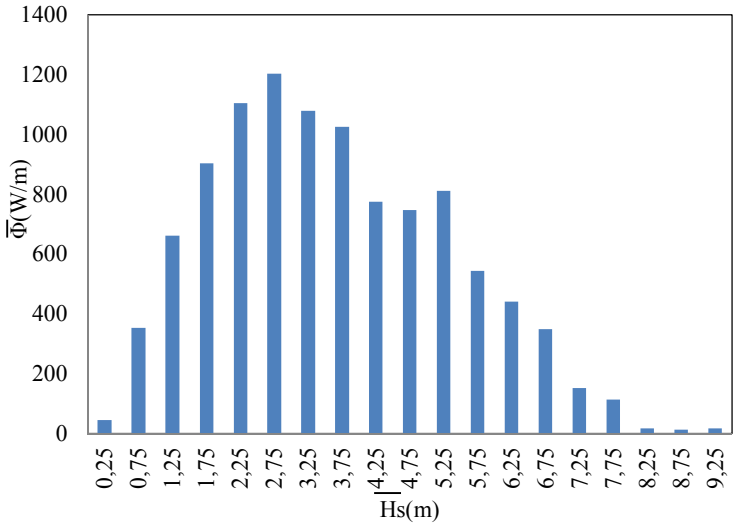


**Figure. 8.3 ï** Average wave power associated with certain significant wave height intervals.

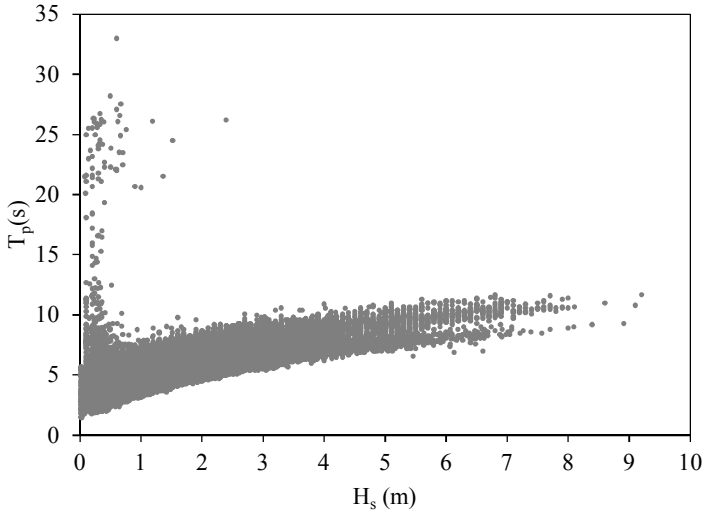


**Figure. 8.4ï** Peak spectral period $T_p$ - significant wave height $H_s$ pairs recorded in Alghero.

where the parameter $\gamma_f$ depends on the frequency spectrum and it is equal to 1.12 for the JONSWAP mean spectrum *(Hasselmann et al. 1973)* and to 1.15 for the PM spectrum *(Pierson & Moskowitz 1964)*, and $f$ is the frequency of occurrence of a certain sea state.

| $d$ | $\gamma_0$ | $b$ | $s\alpha$ | $s\beta$ | $S_a$ | $d_t$ | $q$ |
|---|---|---|---|---|---|---|---|
| 20 | 8 | 4.25 | 2.5 | 4 | 2.75 | 0.75 | 2 |

**Table. 8.1 ï** Geometrical characteristics of the U-OWC in Alghero with $R$=1. Note that $S_a$ denotes the amplitude of the opening between the water column and the vertical duct and $d_t$ denotes the outer diameter of the turbine. Units are in meters.

Figure 8.3 shows that at Alghero the maximum wave power relates to a sea state with significant wave height $H_s$=2.75m. The associated peak period is determined from a $T_p - H_s$ regression. Specifically, the peak spectral period associated with the significant wave height is $T_p$ = 9.42s.

### 8.3.2 Plant design

An U-OWC is designed considering the "design" sea state identified in section 8.3.1. Obviously, the mentioned parameters provide only a synthetic description of the sea state, while the complete frequency domain representation is needed for conducting the simulations. In this regard, a variety of spectral shapes could be selected for describing the incident wave field. However, considering the mentioned $H_s$ - $T_p$ pair and the peculiarities of the site under examination, the six parameter spectrum is adopted *(Ochi and Hubble 1976)*. The turbine adopted for pursuing the simulations is the monoplane Wells without guide vanes. These turbines were investigated by *Curran and Gato (1997)*. Their experimental data are used in conjunction with the described numerical algorithm. Further, the turbine has 2/3 ratio between the inner and the outer diameter. Considering these input data and the dynamical model described in section 8.2, the U-OWC has been designed. Specifically, the plant with the geometrical characteristics shown in Table 8.1 relates to a plant with $R$=1.008, $A$=0.46 and $A_p$=0.16. In this regard, note that the designed geometrical configuration is such that $l_{\hat{o}}=d-q$. That is, the floor of the U-OWC is at the water depth level. Obviously, this is a specific design solution, which has been invoked for accommodating the identification of a "resonant" U-OWC. Nevertheless, different solutions could be adopted, as well.

### 8.3.3 Parametric analysis

The parametric analysis is developed starting from the plant with the geometrical characteristics shown in Table 8.1. The analysis is conducted by varying one parameter per simulation. So that, its influence is investigated by referring to resonance index $R$, absorption coefficient $A$ and production coefficient $A_p$. Figure 8.5 shows the results related to the parameters $\vartheta_0$, $b$, $s'$, $s''$, $q$ and $S_a$. A common feature of all the figures is the sensibility of the resonance index $R$. Indeed, it is seen that even a small change in one parameter relates to a strong deviation of the system from resonance. The energy related parameters are less sensible, but it is worth-mentioning that their maxima may be close to, but do not coincide with, $R$=1. Such evidence is relevant from a design perspective, as it implies that by designing a plant via

the resonance index does not ensure the maximum production coefficient. The parameters $b$ and $q$ are seen to have a small influence on $A$ and $A_p$, while they modify the eigenperiod of the plant. On the other hand, $s$' and $s$" relate to a modification of all parameters. The significant influence of $s$' and $s$" on $A$ and $A_p$ is connected to the head losses computed in the vertical duct and in the water column dynamics. Indeed, by imposing an excessively small duct or water column, the water flow is affected by an excess of head loss that dissipates the energy absorbed by the system or may even reduce drastically the capability of absorbing wave energy. The parameters $b$ and $q$ have a small influence on $A$ and $A_p$. Obviously, this fact does not imply that the absorbed energy in kept unchanged, as the parameters provide merely a percentage of the absorbed/converted wave energy. In this context, it is worth-mentioning that by in-creasing $b$ the absorbed wave energy is effectively increased. Thus, the converted power is increased, as well. Nevertheless, by increasing the submergence $q$, the absorbed power decreases, as the wave pressure amplitude decays with the submergence. Thus, the converted power decreases. The U-OWC key feature is the capability of reaching naturally the resonance condition. Such a condition is relevant for the energy performance of the plant. Indeed, as mentioned previously, maximum production occurs close to $R$=1. In this regard, the decreasing patter of $A$ and $A_p$ can be read in the light of the fact that the plant is quite far from resonance. The parametric analysis on the other parameters revealed that, despite a change in the resonance index, they do not affect the production coefficient $A_p$. Obviously, this does not apply to the turbine diameter $d_t$, as in this context the flow rate efficiency curve governs the performance of the system *(Curran and Gato 1997)*.

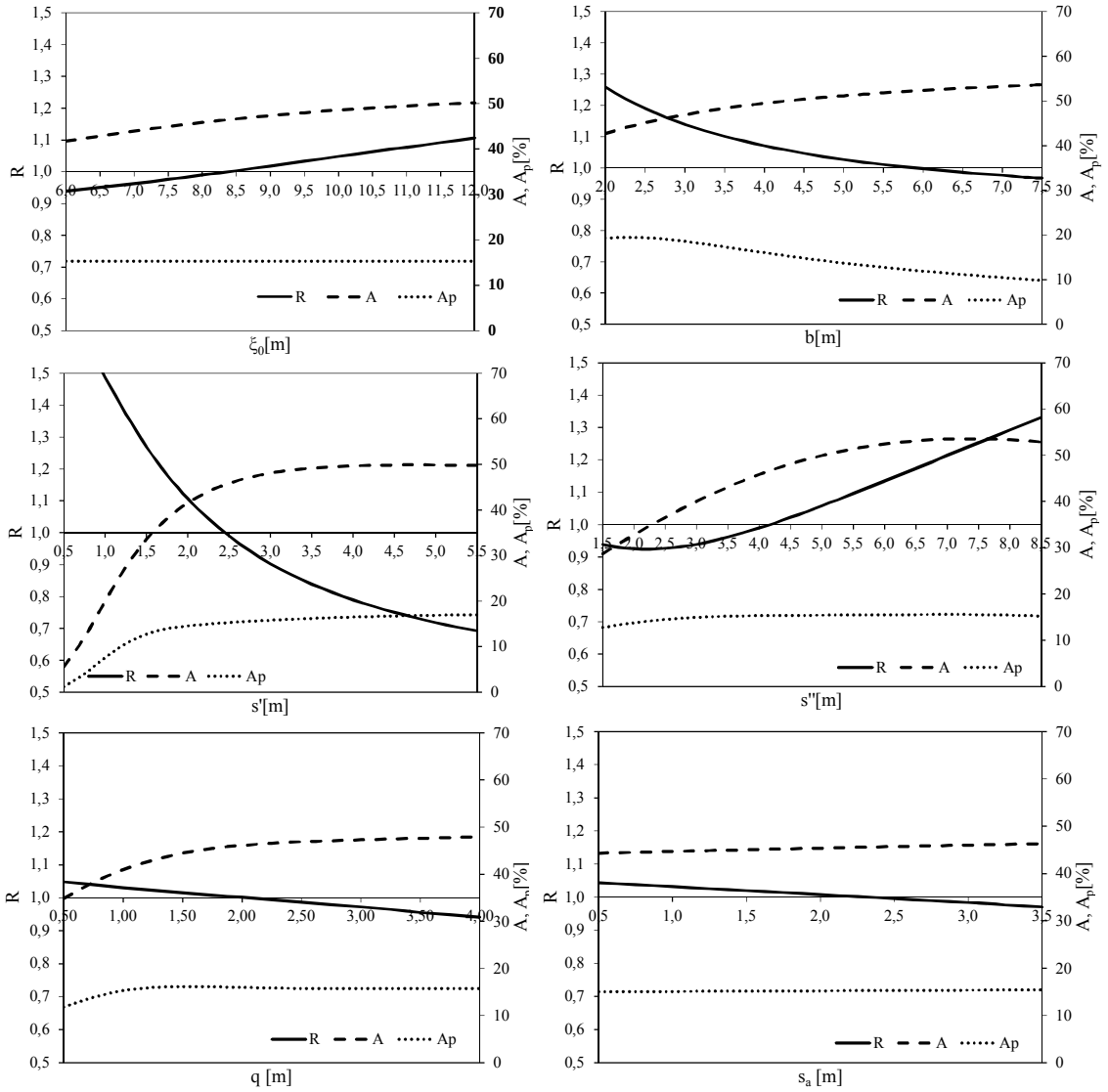


**Figure. 8.5 ï** Resonance index $R$, absorption coefficient $A$, production coefficient $A_p$, versus geometric parameters $\xi_0$, $b$, $s$', $s$'', $q$, $S_a$.

## 8.4 Conclusions

The work presented in this chapter has proposed a parametric analysis focusing on the key coefficients involved in the design of a U-OWC plant: resonance index, absorption coefficient and production coefficient. For the purpose, a case study has been investigated: U-OWC in Alghero. It is seen that $R$ is quite sensible to short variations of the geometrical parameters, while $A$ and $A_p$ are less sensible. Other parameters have been investigated as well. However, it is

seen that their influence on the energy-wise performance of the plant is not relevant. These results are expected to be used in future researches pertaining to the optimal design of U-OWCs. Specifically, given the identified key quantities involved in an optimal design (for instance, based on the maximization of the production coefficient), an algorithm can be constructed for optimizing a plant starting from a certain U-OWC configuration.

# References


Arena, F. and Barbaro, G. (1999). Risk analysis in the Italian seas, Publ. CNR-GNDCI num. 1965, BIOS, 1-136.

Arena, F., (2004), On the prediction of extreme sea waves. Environmental Sciences and Environmental Computing, P. Zanetti, Ed., Enviro Comp Institute, 2, 1-50.

Arena, F., and Pavone, D., (2006), Return period of nonlinear high wave crests. J. Geophys. Res. 111, C08004.

Arena, F., and Pavone, D., (2009), A generalized approach for the long-term modelling of extreme sea waves. Ocean Model. 26, 217–225.

Arena, F., and Puca, S., (2004), The reconstruction of significant wave height time series by using a neural network approach. ASME Journal of Offshore Mechanics and Arctic Engineering. 126, 213-219.

Arena, F., Fiamma, V., Laface, V., Malara, G., Romolo, A., Viviano, A., Sannino, G. & Carillo, A., (2013). Installing U-OWC devices along Italian coasts. In: Proc. of the 32nd International Conference on Ocean, Offshore and Arctic Engineering, OMAE2013, Nantes, France, 9-14 June 2013.

Arena, F., Guedes Soares, C. & Petrova, P., (2010). Theoretical Analysis of Average Wave Steepness Related to Peak Period or to Mean Period. In: Proc. of the 29th Interna-tional Conference on Ocean, Offshore and Arctic Engi-neering, OMAE2010,Shanghai, China, 6-11 June 2010.

Arena, F., Malara, G., Barbaro, G., Romolo, A., Ghiretti, S., (2013), Long-Term Modelling of Wave Run-Up and Overtopping during Sea Storms. Journal of Coastal Research; 29: 419-29.

Arena, F., Malara, G., Romolo, A., (2014), Long-term statistics of nonlinear wave crests via the equivalent power storm model. Prob. Eng. Mech. in press, ISSN: 0266-8920.

Arena, F., Romolo, A., Malara, G., Ascanelli, A., (2013), On design and building of a U-OWC wave energy converter in the Mediterranean Sea: a case study. In: Proceedings of the 32nd International Conference on Ocean, Offshore and Arctic Engineering, OMAE2013, Nantes, France.

Arinaga, R.A., Cheung, K.F., (2012), Atlas of global wave energy from 10 years of reanalysis and hindcast data. Renewable Energy; 39: 49-64.

Ayat, B., (2013), Wave power atlas of Eastern Mediterranean and Aegean Seas. Energy; 54: 251-62.

Aydoğan, B., Ayat, B., Yüksel, Y., (2013), Black Sea wave energy atlas from 13 years hindcasted wave data. Renewable Energy; 57: 436-47.

Barstow, S., Mørk, G., Lønseth, L., Mathisen, J.P., (2009), Worldwaves wave energy resource assessments from the deep ocean to the coast. In: Proceedings of the 8th European wave and tidal energy conference, Uppsala, Sweden.

Bernardino, M., Boukhanovsky, A., and Guedes Soares, C., (2008), Alternative Approaches to Storm Statistics in The Ocean. Proceedings of the 27th International Conference on Offshore Mechanics and Arctic Engineering (OMAE 2008); Estoril, Portugal. New York, USA: ASME; OMAE2008-58053.

Boccotti, P., (1981), On the highest waves in a stationary Gaussian process. Atti Acc. Ligure di Scienze e Lettere 38, 271–302.

Boccotti, P., (1981). On the highest waves in a stationary Gaussian process. Atti Acc. Ligure di Scienze e Lettere, 38, 271-302.

Boccotti, P., (1982). Relations between characteristic sea wave parameters. J. Geophys. Res., 1982, 87, 4267-4268.

Boccotti, P., (1986), On coastal and offshore risk analysis. Excerpta of the Italian Contribution to the Field of Hydraulic Eng., 19–36.

Boccotti, P., (1989). On mechanics of irregular gravity waves. Atti Acc. Naz. Lincei, Memorie, VIII, 111-170.

Boccotti, P., (1997), A general theory of three-dimensional wave groups. Ocean Eng. 24, 265–300.

Boccotti, P., (2000), Wave Mechanics for Ocean Engineering. Elsevier Science, New York.

Boccotti, P., (2003). On a new wave energy absorber. Ocean Engineering 30(9): 1191-1200.

Boccotti, P., (2007) Comparison between a U-OWC and a conventional OWC. Ocean Engineering; 34: 799-805.

Boccotti, P., (2007a). Comparison between a U-OWC and a conventional OWC. Ocean Engineering 34(5-6): 799-805.

Boccotti, P., (2007b), Caisson breakwaters embodying an OWC with a small opening—Part I: Theory. Ocean En-gineering 34(5-6): 806-819.

Boccotti, P., (2012), Design of breakwater for conversion of wave energy into electrical energy. Ocean Engineering; 51: 106-18.

Boccotti, P., (2012), Design of breakwater for conversion of wave energy into electrical energy. Ocean Engineering 51: 106-118.

Boccotti, P., Filianoti, P., Fiamma, V. & Arena, F. (2007), Caisson breakwaters embodying an OWC with a small opening-Part II: A small-scale field experiment. Ocean Engineering 34(5-6): 820-841.

Borgman, L. E., (1970), Maximum wave height probabilities for a random number of random intensity storms. Proc. 12th Conf. Coastal Eng., Washington, DC, ASCE, 53–64.

Borgman, L. E., (1973), Probabilities for highest wave in hurricane. J. Waterw. Harbors Coastal Eng., Div., Amer. Soc. Civ. Eng. 99, 185–207.

Boudiere E., Maisondieu C., Ardhuin F., Accensi M., Pineau-Guillou L., LepesqueurJ.,(2013). A suitable metocean hindcast database for the design of Marine energy converters. International Journal of Marine Energy, 3-4, e40-e52.

Coles, S., (2001), An introduction to Satatistical modelling of extreme values. Springer-Verlag, 208 pp.

Cornett, A.M. (2008), A global wave energy resource assessment. In: Proceedings of the 18th international offshore and polar engineering conference, Vancouver, BC, Canada.

Cruz., J., (2008), Ocean wave energy: current status and future perspectives. Bristol, United Kingdom: Springer.

Curran, R. & Gato, L.M.C., (1997), The energy conversion performance of several types of Wells turbine designs. Proceedings of the Institution of Mechanical Engineers, Part A: Journal of Power and Energy 211: 133-145.

Draper, L. (1966). The analysis and presentation of wave data - a plea for uniformity, Proc. 10th ICCE, pp. 1-11.

Earle, M.D., (1975). Extreme wave conditions during Hurricane Camille. J. Geophys. Res., 80, 377-379.

Falcão, A.F.d.O, (2010), Wave energy utilization: A review of the technologies. Renewable and Sustainable Energy Reviews; 14: 899-918.

Fedele, F., and Arena, F., (2005), Weakly nonlinear statistics of high random waves. Phys. Fluids, 17(2), 026601, 1–10.

Fedele, F., and Arena, F., (2010), The equivalent power storm model for long-term predictions of extreme wave events. J. Phys. Oceanogr. 40, 1106–1117.

Fedele, F., Arena, F., (2010), Long-Term Statistics and Extreme Waves of Sea Storms. Journal of Physical Oceanography; 40: 1106-17.

Ferreira, J.A., Guedes Soares, C., (1998), An application of the peaks over threshold method to predict extremes of significant wave height. J. Offshore Mech. Arct. 120, 165–176.

Ferreira, J.A., Guedes Soares, C., (1999). Modelling the long-term distribution of significant wave height with the beta and gamma models. Ocean Eng. 26 _8, 713–725.

Ferreira, J.A., Guedes Soares, C., (2000) Modelling distributions of significant wave height. Coastal Engineering; 40: 361-74.

Forristall, G. Z. (1978). On the statistical distribution of wave heights in a storm. J. Geophys. Res., 83, 2353-2358.

Forristall, G. Z., (1984). The distribution of measured and simulated wave heights as a function of spectral shape. J. Geophys. Res., 89, 10547-10552.

Forristall, G. Z., (2000), Wave crest distributions: Observations and second-order theory, J. Phys. Oceanogr. 30 (8), 1931–1943.

GEBCO, http://www.gebco.net/data_and_products/gridded_bathymetry_data/.

Goda, Y. (1979). A review on statistical interpretation of wave data. Rent. Port & Harb. Res. Inst., 18(1), pp. 5-32.

Goda, Y., (1992), Uncertainty of design parameters from viewpoint of extreme statistics. J. Offshore Mech. Arct., ASME 114, 76–82.

Goda, Y., (1999), Random Seas and Design of Maritime Structures. World Scientific, 443 pp.

Goda, Y., (2000), Random Seas and Design of Maritime Structures. World Scientific, 443 pp.

Goda, Y., (2010) Random Seas and Design of Maritime Structures. Singapore: World Scientific.

Goda, Y., Hawkes P. J., Mansard E., Martin M. J., Mathiesen M., Peltier E., Thompson E. and Van Vledder G., (1994). Recommended practice for extreme wave analysis, Journal of idraulic research, vol. 32, pp. 803-813.

Goda, Y., Hawkes, P., Mansard, E., Martin, M.J., Mathiesen, E., Peltier, E., Thompson, E., Van Vledder, G., (1993), Intercomparison of extremal wave analysis methods using numerically simulated data. Proceedings of the Second International Symposium On Ocean Wave Measurement and Analysis, ASCE, New Orleans, pp. 963–977.

Gómez Lahoz, M., and Carretero Albiach, J.C., (1997), A two-way nesting procedure for the WAM model: application to the Spanish coast. J. Offshore Mech. Arct. Eng. 119, 20–24.

Guedes Soares, C., (1986), Assessment of the uncertainty in visual observations of wave height. Ocean Engineering; 13: 37-56.

Guedes Soares, C., (1989), Bayesian prediction of design wave height. In: Reliability and Optimization of Structural Systems ’88, Thoft-Christensen, P., Ed., Springer-Verlag, 311–323.

Guedes Soares, C., Bento, A.R., Gonçalves, M., Silva, D., Martinho, P., (2014), Numerical evaluation of the wave energy resource along the Atlantic European coast. Computers & Geosciences; 71: 37-49.

Guedes Soares, C., Henriques, A.C., (1996). Statistical uncertainty in long-term distributions of significant wave height. J. Offshore Mech. Arctic Eng. 11, 284–291.

Guedes Soares, C., Scotto, M., (2001), Modelling uncertainty in long-term predictions of significant wave height. Ocean Engineering; 28: 329-42.

Guedes Soares, C., Weisse , R. , Carretero, J.C., and E. Alvarez , (2002), A 40 years hindcast of wind, sea level and waves in European waters. Pro-ceedings of the 21st International Conference on Offshore Mechanics and Arctic Engineering (OMAE'02), ASME Paper OMAE2002-SR28604.

Gumbel, E. J., (1958), Statistics of Extremes. Columbia University Press, New York.

Günther, H., Behrens, A., (2011), The WAM model validation document version 4.5.3. Report of the Institute of Coastal Research Helmholtz-Zentrum Geesthacht (HZG).

Haring, R. E., Osborne, A. R., and Spencer L. P. (1976). Extreme wave parameters based on continental shelf storm wave records. Proc. 15th Conf. on Coastal Eng., ASCE, New York.

Hasselmann, K., Barnett, T. P., Bouws, E., Carlson, H., Cartwright, D. E., Enke, E., Ewing, J. A., Gienapp, H., Hasselmann, D. E., Krusemann, P., Meerburg, A., Müller, P., Olbers, D. J., Richter, K., Sell, W., and Walden, H., (1973), Measurements of wind-wave growth and swell decay during the Joint North Sea Wave Project (JONSWAP). Dtsch. Hydrogr. Zeit. A12, 1–95.

Haver, S., (1985), Wave climate off northern Norway. Applied Ocean Research; 7: 85-92.

Haver, S., (1985). Wave climate off Northern Norway. Appl. Ocean Res. 7, 85–92.

Isaacson, M. and Mackenzie, N. G., (1981), Long-term distributions of ocean waves: a review. J. Waterway, Port, Coastal Ocean Div., 107, 93–109.

Isaacson, M., and N. G. Mackenzie, (1981), Long-term distribution of ocean waves. A review. J. Waterw., Port Coastal Ocean Div., Amer. Soc. Civ. Eng., 97, 93-109.

Jasper, N. H., (1956). Statistical distribution patterns of ocean waves and wave-induced ship stresses and motions, with engineering applications. Trans. Soc. Nav. Arch. & Mar. Eng., 64, 375-432.

Jonhatan, P., and Ewans , K. , (2007), The effect of directionality on extreme waves design criteria. Ocean Eng. 34, 1977-1994.

Jonhatan, P., Ewans, K., and Forristall, G., (2008), Statistical estimation of extreme ocean environments: The requirements for modelling directionality and other covariate effects. Ocean Eng. 35, 1211-1225.

Krogstad, H. E., (1985), Height and period distributions of extreme waves. Appl. Ocean Res. 7(3), 158–165.

Laface, V., and Arena, F., (2014), A new equivalent exponential storm model for long-term statistics of ocean waves. Natural Hazards and Earth System Sciences, under review.

Liberti, L., Carillo, A., Sannino, G., (2013), Wave energy resource assessment in the Mediterranean, the Italian perspective. Renewable Energy; 50: 938-49.

Longuet-Higgins, M. S., (1952). On the statistical distribution of the heights of sea waves. J. Mar. Res., 11, 245-266.

Longuet-Higgins, M. S., (1980). On the distribution of the heights of sea waves: Some effects of nonlinearity and finite band width. J. Geophys. Res., 85, 1519-1523.

Malara, G., Arena, F., (2013), Analytical modelling of an U-Oscillating Water Column and performance in random waves. Renewable Energy; 60: 116-26.

Mardia, K.V., Jupp, P.E., (2000), Directional statistics.

Mathiesen, M., Hawakes, P., Martin, M. J., Thompson, E., Goda, Y., Mansard, E., Peltier, E. and Van Vledder, G., (1994), Recommended practice for Extreme wave analysis. J. Hydr. Res., IAHR, Vol. 32, pp. 803-814.

Mørk, G., Barstow, S., Kabuth, A., Pontes, M.T., (2010), Assessing the global wave energy potential. In: Proceedings of the 29th international conference on Ocean, Offshore and Arctic Engineering, Shanghai, China.

Neelamani, S., (2009), Influence Of threshold value on Peak Over Threshold Method on the predicted extreme significant wave heights in Kuwaiti territorial waters. J. Coast. Res., Special Issue 56 564-568.

Ochi, M. K., Hubble, E.N., (1976), On six parameters wave spectra. Proceedings of 15th Coastal Engineering Con-ference Vol. 1: 301-328.

Ochi, M.K., (1992). New approach for estimating the severest sea state from statistical data. Proc. Coastal Eng. Conf., 512–525.

Ochi, M.K., (2005), Ocean Waves: The Stochastic Approach. Cambridge, United Kingdom: Cambridge University Press.

Pierson, W. J., and Moskowitz, L. A., (1964), A proposed spectral form for fully developed waves based on the similarity theory of S. A. Kitaigorodskii. J. Geophys. Res. 69, 5181–5190.

Pilar, P., Guedes Soares, C., and Carretero, (2008), Hindcast for the North East Atlantic European Coast. Coast. Eng. 55, 861-871.

Prevosto, M., Krogstad, H. E., and Robin, A., (2000) Probability distribution for maximum wave and crest heights. Coastal Eng. 40, 329–360.

Rice, (1958), Distribution of the duration of fades in ration transmission. Bell Syst. Tech. J. 37, 581-635.

Rice, S. O., (1944) Mathematical analysis of random noise. Bell Syst. Tech. J., 23, 282–332.

Rusu, E., Guedes Soares, C., (2012), Wave energy pattern around the Madeira Islands. Energy; 45: 771-85.

Rusu, L., Guedes Soares, C., (2012), Wave energy assessments in the Azores islands. Renewable Energy; 45: 183-96.

Sierra, J.P., Mösso, C., González-Marco, D., (2014), Wave energy resource assessment in Menorca (Spain). Renewable Energy; 71: 51-60.

T.W. Group., (1988), The WAM Model—A Third Generation Ocean Wave Prediction Model. Journal of Physical Oceanography; 18: 1775-810.

Vicinanza, D., Contestabile, P. & Ferrante, V., (2013), Wave energy potential in the north-west of Sardinia (Italy). Renewable Energy 50: 506-521.

# Abstract

The thesis deals with advanced analyses of wave data for predictions of severe storms and wave energy resource estimations, in the Mediterranean Sea and Atlantic and Pacific Oceans. The correct evaluation of extreme values of significant wave height is one of the most important topics of scientific interest in maritime engineering because of its relevance for the design of maritime structures and marine energy devices. The thesis gives an overview of the various methodologies employed in extreme values analysis of wave height focusing on the "Equivalent Storm Models" (ESM). Several typologies of wave data are processed, considering time series of significant wave height and wave direction by applying the ESMs. The study of existing methodologies in conjunction with the obtained results from the performed analysis has allowed the development of a new approach belonging to the category of ESM called Equivalent Exponential Storm (EES) model, whose crucial element relates to the fact that it joins in a single model the benefits of the previous ones. One of the main contribution given here concerns the introduction of a directional criterion for classifying sea storms as "directional storm" pertaining to a directional sector of given characteristics, which is useful in a lot of coastal engineering applications. Concerning the estimation of wave energy resource, in the thesis a simplified formula for the calculation of average wave power in deep water is applied for wave energy mapping of Mediterranean Sea, in conjunction with extreme values mapping, showing how the coupling of these two data is fundamental at the design stage of a wave energy device.

THIS PAGE INTENTIONALLY LEFT BLANK

# Acknowledgments

It is a very strange feeling to write the last page of my PhD thesis because it does not represent just only the gathering of the researches done during these three years, but the balance of a unique experience: a real opportunity of both professional and human growth. I am grateful to my advisor Professor Felice Arena and to all the people working in his research group, for useful and fruitful teachings. It is worth mentioning all the national and international research institutions that hosted me giving me the opportunity to utilize their database to perform the analyses presented here. In order of time the National Agency for New Technologies, Energy and Sustainable Economic Development (ENEA) of Casaccia (Italy), the Centre for Marine Technology and Ocean Engineering (CENTEC) of Lisbon (Portugal), and finally the French Research Institute for Exploitation of the Sea (IFREMER) of Brest (France). I would like to thank all the people that gave a contribution to my thesis: researchers Gianmaria Sannino and Adriana Carillo from ENEA, my co-advisor Professor Carlos Guedes Soares from CENTEC, and researchers Michel Olagnon and Cristophe Maisondue from Ifremer. Each person I have met during this experience has contributed to improve the sense of this path allowing me to find my way…

Finally, a last acknowledgement is addressed to the European Commission, the European Social Fund and to the "Regione Calabria" for funding the scholarship of my PhD program.